5th. year Internship
Activity report

LIGO-II Seismic Attenuation System

Nicolas Viboud

Institut National des Sciences Appliquées (INSA) de Lyon,
Département Génie Mécanique Développement

Mentors:

Dr. Riccardo DeSalvo

California Institute of Technology

LIGO Project

Pr. Regis Dufour

Laboratoire de Mecanique des Structures

INSA de Lyon

July-December 1999

LIGO-T000007-00-D

Contents

1 Introduction **1**
- 1.1 Gravitational Waves . . . 1
- 1.2 Large interferometers . . . 1
- 1.3 The LIGO-II Seismic Attenuation System . . . 2
- 1.4 Finite elements modeling . . . 2

2 Inverted pendulum leg modal analysis **4**
- 2.1 Introduction: VIRGO Superattenuator example . . . 4
- 2.2 Geometry . . . 4
- 2.3 Mesh . . . 4
- 2.4 Boundary Conditions . . . 6
- 2.5 Flex joint . . . 6
- 2.6 Top short-pendulum . . . 6
- 2.7 Results . . . 7
  - 2.7.1 free-free boundary conditions . . . 7
  - 2.7.2 ground-free boundary conditions . . . 12
  - 2.7.3 "in-situ" boundary conditions . . . 17
- 2.8 Measurements . . . 23
  - 2.8.1 First mode . . . 27
  - 2.8.2 Second mode . . . 28
  - 2.8.3 Third mode . . . 29
  - 2.8.4 Fourth and fifth modes . . . 30
  - 2.8.5 Comparison between measurements and predicitions . . . 30
- 2.9 Conclusion . . . 30

3 Blade-tip built-in flex joint for the filters **31**
- 3.1 Introduction . . . 31
- 3.2 Design of the flex joint . . . 33
- 3.3 Initial geometry . . . 33
  - 3.3.1 Mesh . . . 35
  - 3.3.2 Boundary conditions . . . 36
  - 3.3.3 Results for the initial geometry . . . 37

3.3.4 Conclusion on the first geometry . . . 38
3.4 Improved geometry . . . 39

4 Clamped-Clamped blades **43**
4.1 Introduction . . . 43
4.2 Geometry . . . 44
4.3 Mesh . . . 44
4.4 Boundary Conditions . . . 46
4.5 Solver . . . 46
4.6 Simulation results . . . 47
4.6.1 Stress . . . 47
4.6.2 Stiffness and vertical resonant frequency . . . 47
4.7 Prototype . . . 51
4.7.1 Description . . . 51
4.7.2 Assembly of the prototype . . . 53
4.8 Experiments on the prototype . . . 56
4.8.1 First results . . . 56
4.8.2 Geometry modifications . . . 57
4.8.3 Results for the prototype . . . 58
4.9 Comments on the working principle . . . 62
4.10 Simulation of the prototype . . . 66
4.10.1 Introduction . . . 66
4.10.2 Comments on the prototype's geometry . . . 66
4.10.3 Simulation first results . . . 67
4.10.4 Inverse approach . . . 69
4.10.5 Loading procedure . . . 69
4.10.6 Corrections on blade # 1 . . . 70
4.10.7 Corrections on blade # 3 . . . 74
4.10.8 Comment on the geometry corrections . . . 74
4.11 Next prototype . . . 75
4.11.1 Preambule . . . 75
4.11.2 Simulations . . . 75
4.11.3 Limits to the predictions . . . 79
4.11.4 Comment on the stress . . . 79
4.12 Conclusion on the clamped-clamped filter . . . 83

5 Conclusion **84**

6 Acknowledgements **85**

Abstract

The experiments to detect gravitationnal waves (large interferometers LIGO, VIRGO) require an excellent isolation from the seismic noise, which is much larger (10^6) than the expected signal.

An update project for the LIGO-II interferometer is being developped in order to achieve the required seismic isolation.

The requirements on the mechanics of the seismic attenuation system are stringent. The parts must be designed in a way that their resonant frequencies are located as much as possible away from the typical seismic noise frequency range. Or the effects of an unwanted resonant frequency must be properly neutralized. Some parts (filter links for example) are subject to very high stress and one must be sure they will not break, or even creep. Some alternative designs must be studied (wireless filters for example) and compared to the current designs. After each part is analysed separately, some subsystems (filters for example, in the dynamic behavior study) should be re-assembled and studied, in order to take into account the interactions between the parts.

The main purpose of this internship is to perform finite elements simulations on the mechanics of the seismic attenuation system, in order to meet the above requirements.

Chapter 1

Introduction

1.1 Gravitational Waves

At the beginning of the 20th century Einstein came out with General Relativity (G.R.). In Special Relativity, gravitational interactions, being instant, were allowed to exceed speed of light. Einstein addressed that problem by producing G.R., a wider theory that includes gravitation. In this theory, gravitational interactions travel at the speed of light. G.R. equations admit a solution in terms of waves, gravitational waves (G.W.), in an analog way to Maxwell's equations and electromagnetic waves.

G.W. stretch and compress space, and they are quadrupolar. If the direction of propagation is Z, then when space is streched along X, it is also compressed along Y.

So far nobody has detected G.W. directly. Taylor and Hulse proved indirectly that they exist and won the 1993 Nobel Prize. The gravitationnal waves should be emitted most strongly by large-scale, coherent vibrations/motion of matter or spacetime curvature: collisions of black holes, the implosion of the core of a star triggering a supernova, the inspiral and merger of two neutron stars that are orbiting each other etc...

The difficulty of detecting G.W. comes from the fact that their effects are very small. The relative elongation, strain of space, that one could expect from the above events would be, on earth, of about $h = 10^{-21}$.

1.2 Large interferometers

G.W. are difficult to detect because they cause very small strain and very small displacements. Interferometry is attractive when one needs to measure small displacements. For LIGO (Laser Interferometer Gravitatinal-wave Observatory), a giant Michelson-like interferometer is being built. The laser beam is the length reference, and if space was stretched by a G.W., the mirrors would follow and the interference pattern would be changed. Over its 4 km-long arms, strains of 10^{-21} would move the mirrors of about 10^{-18} m. Practically, the interferometer is "locked" on a dark fringe, and if we need to translate the mirrors to

maintain lock, then it means we are compensating for the effect of a G.W.. Therefore the observation is done by monitoring the servo signal, which includes compensation for G.W. But it also contains compensation for all kinds of noises when we look at a level of 10^{-18} m.

Seismic motion is the first source of noise that comes to our mind. Typical amplitude of seismic noise is of the order of 10^{-6} m, twelwe orders of magnitude larger than the signal of interest. The interferometer's optics require seismic isolation, so that we bring the seismic noise amplitude below the displacements we want to detect.

1.3 The LIGO-II Seismic Attenuation System

It is essentially a chain of low frequency mechanical, passive oscillators. Actuators and electronics are present to control the system and damp its resonances, but not to provide isolation in the frequency range of interest.

The success in attenuating seismic noise depends on the mechanics on the system. Therefore a large effort is made to fully understand the behaviorof the system, theoretically and experimentally.

1.4 Finite elements modeling

The behavior of real "solids" (which are not perfectly solid) is ruled by elasticity equations, also named solid mechanics equations. These equations have in general no analytical solutions. Therefore we solve them with numerical methods. Among all the available numerical techniques, Finite Elements are the most commonly used.

In this project we used the Finite Elements capabilities of I-DEAS Master Series 5m3, a software from Structural Dynamics Research Corporation (SDRC). The software was running most of the time on a remote, powerful workstation (canopus.ligo.caltech.edu, a SUN Ultra-60 with 384 MegaBytes of RAM).

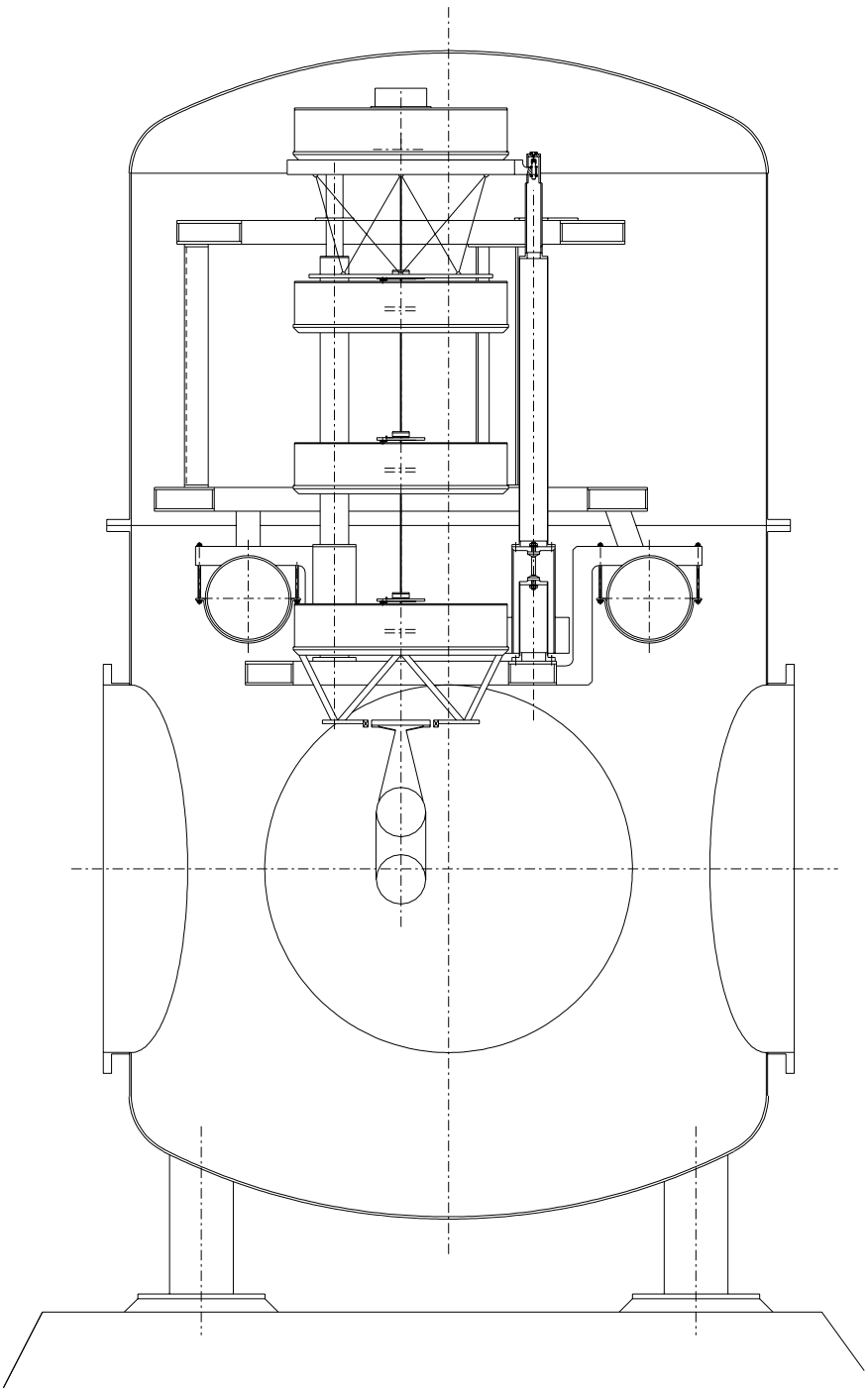

Figure 1.1: LIGO BeamSplitter Chamber, with the seismic attenuation system used to hang the mirror.

Chapter 2

Inverted pendulum leg modal analysis

2.1 Introduction: VIRGO Superattenuator example

The inverted pendulum is a quite simple device. For the seismic isolation we design it with a very low resonant frequency (about 0.01 Hz). Therefore at frequencies above the pendulum's, we will attenuate seismic noise with an increasing attenuation factor proportionnal to f^2.

This is true only in theory, for a perfect pendulum. With real solids, we are limited by the internal resonant frequencies of the system.

The VIRGO interferometer suffers from this problem at 9 Hz, where the inverted pendulum leg has its first internal mode. The system does not attenuate as expected. For the LIGO Seismic Attenuation System we wanted to avoid such a bad surprise, making a modal analysis of the leg.

2.2 Geometry

Three cylinders on top of each other, on which the mesh was put. The main part of the leg is the middle (hollow) cylinder. The short, bottom cylinder is the counterweight bell. The counterweight is here for center of percussion tuning purposes. On top of the main cylinder is located a very small cylinder with a short pendulum to hold the filter 0.

2.3 Mesh

Semi-automatic mapped mesh was used (see 2.3). It included elements of the following types:

'95 - thin shell parabolic quadrilateral' (8 nodes, 6 dof/node)
'92 - thin shell parabolic triangle' (6 nodes, 6 dof/node)
'161 - lumped mass'
'21 - linear beam'
'136 - node to node translational spring'
'137 - node to node rotational spring'

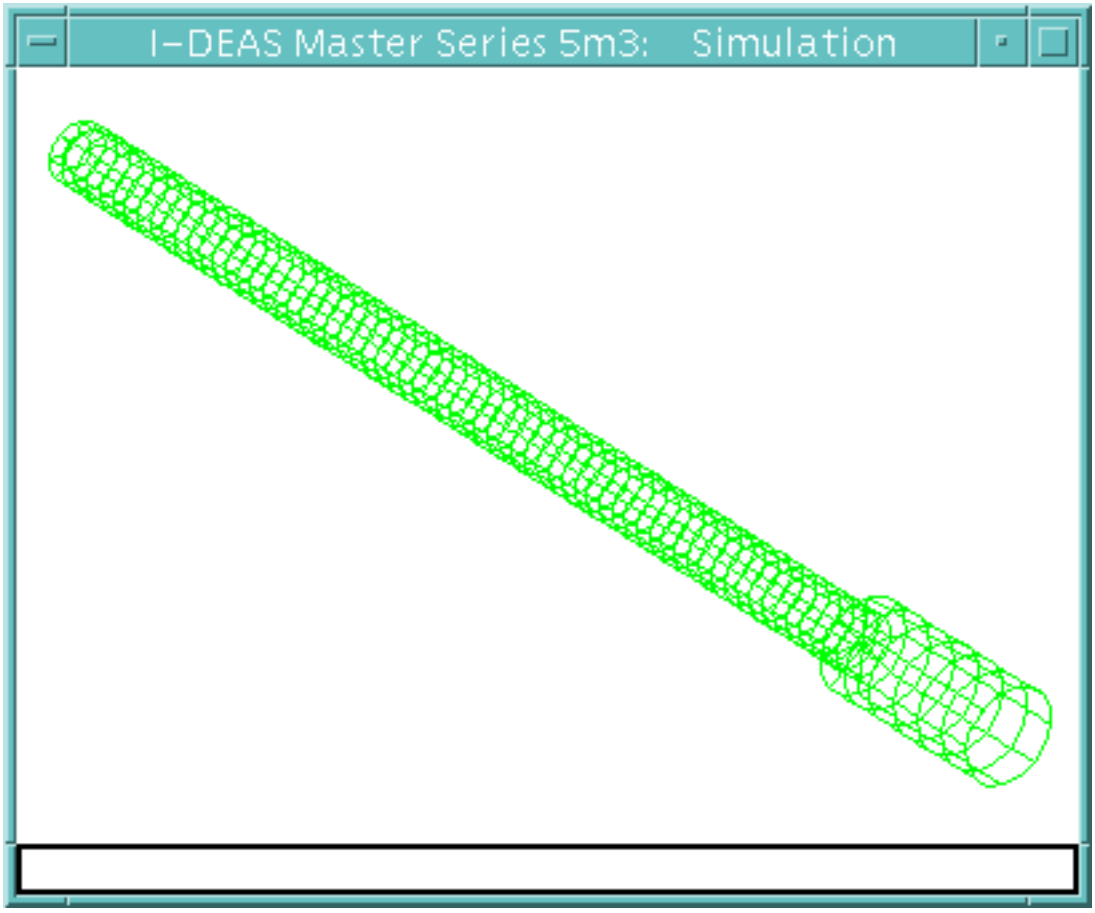

Figure 2.1: Inverted pendulum leg mesh.

1980 degrees of freedom for the leg
673 shell elements
4+1 lumped masses, 1 beam, 1 translational spring, 1 rotationnal spring

The bases of the cylinders (disc between the main cylinder and the counterweight bell, between the main cylinder and the small top cylinder, and eventually the lid on the top cylinder) were also modelled using the same elements, in order to keep the mesh simple. They are quite thick, so the thin-shell elements may not give accurate distributions of stress in these areas. However, the thickness of the shell in these areas was choosen as the actual thickness. Therefore the mass is correct and the deformed curvature of the leg remains continuous at the interface between the different cylinders.

For simplicity, 4 lumped masses (3.3 kg) were added at 4 nodes at the bottom of the counterweight bell, instead of the counterweight ring.

2.4 Boundary Conditions

Several boundary conditions were used. In the beginning, the two ends were put on simple-supports, one of them sliding.

Then the leg was left free at both ends (with a small frequency shift added to the solver in order to skip the resulting rigid-body modes).

Then, the upper end was left free and the bottom end was linked to the ground by the flex joint (see 2.5).

Eventually, a feature was added to the model of the leg, in order to roughly take into account the influence of the vertical filter chain (see 2.6).

2.5 Flex joint

The flex-joint provides the restoring force when the inverted pendulum is out of its vertical position, whereas gravity tends to make the pendulum fall acting as a negative spring (non-linear, which makes the system unstable if the displacements become too large). An engineer previously designed the flex joint and had already made a detailed, finite-element static analysis. Therefore a simple beam element was used here to model the flex joint. The cross-section affected to this element was cylindrical, with a diameter corresponding to the main cylinder of the actual flex joint. The roundings at the ends of the flex joint and its really short length (which is unappropriate for beam elements) were ignored. Later on, we had two occurences of the same mode, the only difference being that one of them had an unrealistic deformation for the flex joint. Therefore we concluded a beam element was not suitable and replaced it by a simple rotational spring.

2.6 Top short-pendulum

The load (vertical filter chain + test mass) hangs to the top of the leg via a short (3cm) wire. It is located inside the small upper cylinder, which features a slot on its side to connect filter 0 to the end of the wire. The wire and the chain attached at its end form another pendulum (very short, 3Hz, and not inverted this time). One of the reasons of the use of this device is that it is a frictionless replacement to a ball joint.

In our model it introduces a filtering effect between the heavy-mass vertical chain and the inverted pendulum leg. To study the inverted pendulum mode, whose frequency ($f_i = 100mHz$) is below the top pendulum frequency ($f_t = 3Hz$), a mass corresponding to 100 % of the payload must be taken into account. To study frequencies f_s above 3Hz, only a fraction of the payload remains as an effective mass, because of the f_s/f^2 filtering effect.

It turned out that modelling the top short-pendulum, with a rod and a mass, was not possible. The linear geometric formulation that the software uses for Modal Analysis cannot take into account the effect of the gravity as a recovering force for the rod. Therefore the

rod of the pendulum can rotate without any recovering force appearing. It obviously creates singularities in the matrix system.

The solution was to replace the rod element (link) and the gravity (recovering force) by translational and rotational springs, removing the singularity problems. These springs link the lumped mass to the former wire mount point on the upper cylinder lid. Their stiffness was calculated in order to get the 3Hz resonance.

2.7 Results

2.7.1 free-free boundary conditions

Note that to remove the 6 rigid body modes of the free structure, a frequency shift was introduced into the solver. The software started at 1 Hz instead of 0 Hz.

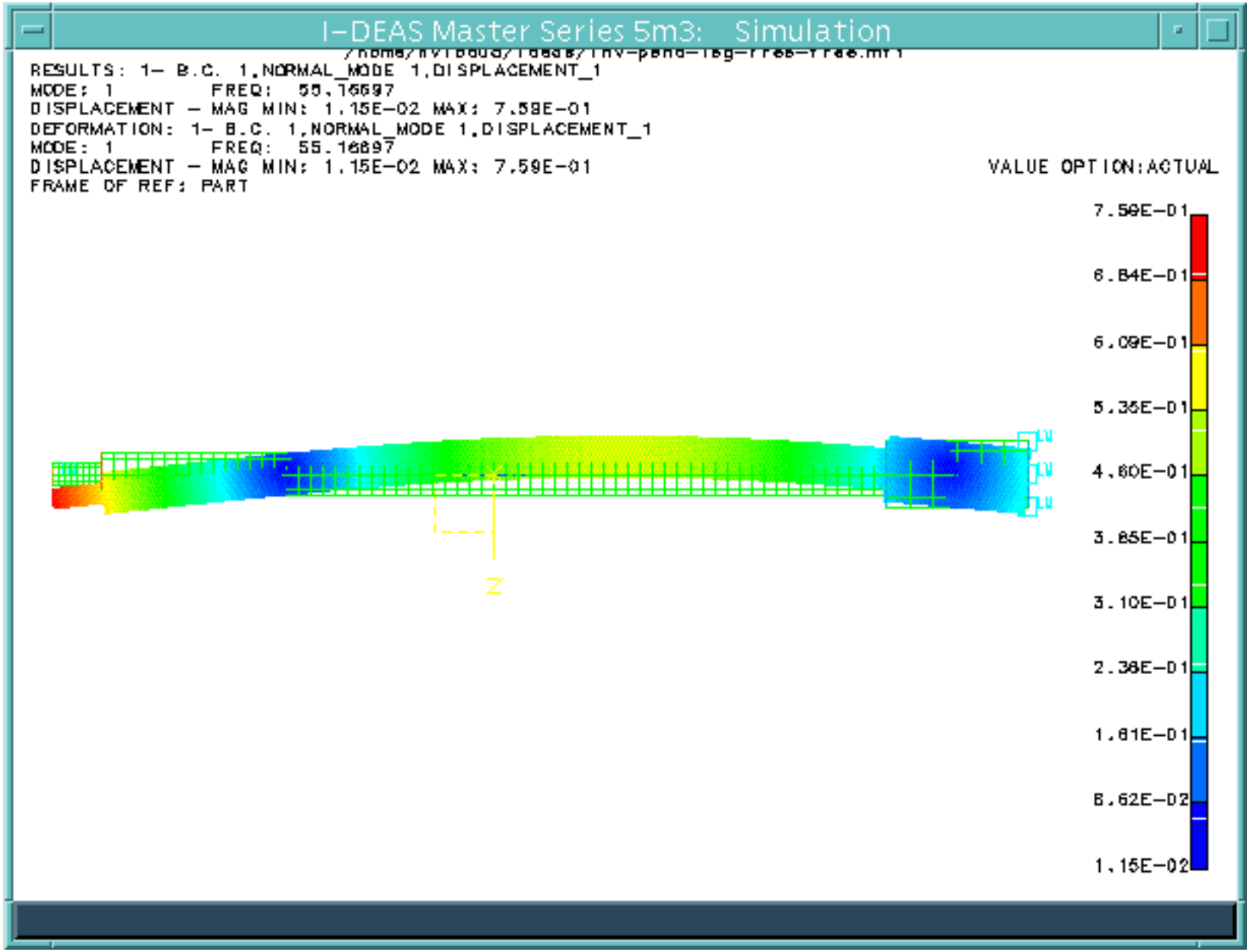
I-DEAS Master Series 5m3: Simulation
RESULTS: 1- B.C. 1,NORMAL_MODE 1,DISPLACEMENT_1
MODE: 1 FREQ: 55.16697
DISPLACEMENT - MAG MIN: 1.15E-02 MAX: 7.59E-01
DEFORMATION: 1- B.C. 1,NORMAL_MODE 1,DISPLACEMENT_1
MODE: 1 FREQ: 55.16697
DISPLACEMENT - MAG MIN: 1.15E-02 MAX: 7.59E-01
FRAME OF REF: PART
VALUE OPTION:ACTUAL
7.59E-01
6.84E-01
6.09E-01
5.35E-01
4.60E-01
3.85E-01
3.10E-01
2.36E-01
1.61E-01
8.62E-02
1.15E-02
Z

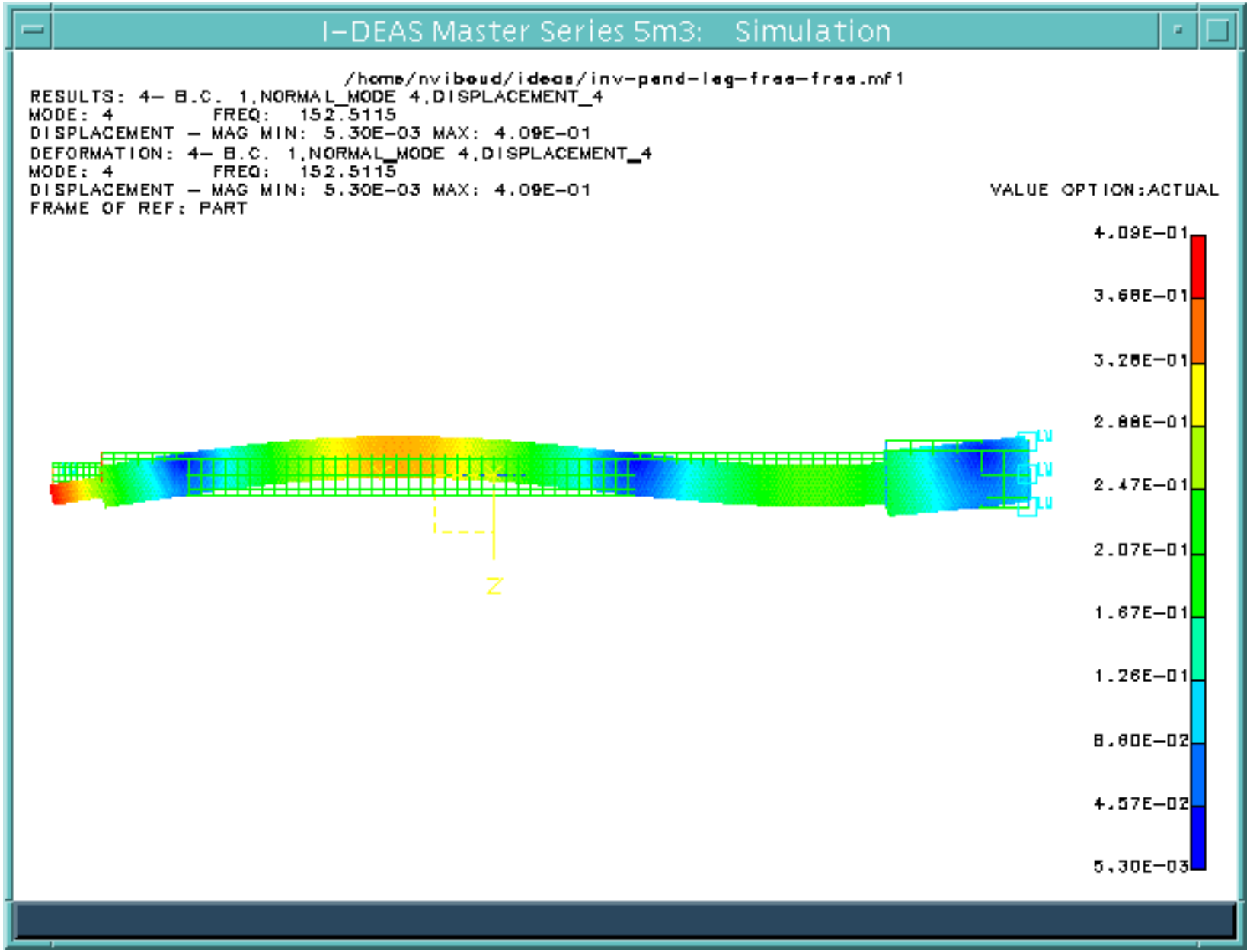
I-DEAS Master Series 5m3: Simulation
/home/nviboud/ideas/inv-pend-leg-free-free.mf1
RESULTS: 4- B.C. 1,NORMAL_MODE 4,DISPLACEMENT_4
MODE: 4 FREQ: 152.5115
DISPLACEMENT - MAG MIN: 5.30E-03 MAX: 4.09E-01
DEFORMATION: 4- B.C. 1,NORMAL_MODE 4,DISPLACEMENT_4
MODE: 4 FREQ: 152.5115
DISPLACEMENT - MAG MIN: 5.30E-03 MAX: 4.09E-01
FRAME OF REF: PART
VALUE OPTION:ACTUAL
4.09E-01
3.68E-01
3.26E-01
2.88E-01
2.47E-01
2.07E-01
1.67E-01
1.26E-01
8.60E-02
4.57E-02
5.30E-03
Z

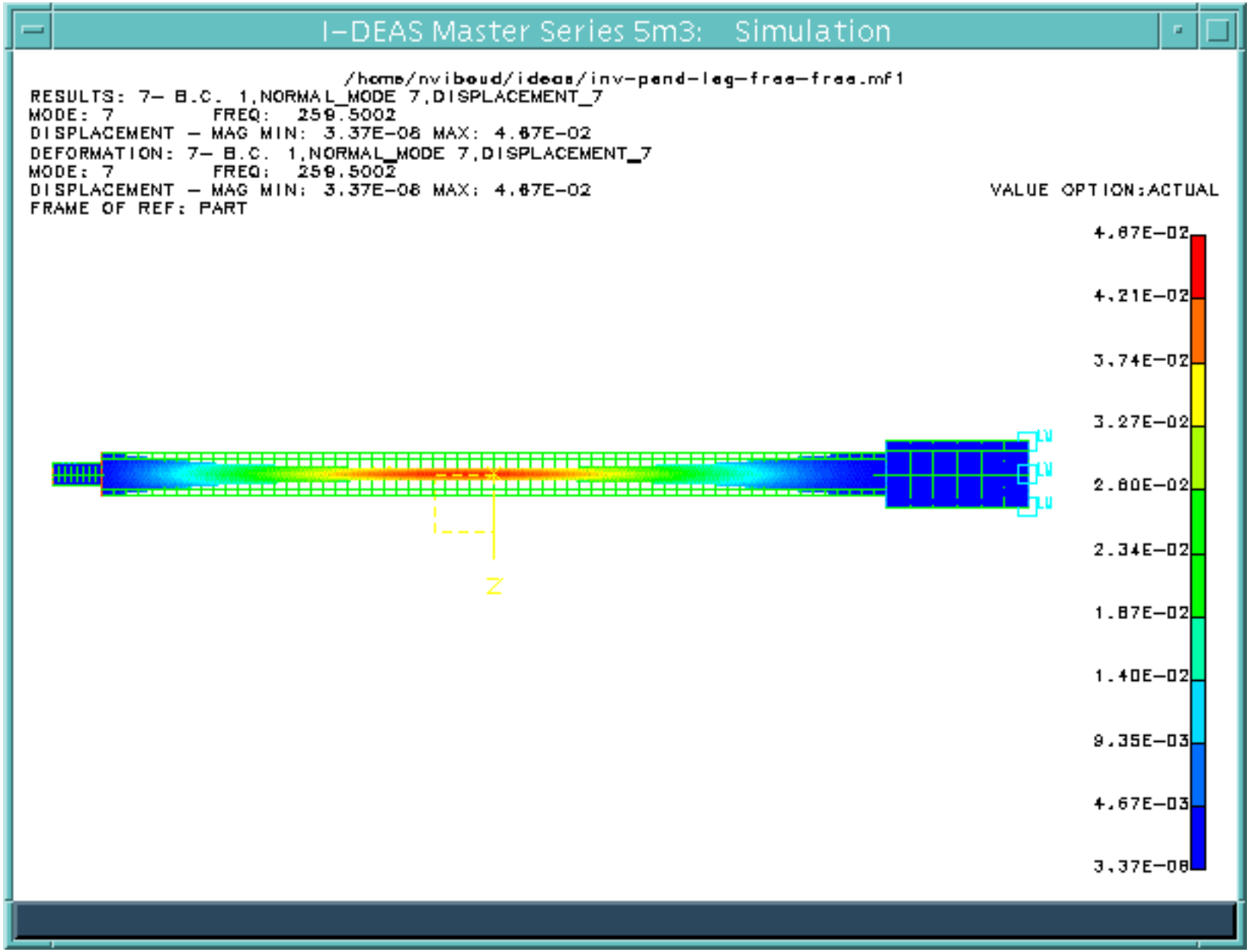
I-DEAS Master Series 5m3: Simulation
/home/nvibeud/ideas/inv-pend-leg-free-free.mf1
RESULTS: 7- B.C. 1,NORMAL_MODE 7,DISPLACEMENT_7
MODE: 7 FREQ: 259.5002
DISPLACEMENT - MAG MIN: 3.37E-08 MAX: 4.67E-02
DEFORMATION: 7- B.C. 1,NORMAL_MODE 7,DISPLACEMENT_7
MODE: 7 FREQ: 259.5002
DISPLACEMENT - MAG MIN: 3.37E-08 MAX: 4.67E-02
FRAME OF REF: PART
VALUE OPTION:ACTUAL
4.67E-02
4.21E-02
3.74E-02
3.27E-02
2.80E-02
2.34E-02
1.87E-02
1.40E-02
9.35E-03
4.67E-03
3.37E-08
Z

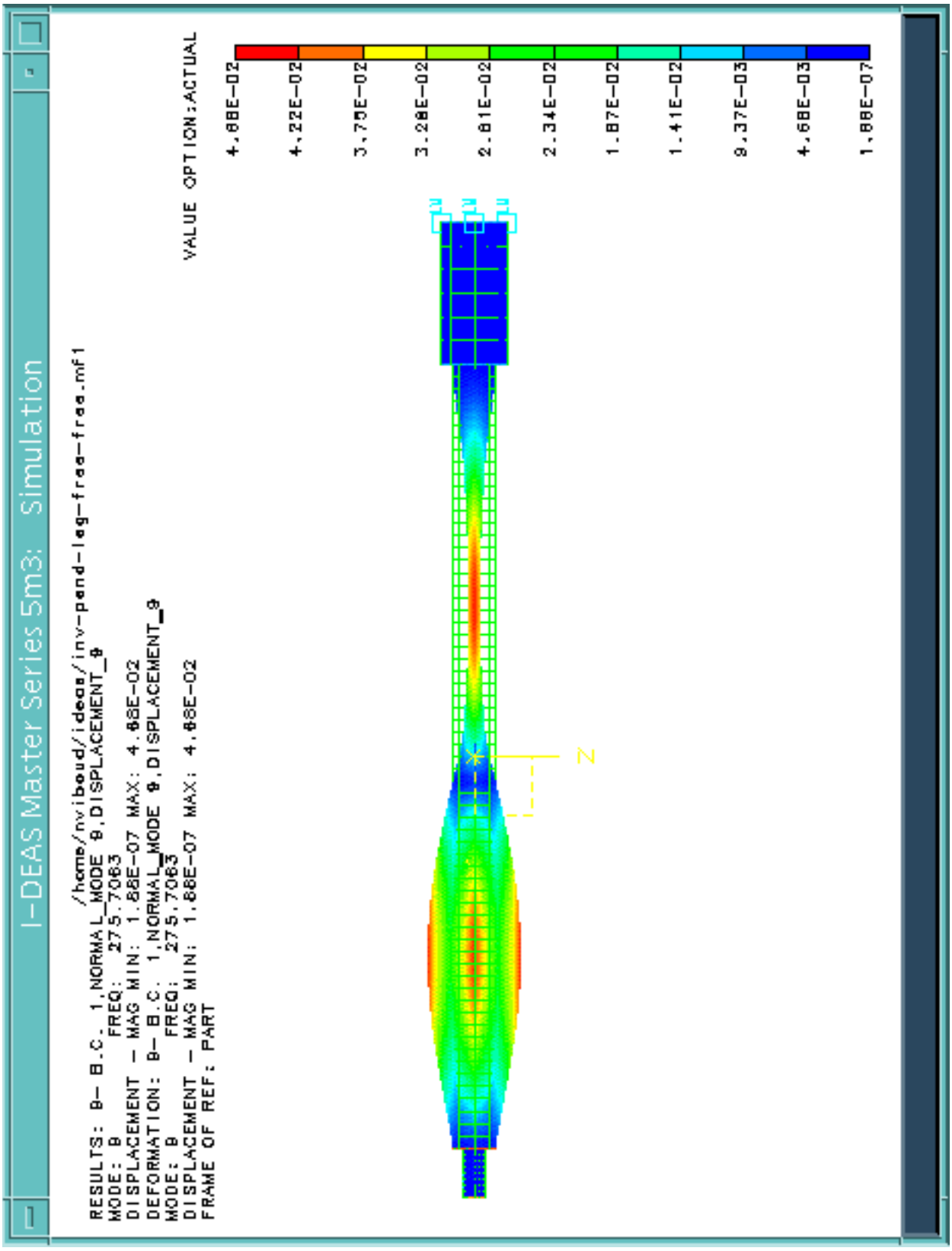
I-DEAS Master Series Sm3: Simulation
/home/nvi6oud/ideas/inv-pend-leg-free-free.mf1
RESULTS: 8- B.C. 1,NORMAL_MODE 8,DISPLACEMENT_8
MODE: 8 FREQ: 275.7063
DISPLACEMENT - MAG MIN: 1.68E-07 MAX: 4.68E-02
DEFORMATION: 8- B.C. 1,NORMAL_MODE 8,DISPLACEMENT_8
MODE: 8 FREQ: 275.7063
DISPLACEMENT - MAG MIN: 1.68E-07 MAX: 4.68E-02
FRAME OF REF: PART
VALUE OPTION:ACTUAL
4.68E-02
4.22E-02
3.75E-02
3.28E-02
2.81E-02
2.34E-02
1.87E-02
1.41E-02
9.37E-03
4.68E-03
1.68E-07
N

2.7.2 ground-free boundary conditions

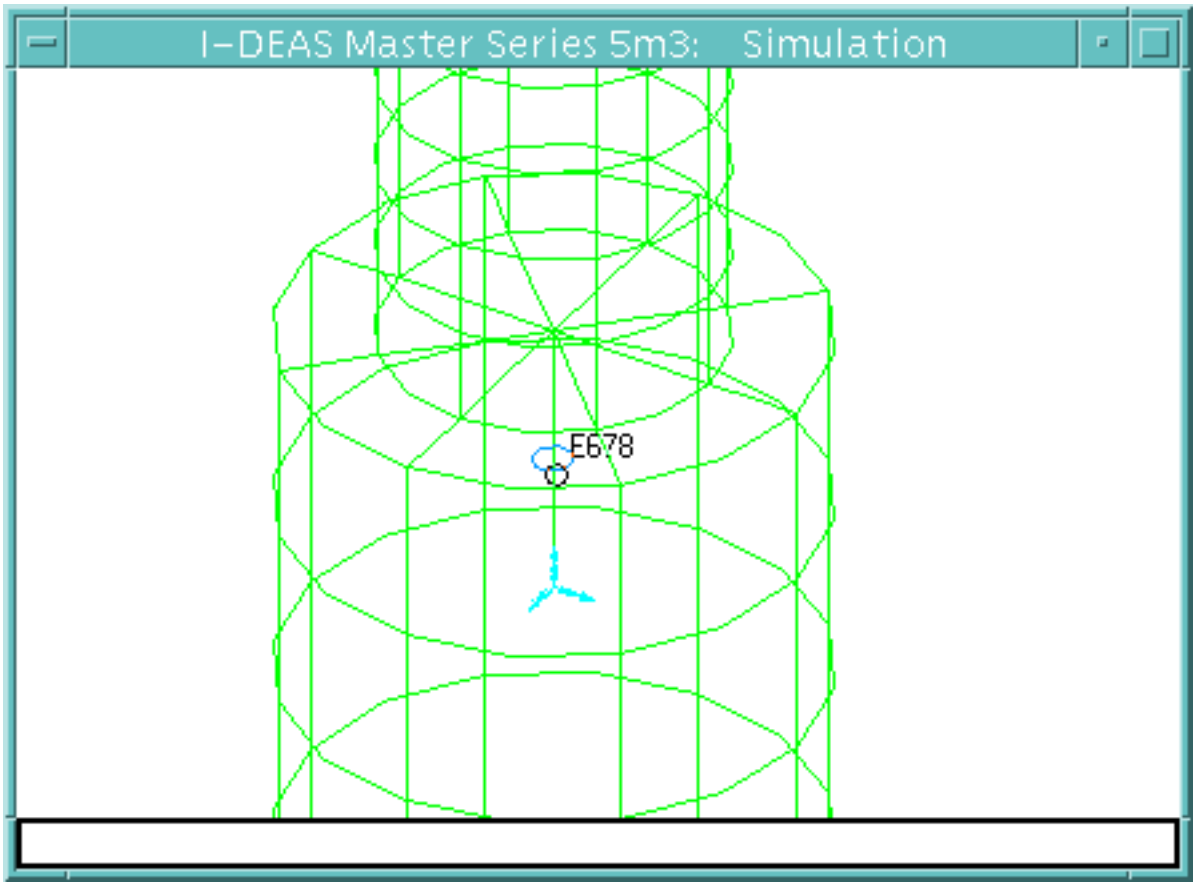

The beam element used to simulate the flex joint is the green, vertical line labelled E678 on the picture. The top-end node is connected to the center of the horizontal disk, and the bottom-end node is clamped to the ground.

The addition of this feature to the model decreased the resonant frequencies of the former first and second modes of the leg. It also created other modes:

- the pendulum mode (where the leg oscillates away from the vertical position)
- a torsional mode about the flex joint's axis
- a vertical translation mode due to the "well" deformation of the disc connected to the flex joint

  This last mode is certainly unreal because of the thin shell approximation made for the thick disc.

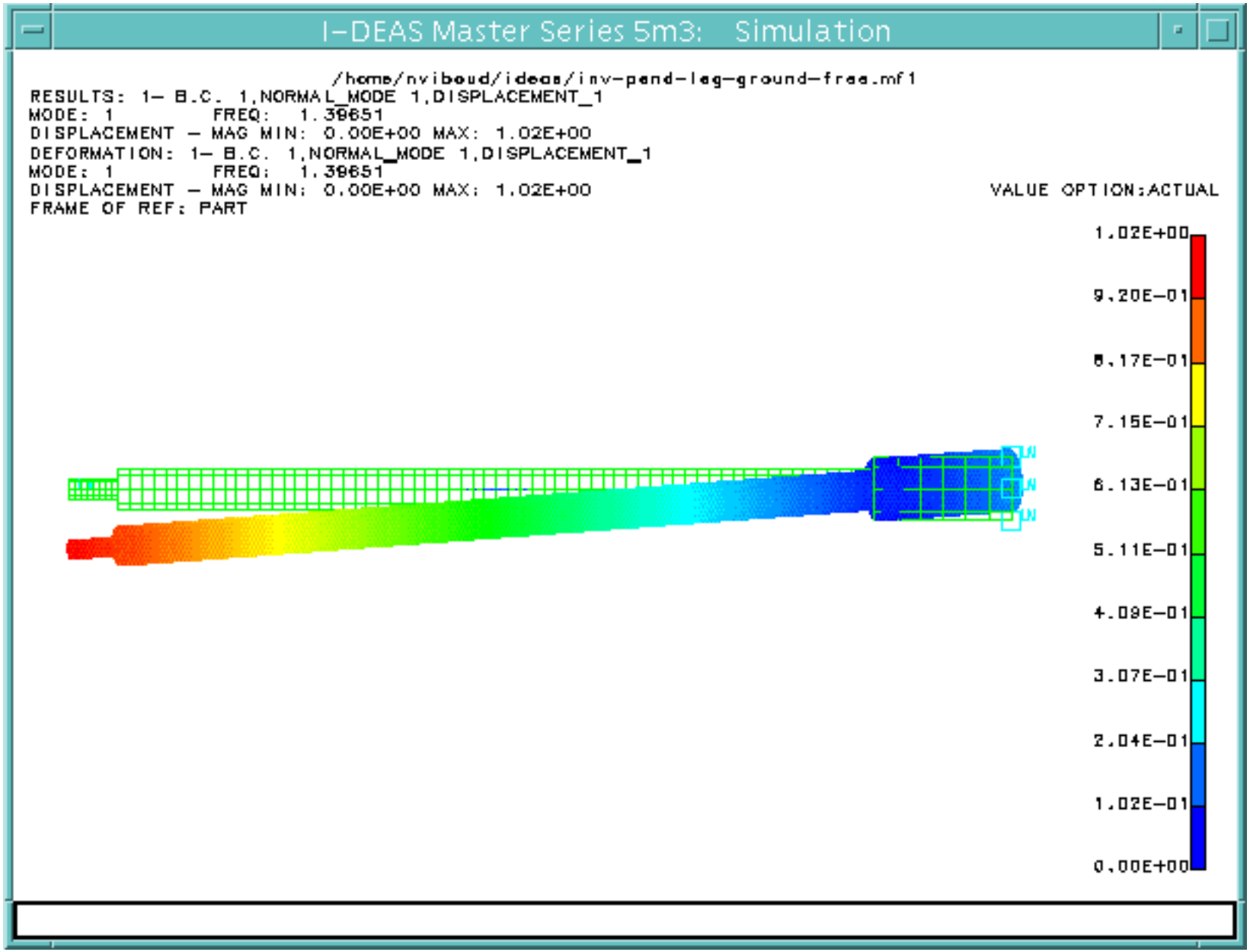
I-DEAS Master Series 5m3: Simulation
/home/nvibeud/ideas/inv-pend-leg-ground-free.mf1
RESULTS: 1- B.C. 1,NORMAL_MODE 1,DISPLACEMENT_1
MODE: 1 FREQ: 1.39651
DISPLACEMENT - MAG MIN: 0.00E+00 MAX: 1.02E+00
DEFORMATION: 1- B.C. 1,NORMAL_MODE 1,DISPLACEMENT_1
MODE: 1 FREQ: 1.39651
DISPLACEMENT - MAG MIN: 0.00E+00 MAX: 1.02E+00
FRAME OF REF: PART
VALUE OPTION:ACTUAL
1.02E+00
9.20E-01
8.17E-01
7.15E-01
6.13E-01
5.11E-01
4.09E-01
3.07E-01
2.04E-01
1.02E-01
0.00E+00

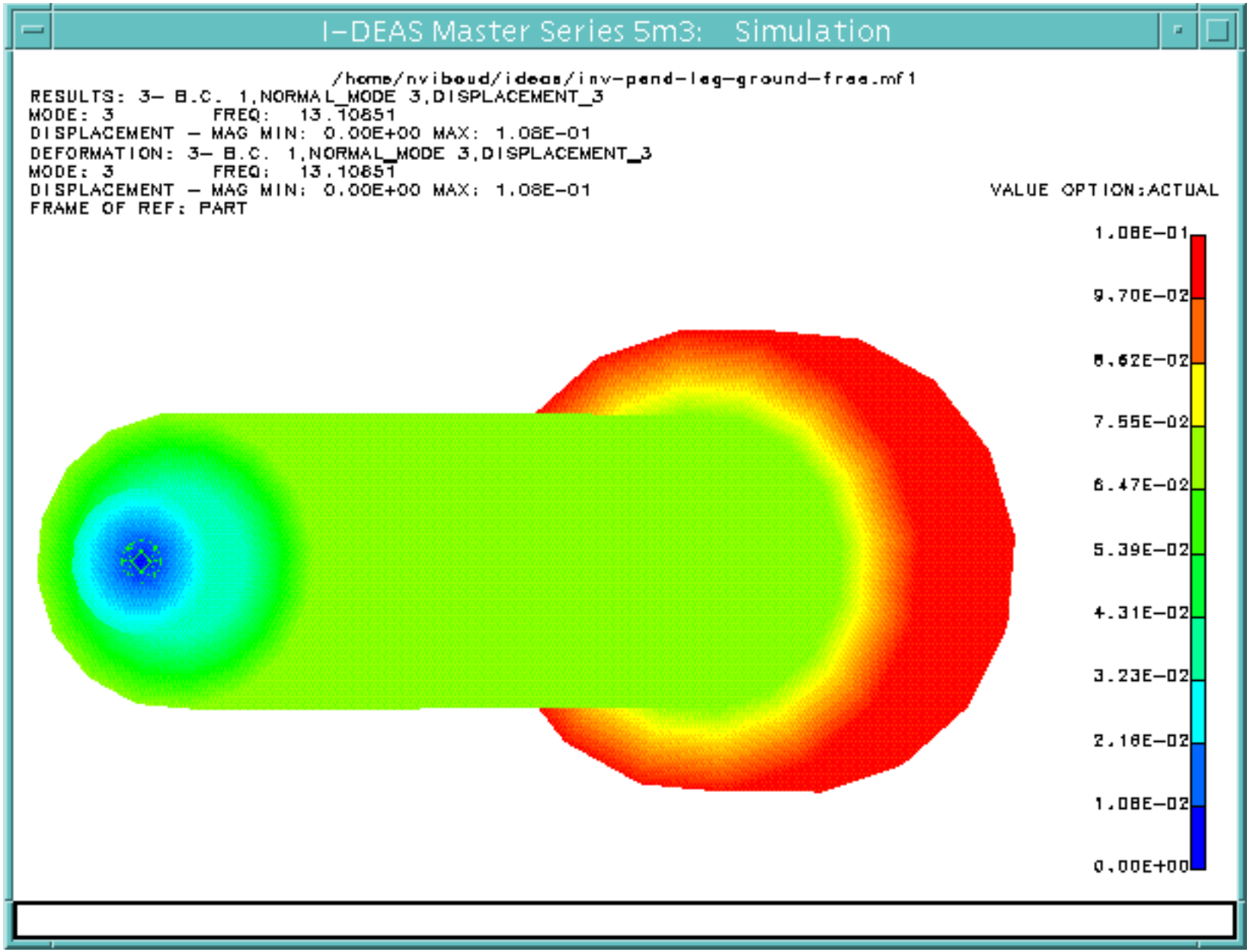
I-DEAS Master Series 5m3: Simulation
/home/nvibeud/ideas/inv-pend-leg-ground-free.mf1
RESULTS: 3- B.C. 1,NORMAL_MODE 3,DISPLACEMENT_3
MODE: 3 FREQ: 13.10851
DISPLACEMENT - MAG MIN: 0.00E+00 MAX: 1.08E-01
DEFORMATION: 3- B.C. 1,NORMAL_MODE 3,DISPLACEMENT_3
MODE: 3 FREQ: 13.10851
DISPLACEMENT - MAG MIN: 0.00E+00 MAX: 1.08E-01
FRAME OF REF: PART
VALUE OPTION:ACTUAL
1.08E-01
9.70E-02
8.62E-02
7.55E-02
6.47E-02
5.39E-02
4.31E-02
3.23E-02
2.16E-02
1.08E-02
0.00E+00

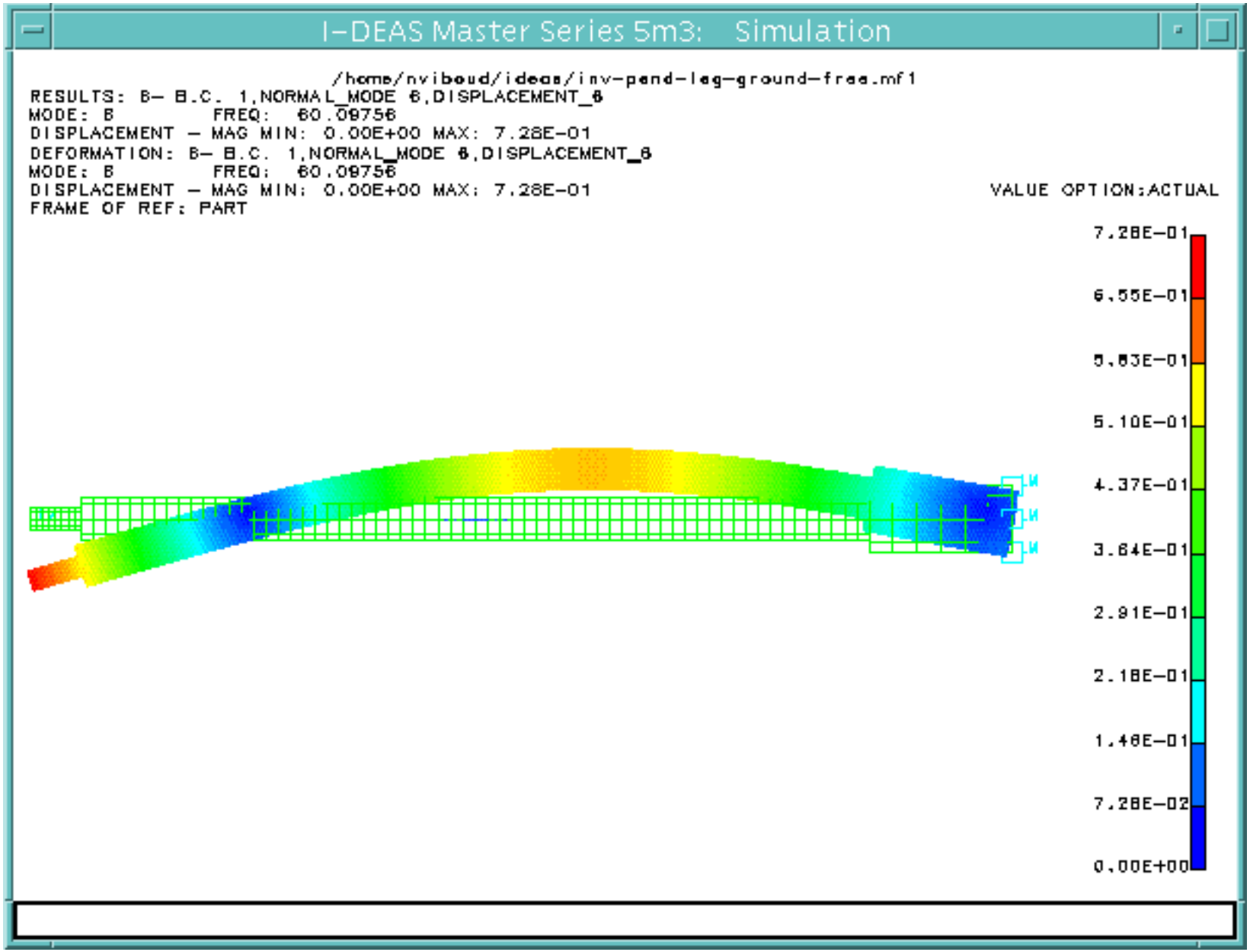
I-DEAS Master Series 5m3: Simulation
/home/nvibeud/ideas/inv-pend-leg-ground-free.mf1
RESULTS: B- B.C. 1,NORMAL_MODE 6,DISPLACEMENT_6
MODE: B FREQ: 60.09756
DISPLACEMENT - MAG MIN: 0.00E+00 MAX: 7.28E-01
DEFORMATION: B- B.C. 1,NORMAL_MODE 6,DISPLACEMENT_6
MODE: B FREQ: 60.09756
DISPLACEMENT - MAG MIN: 0.00E+00 MAX: 7.28E-01
FRAME OF REF: PART
VALUE OPTION:ACTUAL
7.28E-01
6.55E-01
5.83E-01
5.10E-01
4.37E-01
3.64E-01
2.91E-01
2.18E-01
1.46E-01
7.28E-02
0.00E+00

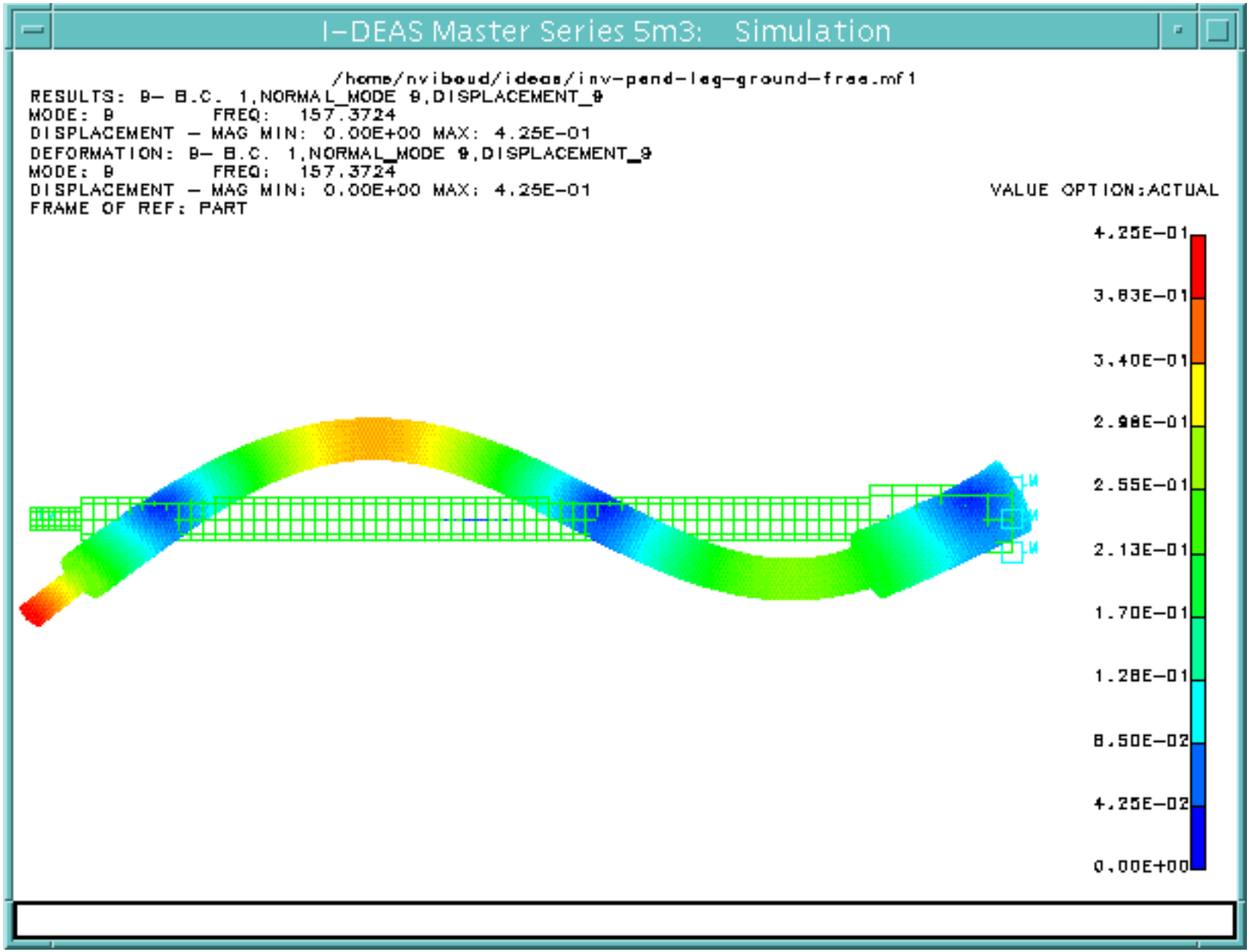
I-DEAS Master Series 5m3: Simulation
/home/nvibeud/ideas/inv-pend-leg-ground-free.mf1
RESULTS: B- B.C. 1,NORMAL_MODE 9,DISPLACEMENT_9
MODE: 9 FREQ: 157.3724
DISPLACEMENT - MAG MIN: 0.00E+00 MAX: 4.25E-01
DEFORMATION: B- B.C. 1,NORMAL_MODE 9,DISPLACEMENT_9
MODE: 9 FREQ: 157.3724
DISPLACEMENT - MAG MIN: 0.00E+00 MAX: 4.25E-01
FRAME OF REF: PART
VALUE OPTION:ACTUAL
4.25E-01
3.83E-01
3.40E-01
2.98E-01
2.55E-01
2.13E-01
1.70E-01
1.28E-01
8.50E-02
4.25E-02
0.00E+00

2.7.3 "in-situ" boundary conditions

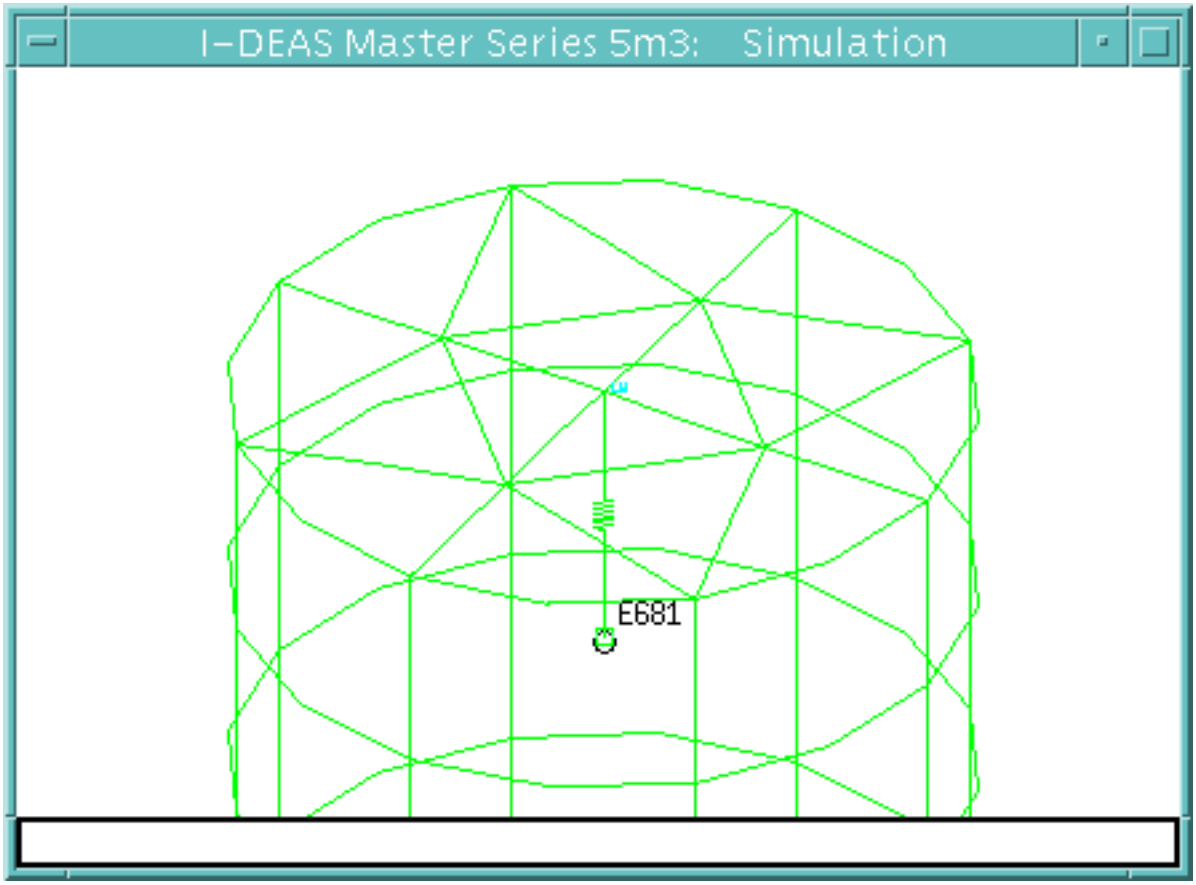

The 160kg lumped mass standing for the vertical filter chain is the green square labelled E681 on the picture. It is connected to the center of the top lid via a spring element. On the picture the spring is shown vertical, but it is actually a spring-link for all the 6 degrees of freedom. It was tuned to $56849 N.m^{-1}$ in the two horizontal directions (X and Z), to get a 3Hz resonant frequency. In the vertical direction it was tuned to $5E9 N.m^{-1}$ in order to push the vertical resonance above the studied frequency range.

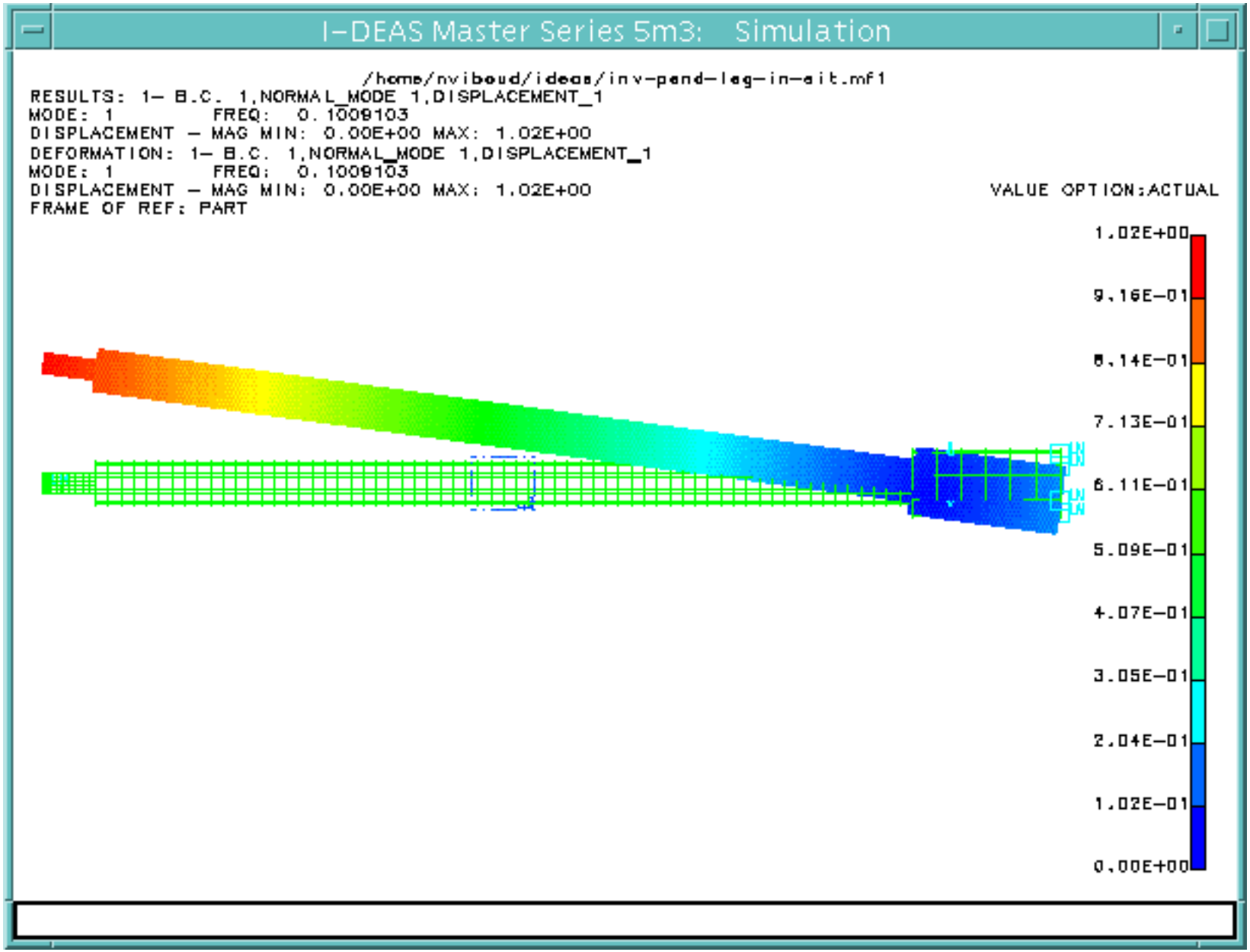
I-DEAS Master Series 5m3: Simulation
/home/nvibeud/ideas/inv-pend-leg-in-ait.mf1
RESULTS: 1- B.C. 1,NORMAL_MODE 1,DISPLACEMENT_1
MODE: 1 FREQ: 0.1009103
DISPLACEMENT - MAG MIN: 0.00E+00 MAX: 1.02E+00
DEFORMATION: 1- B.C. 1,NORMAL_MODE 1,DISPLACEMENT_1
MODE: 1 FREQ: 0.1009103
DISPLACEMENT - MAG MIN: 0.00E+00 MAX: 1.02E+00
FRAME OF REF: PART
VALUE OPTION:ACTUAL
1.02E+00
9.16E-01
8.14E-01
7.13E-01
6.11E-01
5.09E-01
4.07E-01
3.05E-01
2.04E-01
1.02E-01
0.00E+00

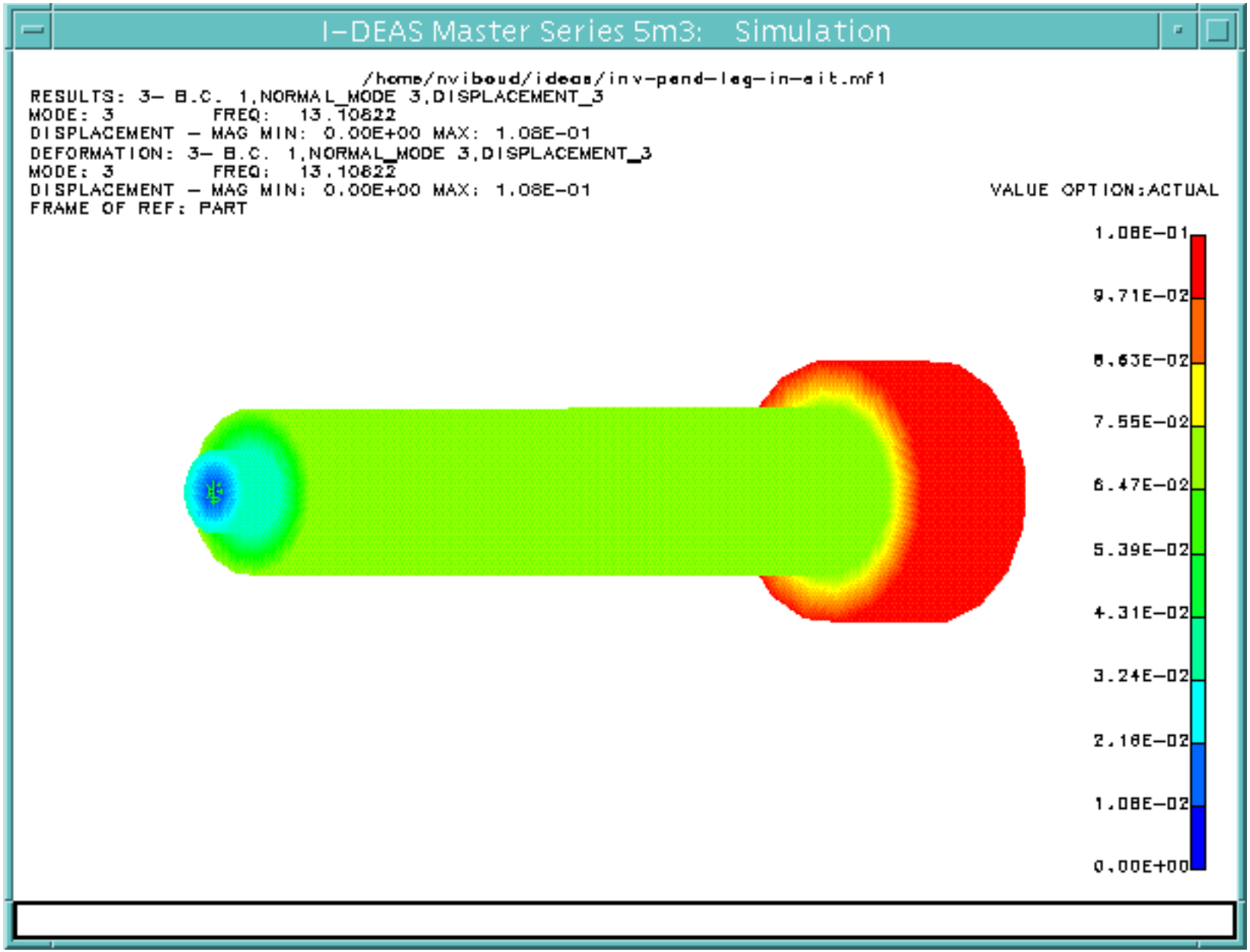
I-DEAS Master Series 5m3: Simulation
/home/nvibeud/ideas/inv-pend-leg-in-air.mf1
RESULTS: 3- B.C. 1,NORMAL_MODE 3,DISPLACEMENT_3
MODE: 3 FREQ: 13.10822
DISPLACEMENT - MAG MIN: 0.00E+00 MAX: 1.08E-01
DEFORMATION: 3- B.C. 1,NORMAL_MODE 3,DISPLACEMENT_3
MODE: 3 FREQ: 13.10822
DISPLACEMENT - MAG MIN: 0.00E+00 MAX: 1.08E-01
FRAME OF REF: PART
VALUE OPTION:ACTUAL
1.08E-01
9.71E-02
8.63E-02
7.55E-02
6.47E-02
5.39E-02
4.31E-02
3.24E-02
2.16E-02
1.08E-02
0.00E+00

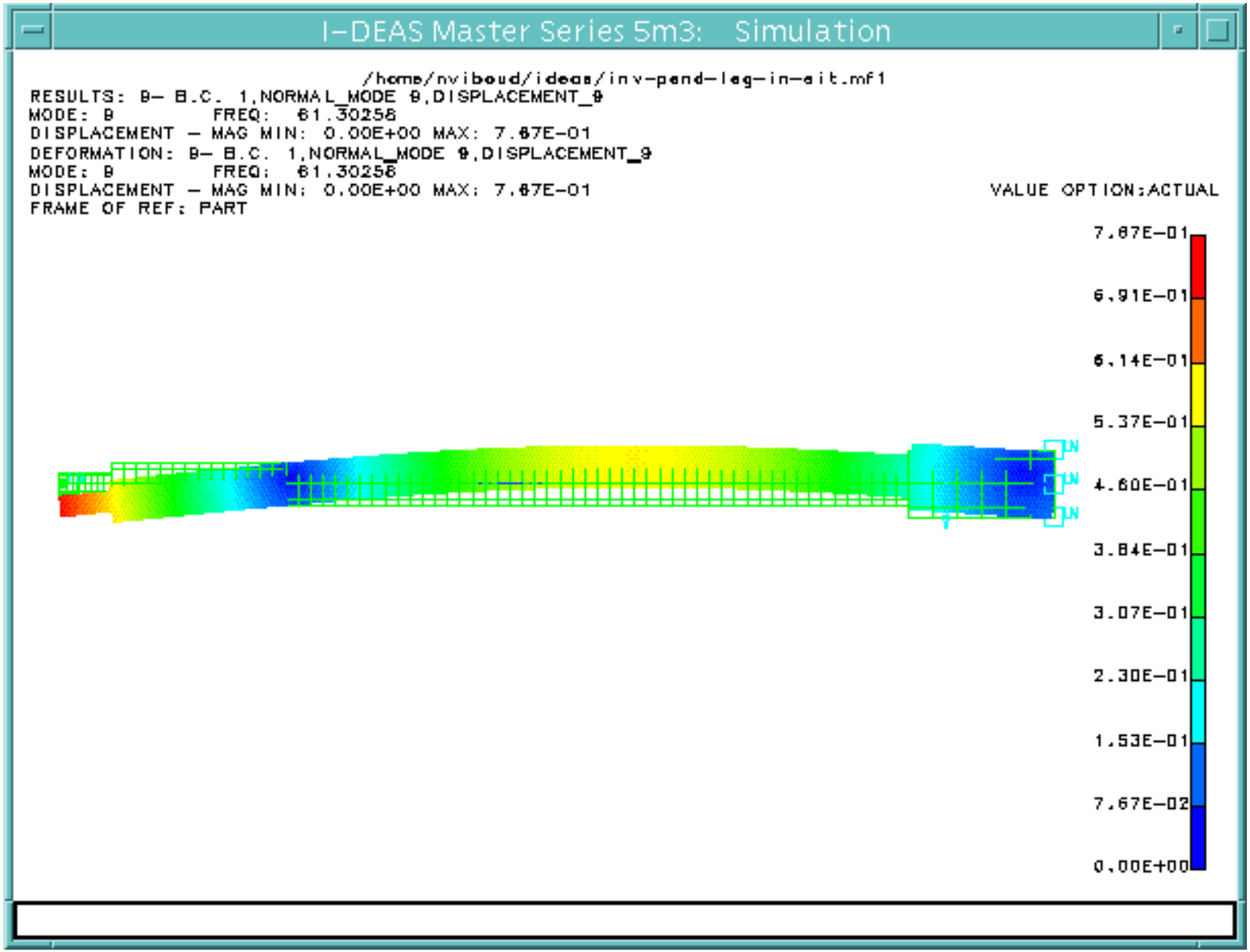
I-DEAS Master Series 5m3: Simulation
/home/nvibeud/ideas/inv-pend-leg-in-ait.mf1
RESULTS: B- B.C. 1,NORMAL_MODE 9,DISPLACEMENT_9
MODE: 9 FREQ: 61.30258
DISPLACEMENT - MAG MIN: 0.00E+00 MAX: 7.67E-01
DEFORMATION: B- B.C. 1,NORMAL_MODE 9,DISPLACEMENT_9
MODE: 9 FREQ: 61.30258
DISPLACEMENT - MAG MIN: 0.00E+00 MAX: 7.67E-01
FRAME OF REF: PART
VALUE OPTION:ACTUAL
7.67E-01
6.91E-01
6.14E-01
5.37E-01
4.60E-01
3.84E-01
3.07E-01
2.30E-01
1.53E-01
7.67E-02
0.00E+00

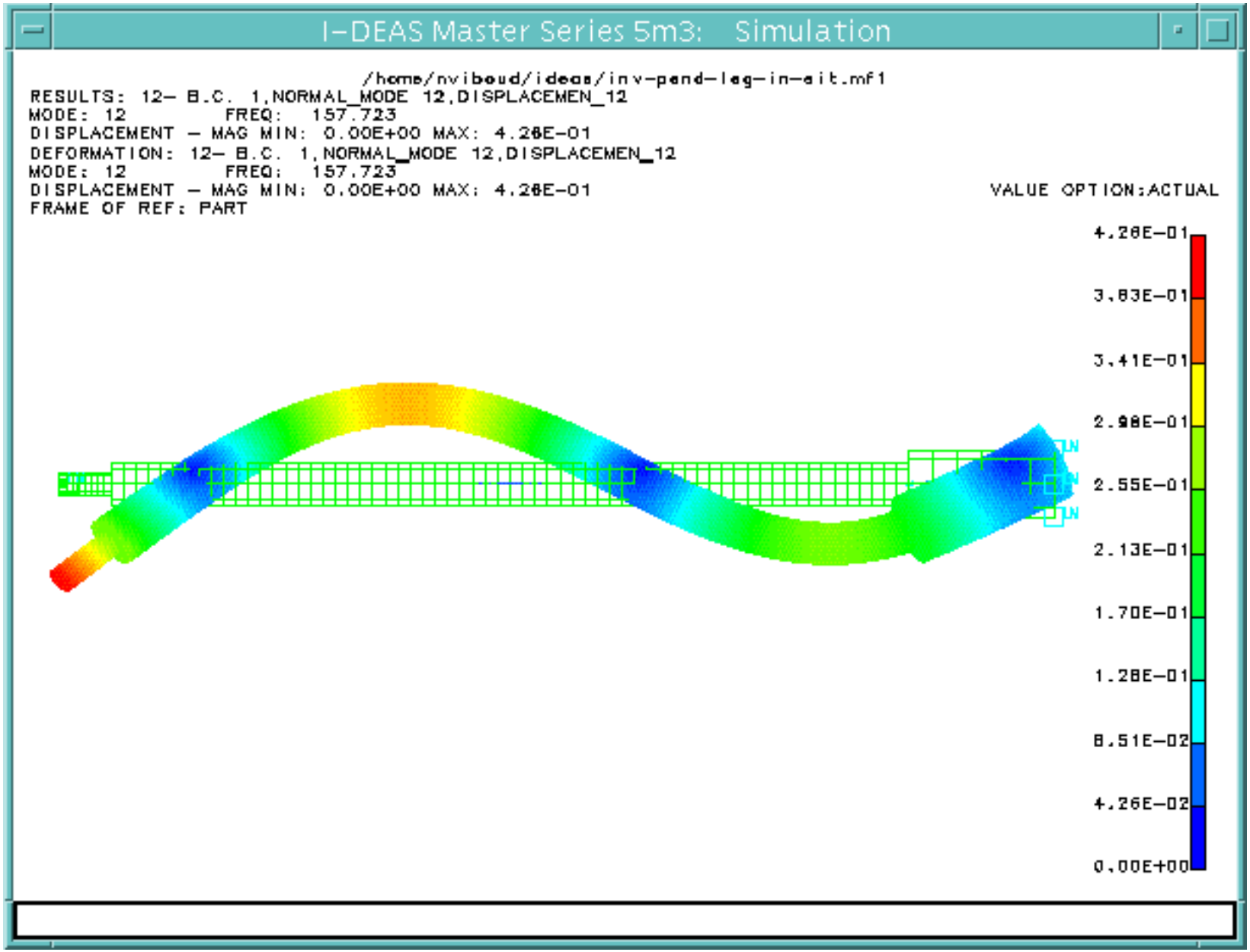
I-DEAS Master Series 5m3: Simulation
/home/nvibeud/ideas/inv-pend-leg-in-ait.mf1
RESULTS: 12- B.C. 1,NORMAL_MODE 12,DISPLACEMEN_12
MODE: 12 FREQ: 157.723
DISPLACEMENT - MAG MIN: 0.00E+00 MAX: 4.26E-01
DEFORMATION: 12- B.C. 1,NORMAL_MODE 12,DISPLACEMEN_12
MODE: 12 FREQ: 157.723
DISPLACEMENT - MAG MIN: 0.00E+00 MAX: 4.26E-01
FRAME OF REF: PART
VALUE OPTION:ACTUAL
4.26E-01
3.83E-01
3.41E-01
2.98E-01
2.55E-01
2.13E-01
1.70E-01
1.28E-01
8.51E-02
4.26E-02
0.00E+00

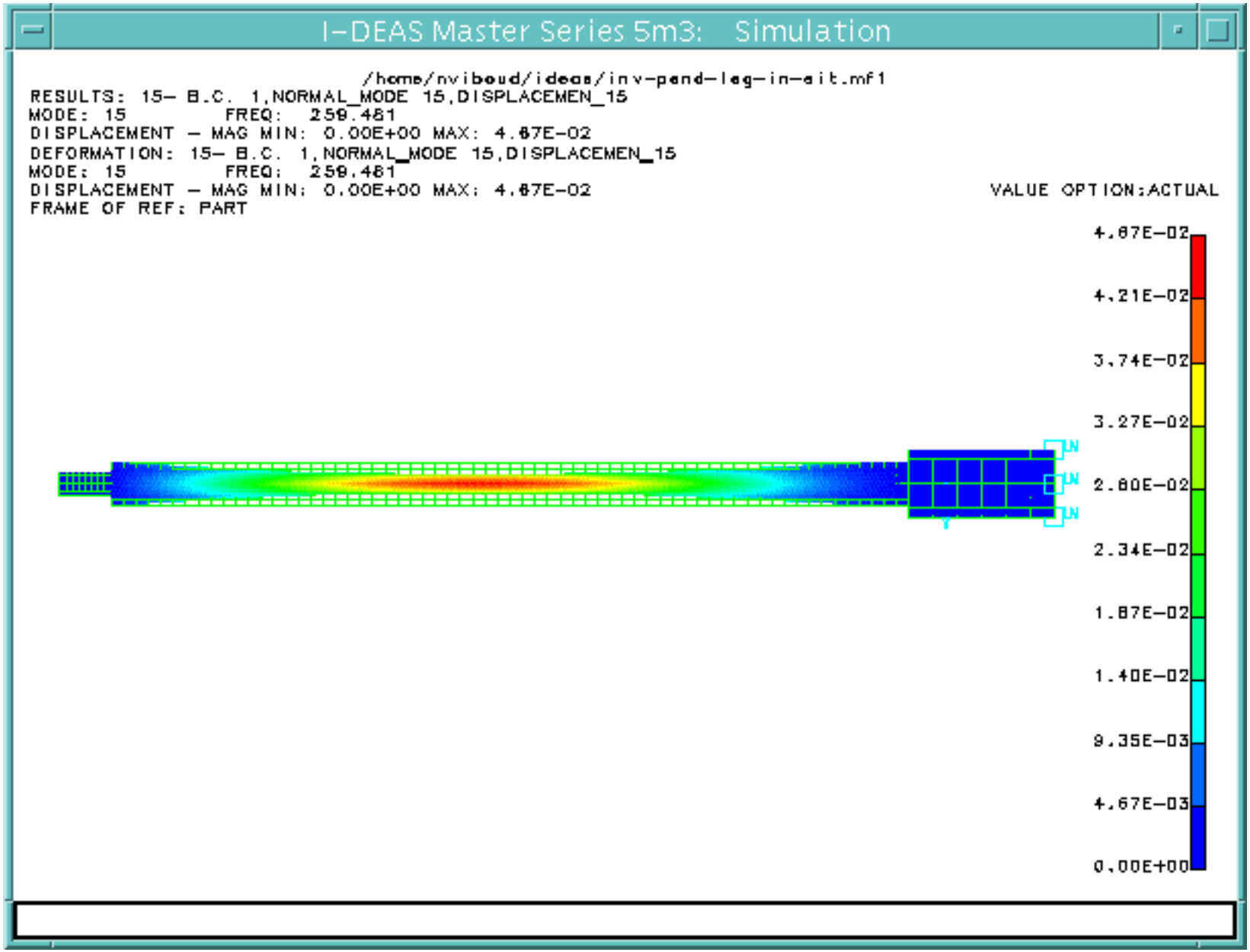
I-DEAS Master Series 5m3: Simulation
/home/nvibeud/ideas/inv-pend-leg-in-ait.mf1
RESULTS: 15- B.C. 1,NORMAL_MODE 15,DISPLACEMEN_15
MODE: 15 FREQ: 259.481
DISPLACEMENT - MAG MIN: 0.00E+00 MAX: 4.67E-02
DEFORMATION: 15- B.C. 1,NORMAL_MODE 15,DISPLACEMEN_15
MODE: 15 FREQ: 259.481
DISPLACEMENT - MAG MIN: 0.00E+00 MAX: 4.67E-02
FRAME OF REF: PART
VALUE OPTION:ACTUAL
4.67E-02
4.21E-02
3.74E-02
3.27E-02
2.80E-02
2.34E-02
1.87E-02
1.40E-02
9.35E-03
4.67E-03
0.00E+00

2.8 Measurements

Once the inverted pendulum leg was built, we measured its resonant frequencies to check the Finite Element model's predicitions. We first suspended it to a crane with a long rope and stuck accelerometers onto the leg. We were looking at the power spectrum at the output of the accelerometer. The excitation was done by banging the leg with a hammer. This experiment did not give us very clear results. Therefore we chose to use a better excitation setup.

We mounted the leg on its flex joint (see picture 2.2) and used a loud speaker supported by the surrounding safety structure, and connected to the leg via a rod (see picture 2.4). The source was the swept sine output of the Spectrum Analyser that we were already using for its FFT capabilities. We obtained better results, the only small drawback being the resonances of the safety structure.

Figure 2.2: Inverted pendulum leg surrounded by the safety structure.

Figure 2.3: Flex joints.

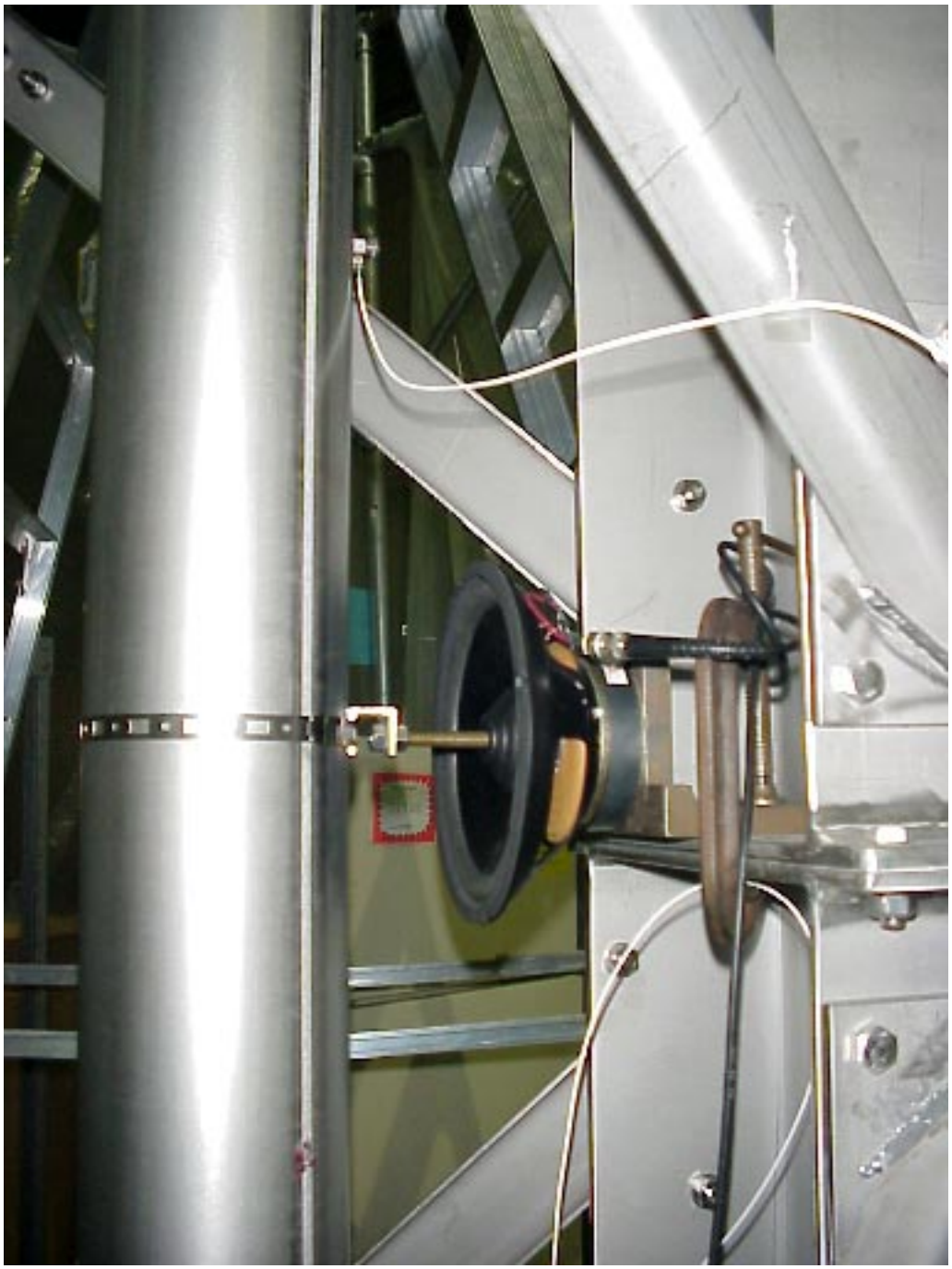

Figure 2.4: Loud speaker used to excite the leg, and accelerometer.

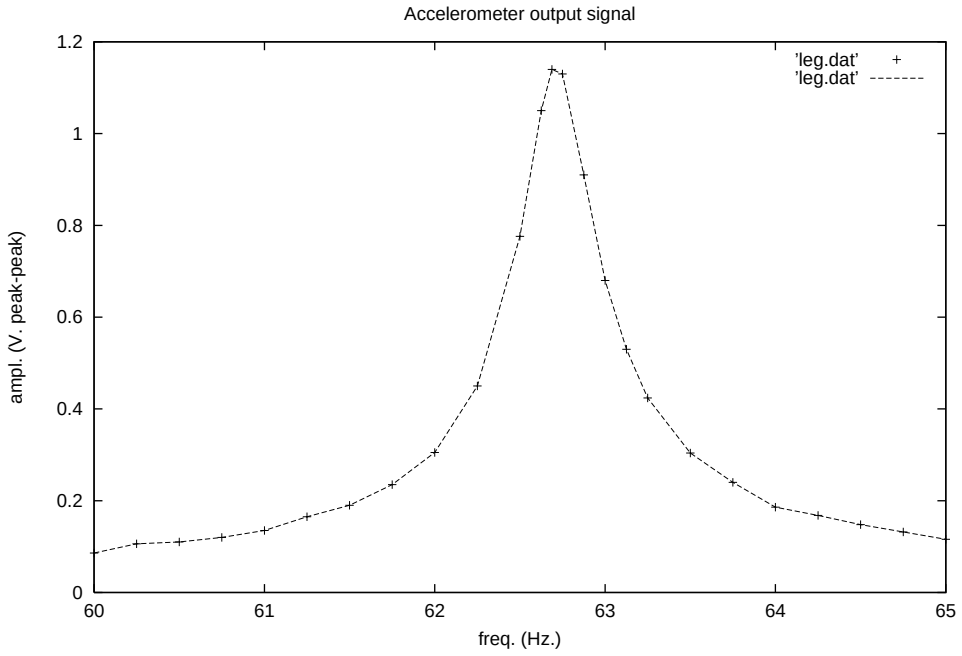

Figure 2.5: Measured data, leg first resonant mode, 62.7 Hz.

2.8.1 First mode

Beginning the frequency sweep from 0.1 Hz. we first came across the 'pendulum' oscillations at about 2 Hz. The next resonance we found was the first internal mode of the leg, at 62.7 Hz (see Figure 2.8.1). We could feel with our fingers the amplitude varying along the leg and we found two nodes, at 226cm from the bottom and about 75 cm from the top. Another proof for the identification of this mode was the increase in its frequency when we removed the counterweight (it shifted from 62.7 to 70.5 Hz.)

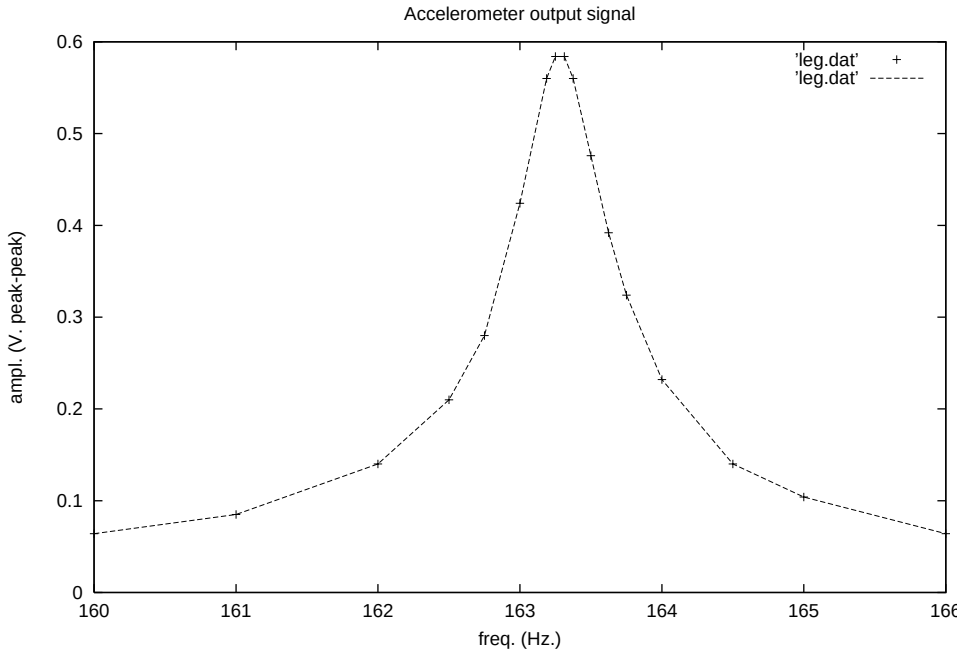

Figure 2.6: Measured data, leg second resonant mode, 163.3 Hz.

2.8.2 Second mode

The next resonance we found was at 163.3 Hz (see Figure 2.8.2). Here also we could feel with our fingers the amplitude variations along the leg and we found three nodes, at 26cm and 127cm from the bottom and about 75 cm from the top. We also found a smaller peak at 145 Hz . This mode is double, because the leg tube doesn't have a perfect cylindrical geometry. There is a welding along the leg. The excitation was done at 139 cm from the bottom, which is a bit too close from the middle node to excite correctly this mode. And the angle between the welding and the actuation axis perhaps gave a bad excitation to the 145 Hz mode and a better excitation to the 163.3 Hz mode. The mean frequency of these twin modes is 154 Hz.

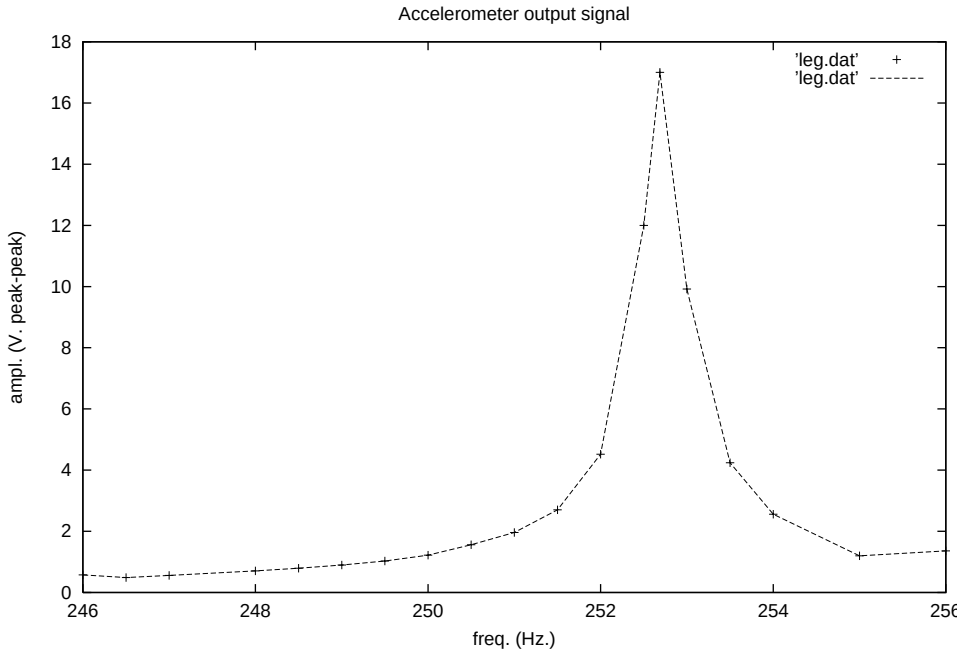

Figure 2.7: Measured data, leg third resonant mode, 252.7 Hz.

2.8.3 Third mode

The next resonance we found was at 220 Hz, but it was a resonance of the safety structure used to hang the actuactor. The next internal mode was found at 252.7 Hz (see Figure 2.8.3). We could feel with our fingers that only the main tube of the leg was moving, the counterweight and its bell did not vibrate. And the washers/flanges at the ends of the tube did not vibrate, so we identified the previously named 'squeeze' mode. Rotating about the leg's axis, we could feel the amplitude variations expected from a quadrupolar movement. Furthermore, putting our finger along certain vertical lines did not affect the output of the accelerometer, whereas putting it on a vibrating spot damped the vibration and reduced the signal's amplitude on the screen.

This mode also is probably double. With this measurement setup we did not see very well the 245 Hz resonance, probably because of the orientation of the excitation axis with respect to the welding. But we had seen it very sharp when we were banging the suspended leg with a hammer. Assuming that 245 Hz is the second occurence of the 'squeeze' mode, we find a mean frequency of 249 Hz.

2.8.4 Fourth and fifth modes

The fourth mode, where there is a node at half length of the tube, with quadrupole movements that occur with opposite phase in each half of the tube, was found at 268.5 and 272 Hz, which makes a mean frequency of 270 Hz.

The fifth mode, a kind of banana with three nodes, was found at 319 Hz.

2.8.5 Comparison between measurements and predicitions

Mode #	1	1bis	2	2bis	3	4	5
Calculated freq. (Hz)	58	63.9	132	173	259.5	275	311
Measured freq. (Hz)	62.7	60	154	?	249	270	319
Error (%)	12	6	17	?	4	2	3

1 bis was mesured with the leg suspended to the crane.

2 bis is computed without the flex joint, we have no valid data at that frequency for the leg suspended to the crane.

The larger error on the banana and s mode (see columns 1 and 2) may be caused by the inaccurate modelling of the flex joint (which has not impact on the tube-squeeze modes, 3 and 4).

Note that the frequencies shown in this table may be a bit different from those you can see in the screen copies of the beginning of this report, because of the removal of the small top cylinder (used to connect the filter zero to the leg).

2.9 Conclusion

It may be required to shift the first internal resonance above 100Hz, instead of 40Hz (the 60 Hz banana mode should decrease when we hang the filter 0 on top of the pendulum). This frequency shift can be done with a larger pipe diameter to increase the 'banana-mode' frequency. The tradeoff will be a lowered 'squeeze-mode' frequency. If necessary a stiffener ring can easily be added inside the leg. We did not alter the geometry of this prototype, because filter 0 was already built and could not accomodate larger leg diameters.

The finite element model used here gave good predictions of the leg's resonant frequencies.

The leg we modelled is a prototype, commonly referred as the 'test tower'. Later on, other different legs may be designed, for example with a greater length to accomodate more stages in the vertical filter chain.

Of course diameter, length changes and stiffener additions can be simulated with this finite element model. It is a re-useable tool to design inverted pendulum legs.

Chapter 3

Blade-tip built-in flex joint for the filters

3.1 Introduction

This chapter discusses a possible change to the current filter design (see 3.1). This change would be to suppress the connecting links that exist between the blade tips and the central disk. The blade tips would fit directly onto the disk, via an integrated flex joint that would be built in the thickness of the blade (see 3.2). It would improve the filter by reducing the number of parts, suppressing the rotational resonance of the central disk, etc... The point of this chapter is to simulate the new configuration to determine whether it is feasible or not.

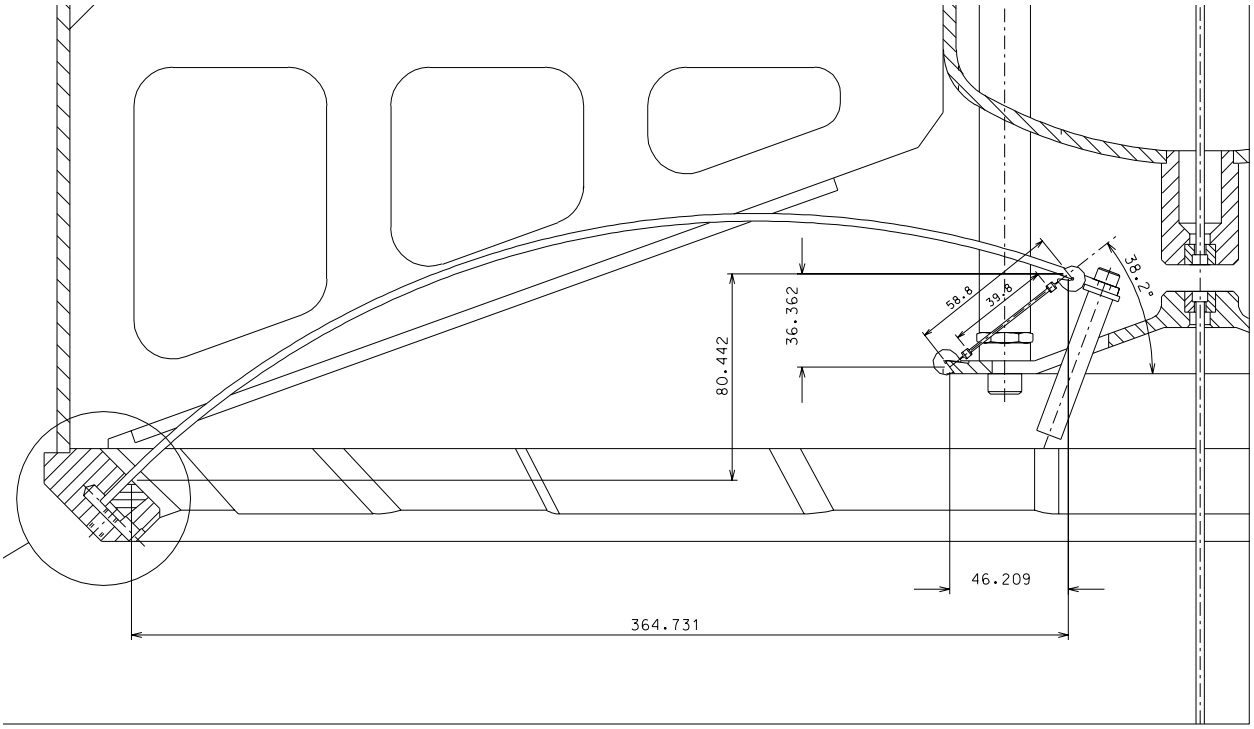

Figure 3.1: "classic" filter with Geometric Anti Springs (GAS)

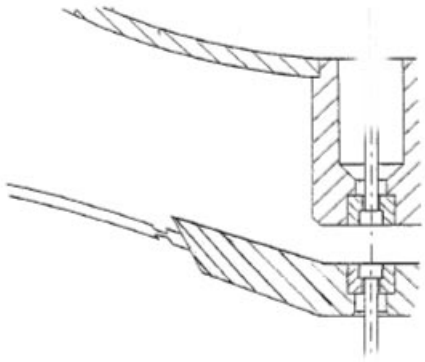

Figure 3.2: "wireless" filter with blade built-in flex joints

3.2 Design of the flex joint

Starting from the idea previously explained, one has now to define the geometry of the flex-joint. As shown on 3.1 it is a part that works in compression. Therefore has one not only to look at the stress but also has to be aware of the buckling problem. A long and narrow flex joint would be really flexible, and therefore would not undergo much stress, but it would buckle. A compromise has to be found. The optimization problem can be described this way: "Knowing the compression force and the range of angles the flex joint will be bent, find a geometry that fits inside the blade thickness, minimizes the stress, and operates below the buckling load". Once the optimum solution is found (i.e. the minimum stress obtained), one has to compare the stress to the material's limit to say whether it will work or break.

3.3 Initial geometry

An arbitrary geometry was designed to be used as a starting point. It is shown on 3.3.

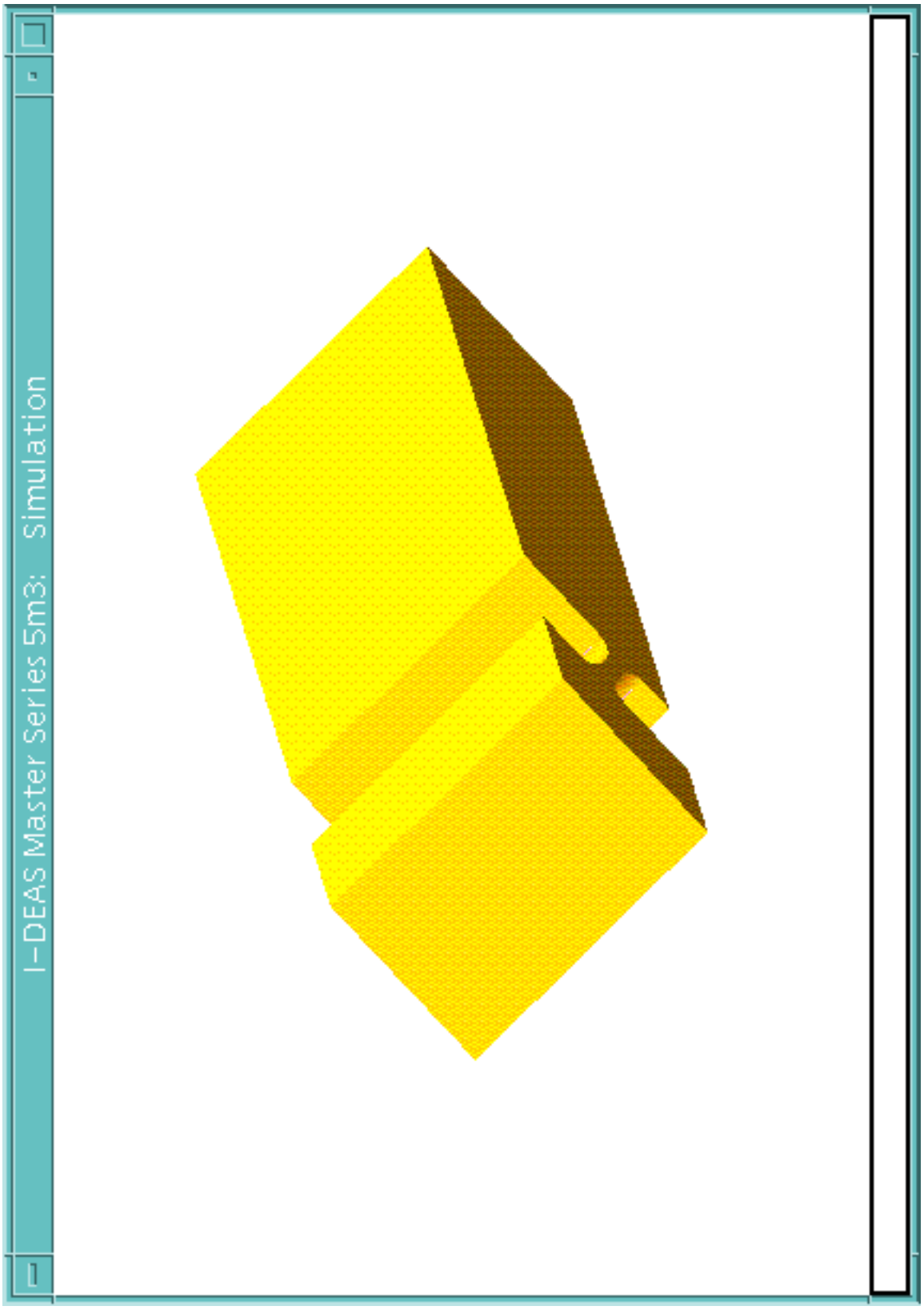

Figure 3.3: blade-tip built-in flex joint, initial geometry

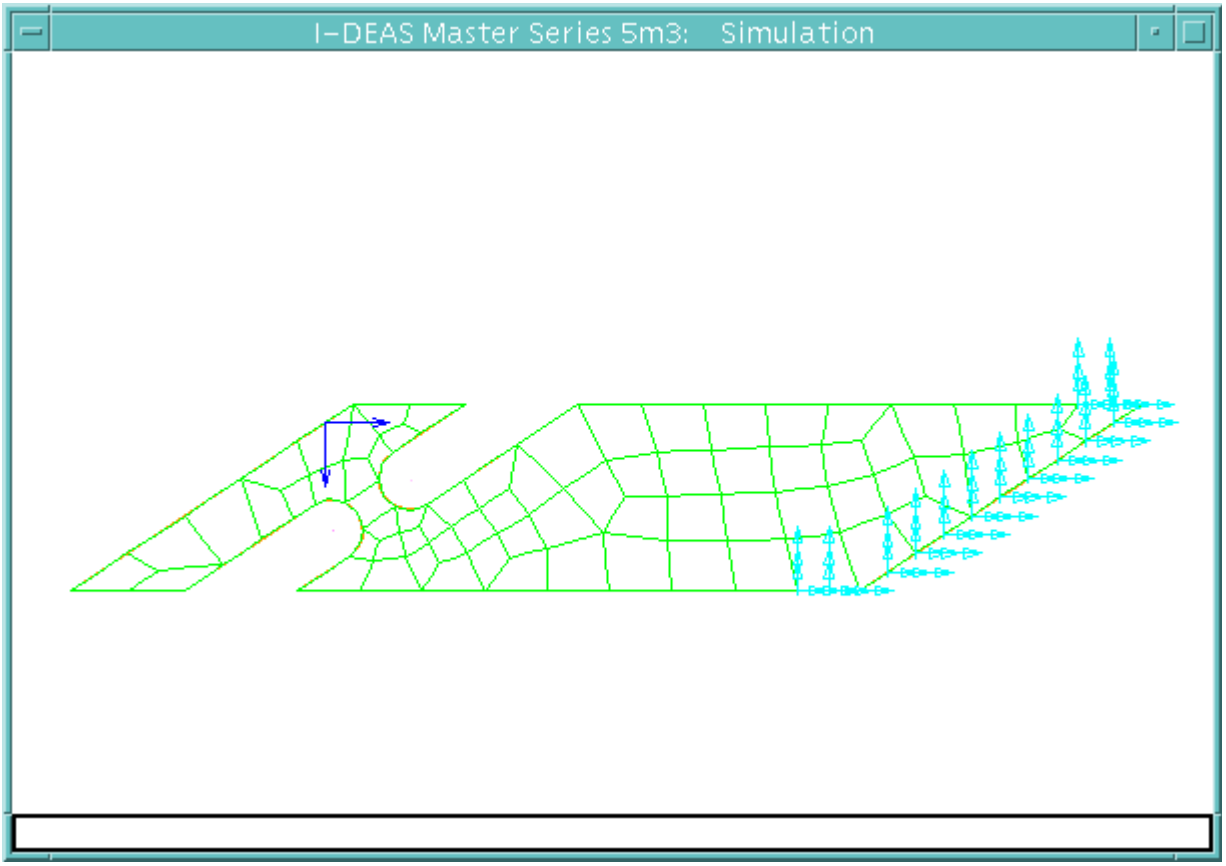

Figure 3.4: coarse mesh (side view of the blade tip)

3.3.1 Mesh

Only the tip of the blade was modelled. The problem was simulated as a plane-stress problem, using type '45 - plane stress parabolic quadrilateral' elements. 8 nodes/elements , 2 translational dofs/node

Automatic free mesh was used, it used 256 nodes and 69 elements.

It can be seen on 3.4 that the mesh is really coarse. Later on it was refined (see 3.5) in order to improve the energy error norm and get a detailed insight of the narrow area.

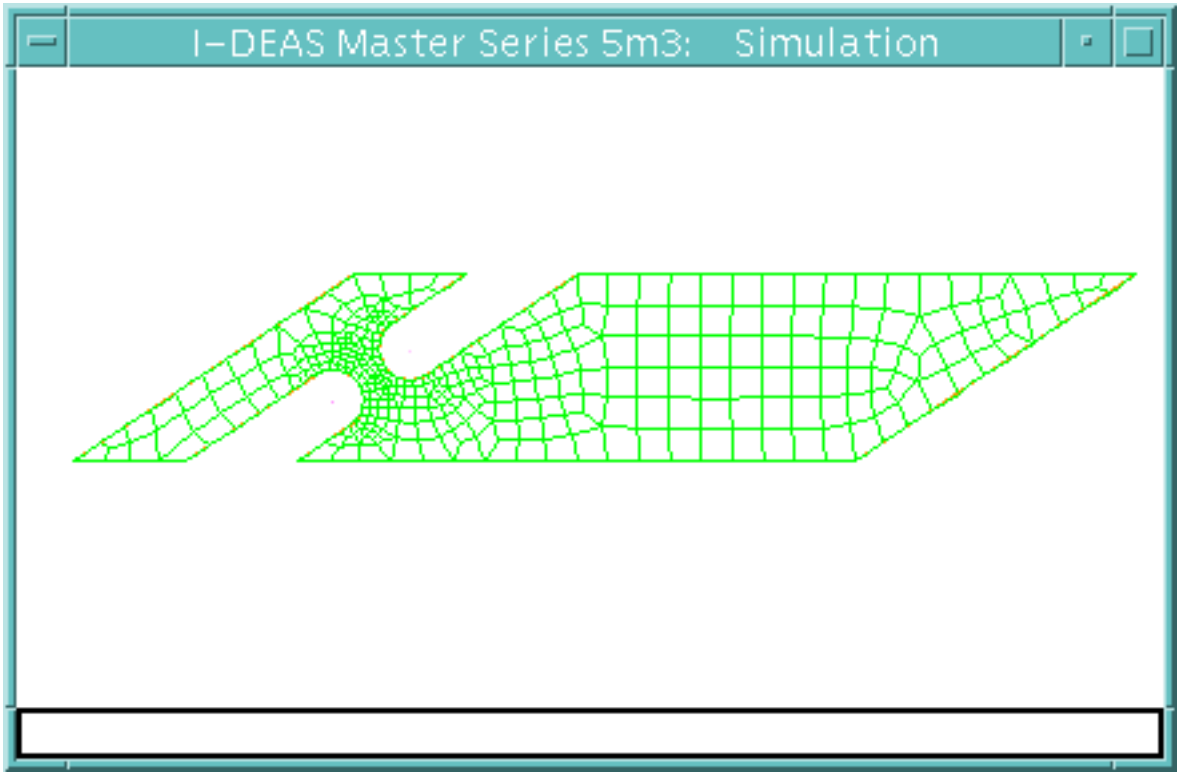

Figure 3.5: fine mesh with low element distortion

3.3.2 Boundary conditions

Since only the tip of the blade was modelled, we clamped the side where the blade was "cut" and we put the compression force on the contact surface, where the disc would sit. It can be seen on 3.4.

The contact force (1170N) was simulated by a point force, and was put on a node as aligned with the flex joint as possible (however it was not a perfect alignment).

Later on we will bend the joint by sliding the force along the surface, away from the alignment. We chose $+or-$ 3^o as a maximum bending angle.

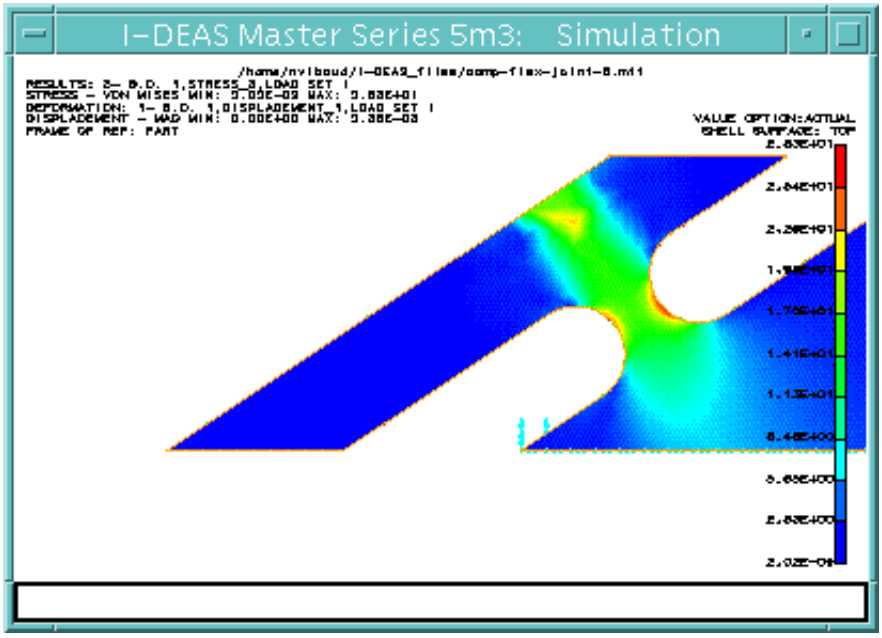

Figure 3.6: stress distribution at 0^o (S.I. units)

3.3.3 Results for the initial geometry

The model is linear geometrically, therefore the bending angle had to be manually computed from the translational displacements.

The first geometry, with the improved mesh gave a maximum stress of 28 kgf/mm2 at 0^o and 408 kgf/mm2 at 3^o. It is shown on picture 3.6 at 0^o and on picture 3.7 at a 2.6^o deflection. The buckling analysis told us that we were at a 16.7x safety factor.

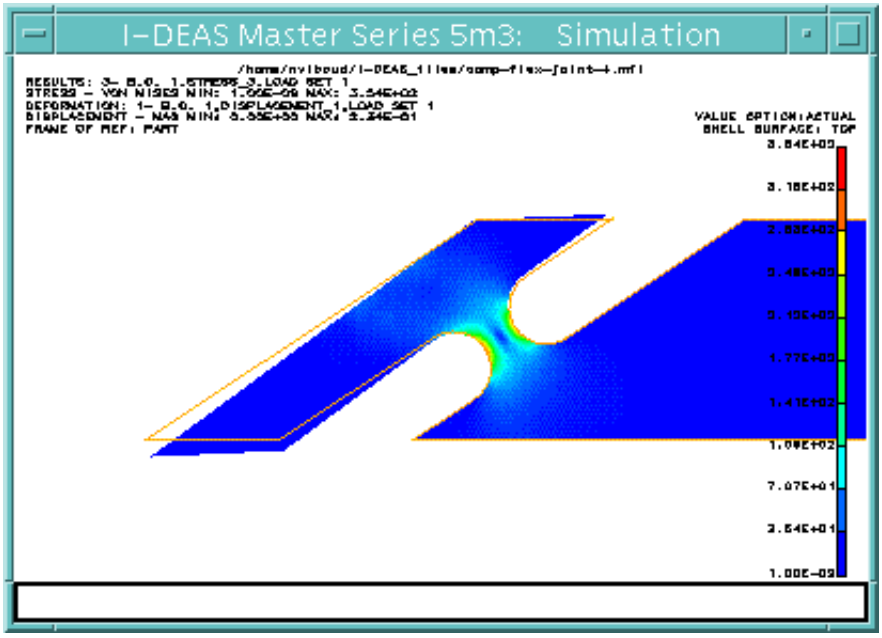

Figure 3.7: stress distribution at 2.6^o (S.I. units)

3.3.4 Conclusion on the first geometry

The stress at 0^o is very low, and it increases too fast when we apply a 3^o bending angle. The buckling limit is very far.

Decreasing the thickness of the joint will:

- increase the stress at 0^o
- decrease the additionnal, bending tension-compression stress
- reduce the buckling safety factor
- decrease the equivalent stiffness of the joint, but we do not worry about it here. It just means that we will have to reduce the applied moment to get the same angle.

Increasing the length of the joint will:

- decrease the equivalent stiffness of the joint
- decrease the part of stress that is due to bending
- not change the stress at 0^o
- reduce the buckling safety factor

We will have to alter these two parameters to improve our geometry.

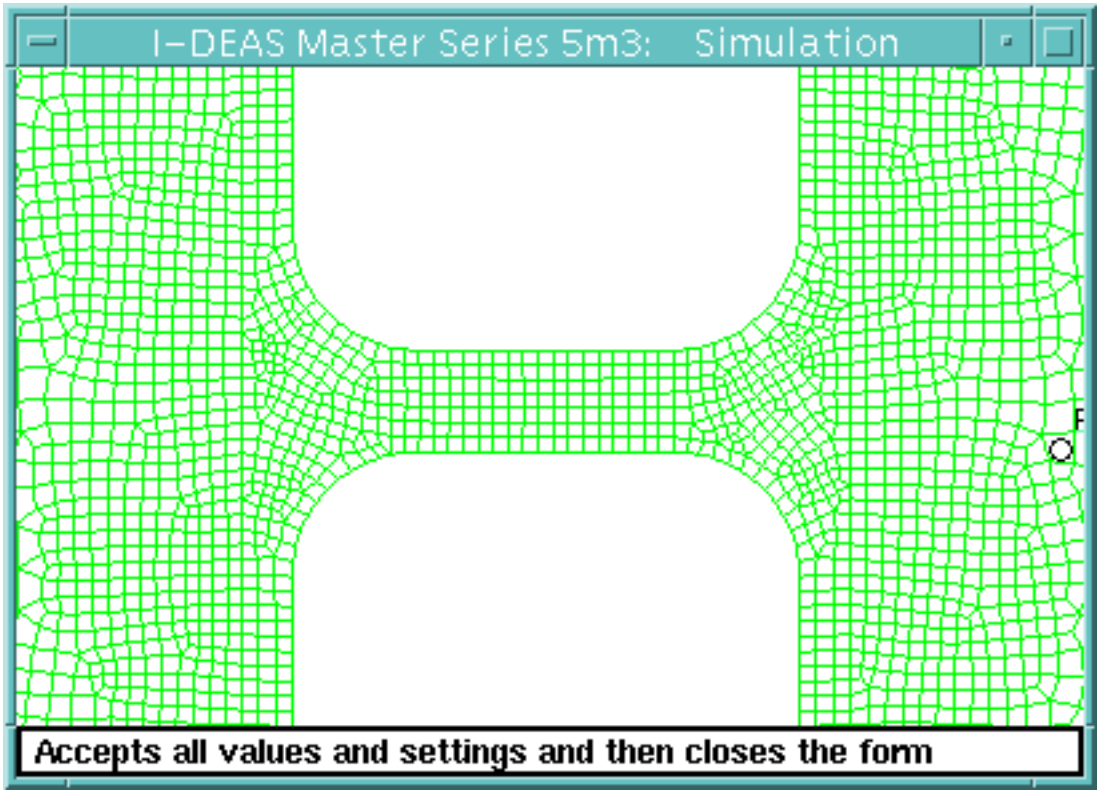

Figure 3.8: New geometry and its mesh

3.4 Improved geometry

A thinner joint was designed, with a 0.2mm thickness a the narrowest point instead of 0.5mm in the previous geometry.

The length (1mm) could not be changed much because we wanted the joint to remain inside the thickness of the blade tip. But we made the effective length greater than before by changing the radius of the roundings. The joint becomes narrow on a greater length.

We made the roundings with a small radius (0.15mm) and with distant centers. Now we have a straight line with a quarter of a circle at each end (see 3.8), whereas before the roundings had the same center, reducing the straight line two zero and joining the two roundings into a half circle profile (see 3.5).

We launched an automatic optimization on the rounding radius with minimizing the stress as a goal. At each iteration, the software changed the radius, updated automatically the mesh, an computed the stress. The optimal radius we obtained from this was 0.25mm, a value which was kept in the following.

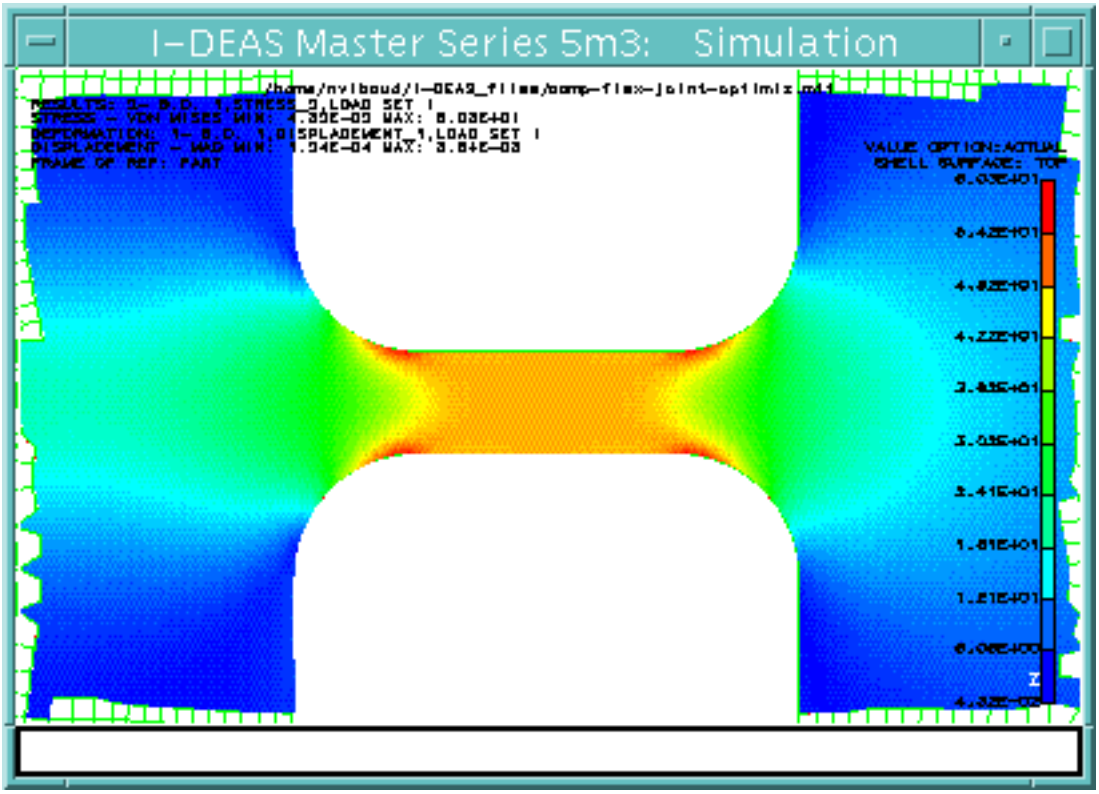

Figure 3.9: stress distribution at 0^o (S.I. units)

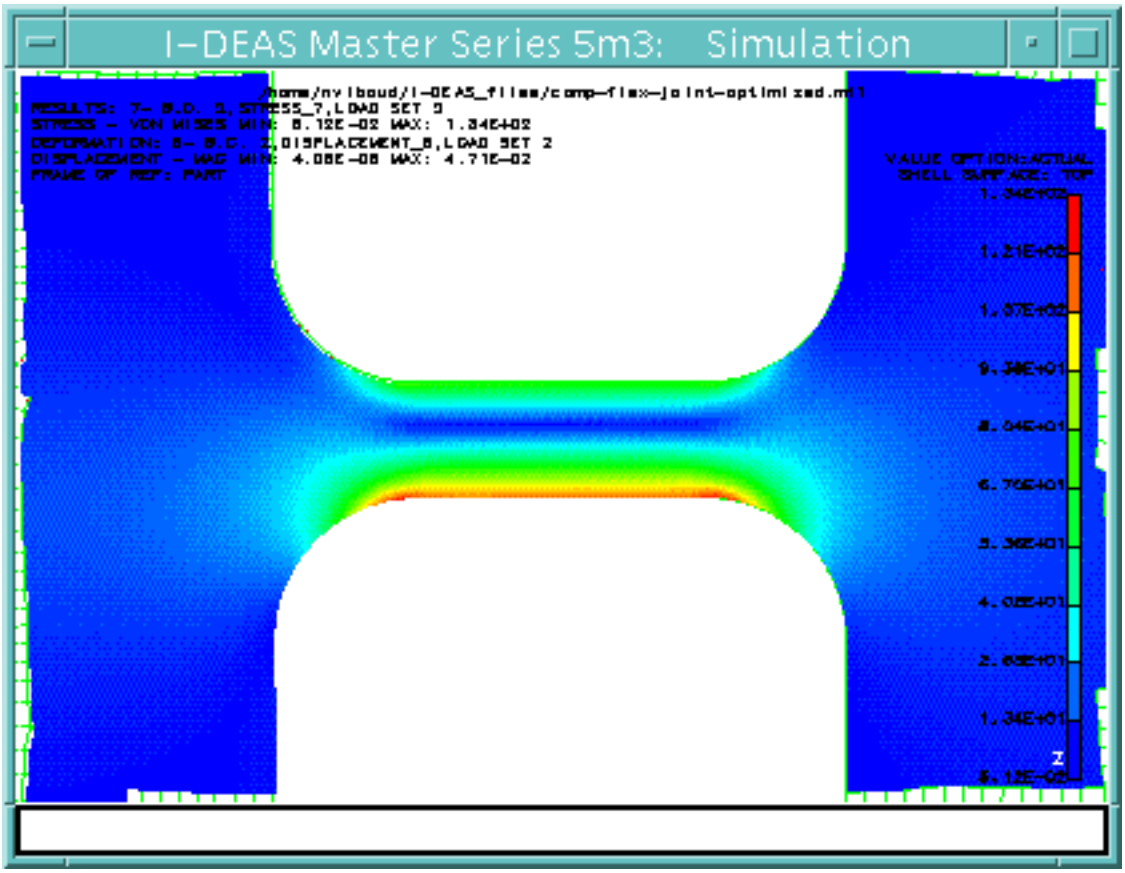

Figure 3.10: stress distribution at 1.7^o (S.I. units)

The stress at 0^o is shown on picture 3.9, the value goes up to 50kgf/mm2. On picture 3.10 it is shown at a 1.7^o bending angle. And at 2.5^o we obtained a stress of 169kgf/mm2. So for the nominal 3^o we would get about 190 kgf/mm2 (which is about the stress limit for maraging steel). It is an improvement compared to the previous geometry (408 kgf/mm2). Also the buckling analysis gave us a too small safety factor: 1.12x.

Therefore we can say that this geometry is our optimum solution. Decreasing again the thickness or making the joint longer would bring us to the buckling limit. But this optimum solution is not acceptable, because of the stress levels we reach (to avoid creep it is necessary to remain under 140 kgf/mm2 for maraging).

Chapter 4

Clamped-Clamped blades

4.1 Introduction

As shown previously, we did not manage to design flex joints that would fit inside the thickness of the blade. Therefore we had to try another solution for a wireless filter. We might have been able to find a solution for the flex joints if we had accepted to add a part to our system instead of remaining in the thickness of the blade (see 4.1).

Rather than trying this option we chose another principle. The idea is to clamp the blade not only at its root, but also at its tip, on the central disk. The blade will be clamped at its natural position, the nominal position it has on the GAS filter with links. This forces the blade tip to keep its nominal orientation and radial position.

When the blade moves up or down, away from its nominal position, the blade tip will only translate along the vertical axis. All of the 5 others degrees of freedom will remain fixed. For example, the slope of the tip will not change, whereas on the GAS filters it is allowed to change. It is likely that it will increase the stress of the blade, but the stress increase can probably be designed by modulating the blade transversal profile.

The purpose of the following is first to address this stress issue, and later to study more generally the properties/performances/stiffness etc... of such a clamped-clamped filter.

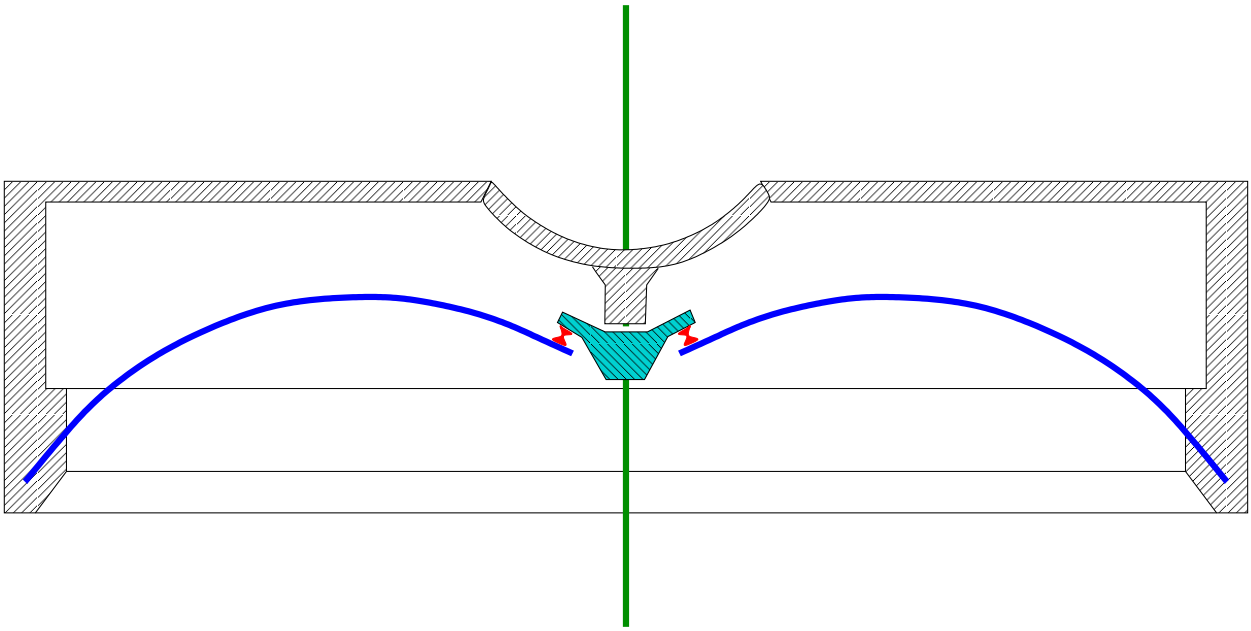

Figure 4.1: sketch of a filter featruing external flex joints

4.2 Geometry

We will study only half of a single blade, using symmetry properties to reduce the size of the Finite Element model.

We used the straight, unloaded geometry of the blade (see 4.2). A plane profile was created in the solid modeller. We could not hook a mesh on this bidimensionnal geometry until we transformed it into a (thin) prismatic volume.

4.3 Mesh

The semi-automatic mapped meshing process was used (see 4.2). Type '95 - thin shell parabolic quadrilateral' elements were used (8 nodes, 6 dof/node). Near the tip of the blade, where the curved profile ends, a triangular element was added manually (type '92 - thin shell parabolic triangle' element with 6 nodes, 6 dof/node).

A simplified link was connected to the tip of the blade. It was modelled by a type '11 - rod' element (2 nodes) which transmits only translations (3 dof/node).

The model has 650 nodes, 3900 d.o.f., 189 elements.

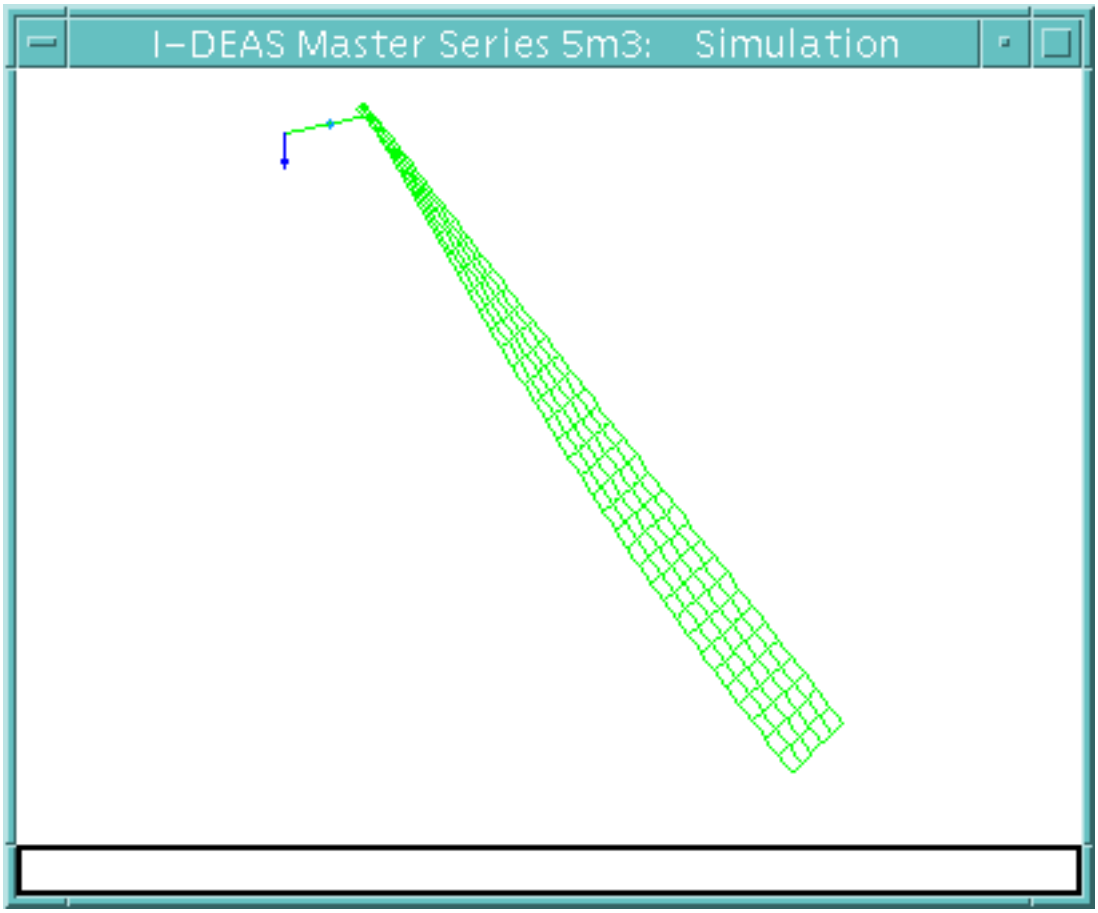

Figure 4.2: Unloaded half-blade and its mesh.

4.4 Boundary Conditions

The root of the blade was clamped (all degrees of freedom restrained to zero). The half-width line was restrained so that only symmetrical displacements were allowed: no lateral translation, no rotation about the longitudinal axis (half-width line).

A the beginning, a vertical force corresponding to the payload was put at the end of the link/rod, where the central disk would normally be. This was done in order to calculate the nominal position of the GAS filters.

After having solved this first problem, the obtained diplacements were recorded for future re-use. Later on the force at the end of the link was suppressed. The boundary condition on the tip was changed from force to displacement. To simulate the clamping, the previously recorded displacements were used as restraints for the tip. We translated them vertically by various amounts up and down, in order to explore the vertical dynamic range.

4.5 Solver

The filter blade is a system with geometric non linearities. The stressed blade undergoes a deflection of about 60^o at its tip. Therefore it cannot be solved by linear, small-displacement solvers.

The static non-linear solver of I-DEAS offers limited possibilities. For example it is not allowed to choose displacements boundary conditions that would stress the structure. And even with a loading expressed in terms of a force, we came across convergence difficulties. Therefore we switched to the ANSYS 5.5.3 solver. Once built with I-DEAS, the finite element model was exported to be solved by ANSYS [1].

The algorithm chosen was "Full Newton-Raphson". The loading of the structure is applied in a progressive way, with loading substeps. For each substep, equilibrium iterations are performed in order to converge (i.e. reduce the force unbalance in the model). And before each equilibrium iteration, the stiffness matrix of the blade is refreshed according to the current geometry.

During the process, the solver is able to refine automatically the substeps to avoid divergence (step cutback) or improve the convergence speed (step increase).

For the first problem to solve, a first try was made with 1/6 substeps as an user input. It led to a cutback (1/15), which worked but later proved to be an unnecessarily high number of substeps: a substep increase (1/10) eventually corrected it. The following times we launched the solving process, we put 1/10 for the initial substep size, which seemed to be the optimal value, at least for the first half of the loading process.

[1] Provided by the Laboratoire de Mecanique des Structures (LMSt)

4.6 Simulation results

4.6.1 Stress

The solution for the nominal position of the GAS filter is shown on figure 4.3. Our calculations give a smaller deflexion than what we measured (the blade tip is too high) but we did not investigate further because we were interested in variations. The results when we clamp the tip, and move away from the nominal position are shown on figures 4.4 and 4.5. Note that on these last two figures the link is still shown but has no functionnality.

What we first saw was that the stress underwent no dramatical change. We feared that clamping all the degrees of freedom would overconstraint the blade tip when we move it away from the nominal position. It is not the case. The curvature of the blade changes, and the point where the stress is maximum is moved along the blade, but the change in the maximum's value is small and acceptable.

At this point we decided to build quickly a prototype.

4.6.2 Stiffness and vertical resonant frequency

As it was said earlier, we computed several vertical positions, and got the vertical force for each of them. With the ratio of the force difference and the height difference we get the vertical stiffness of the filter around its nominal position. We can also translate the vertical force into a corresponding loadcarrying capacity (payload mass). At the end we can compute the vertical resonant frequency of the oscillator. We obtained 2.2Hz, which was much higher than the 450mHz we had measured for the GAS filter we based our geometry on. The difference was of a factor 4.4 in frequency and 19 in stiffness. At this point we were worried about getting a system that would not break (as explained in 4.6.1 the stress did not increase) but that would be too stiff for the purpose of seismic isolation. We thought that we would be able to decrease the stiffness by compressing a bit more more the blades, to increase their curvature. Having a prototype helped us a lot to address this issue.

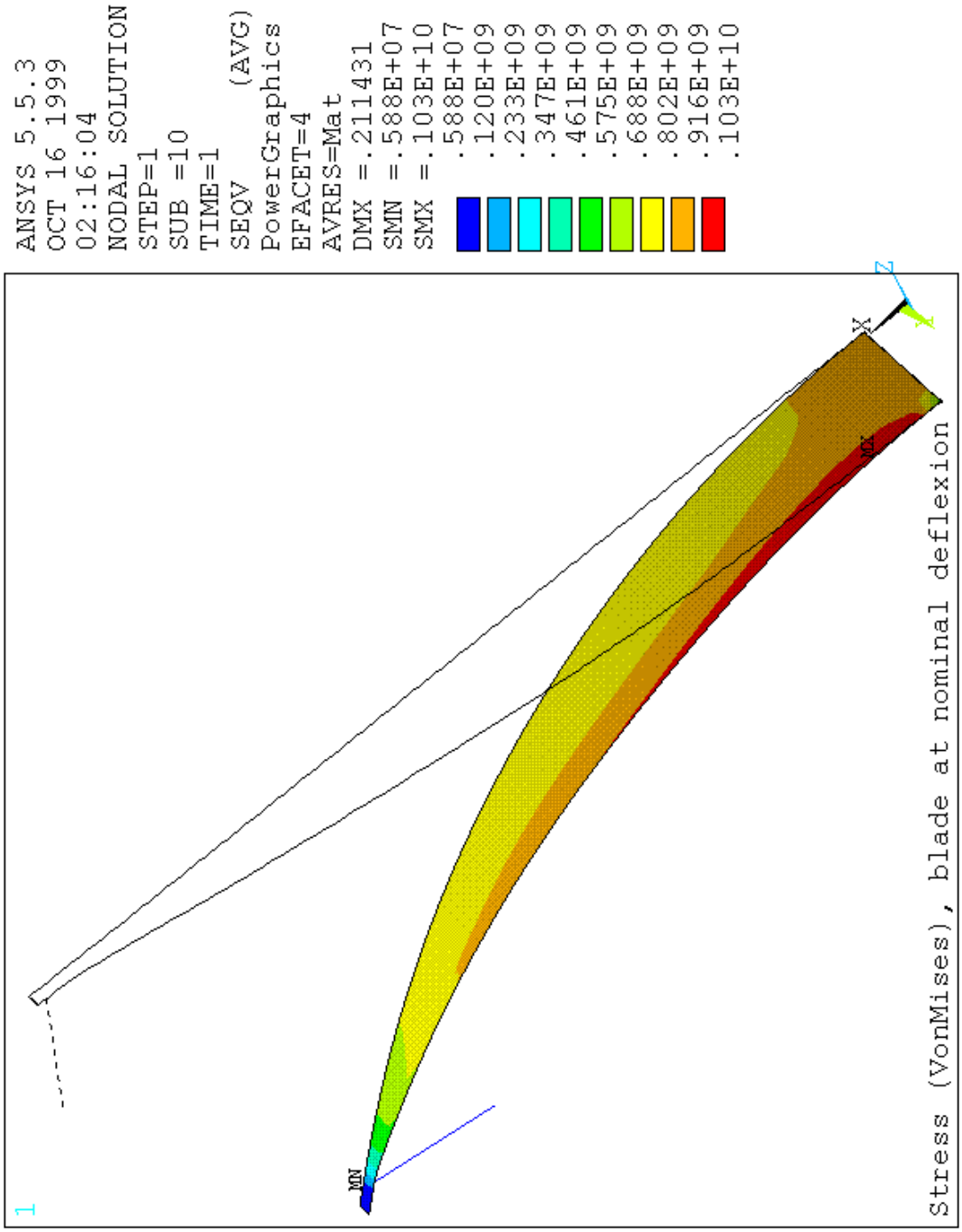

Figure 4.3: ANSYS stres output, nominal position (=GAS nominal position)

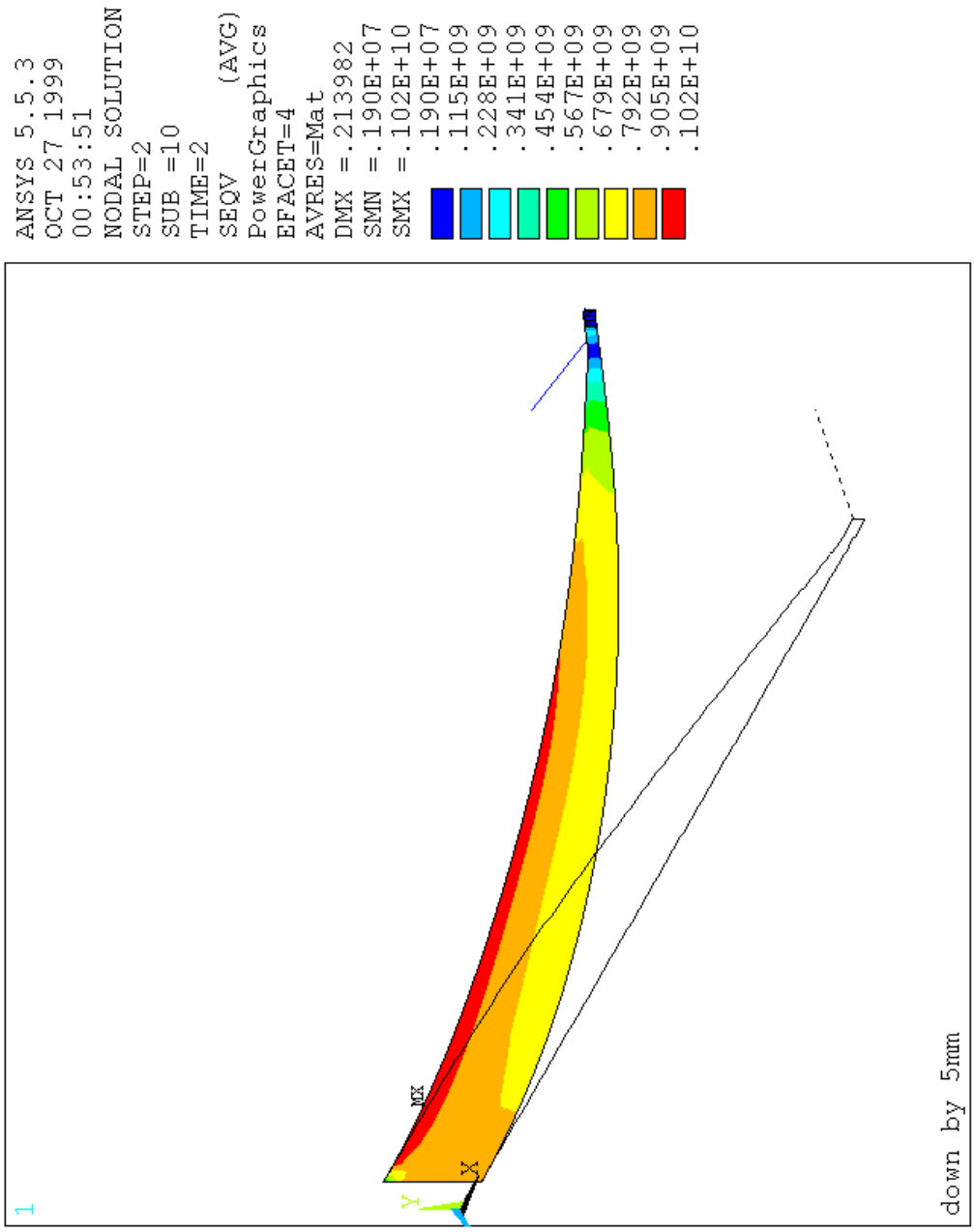

Figure 4.4: ANSYS stress output, down by 5mm

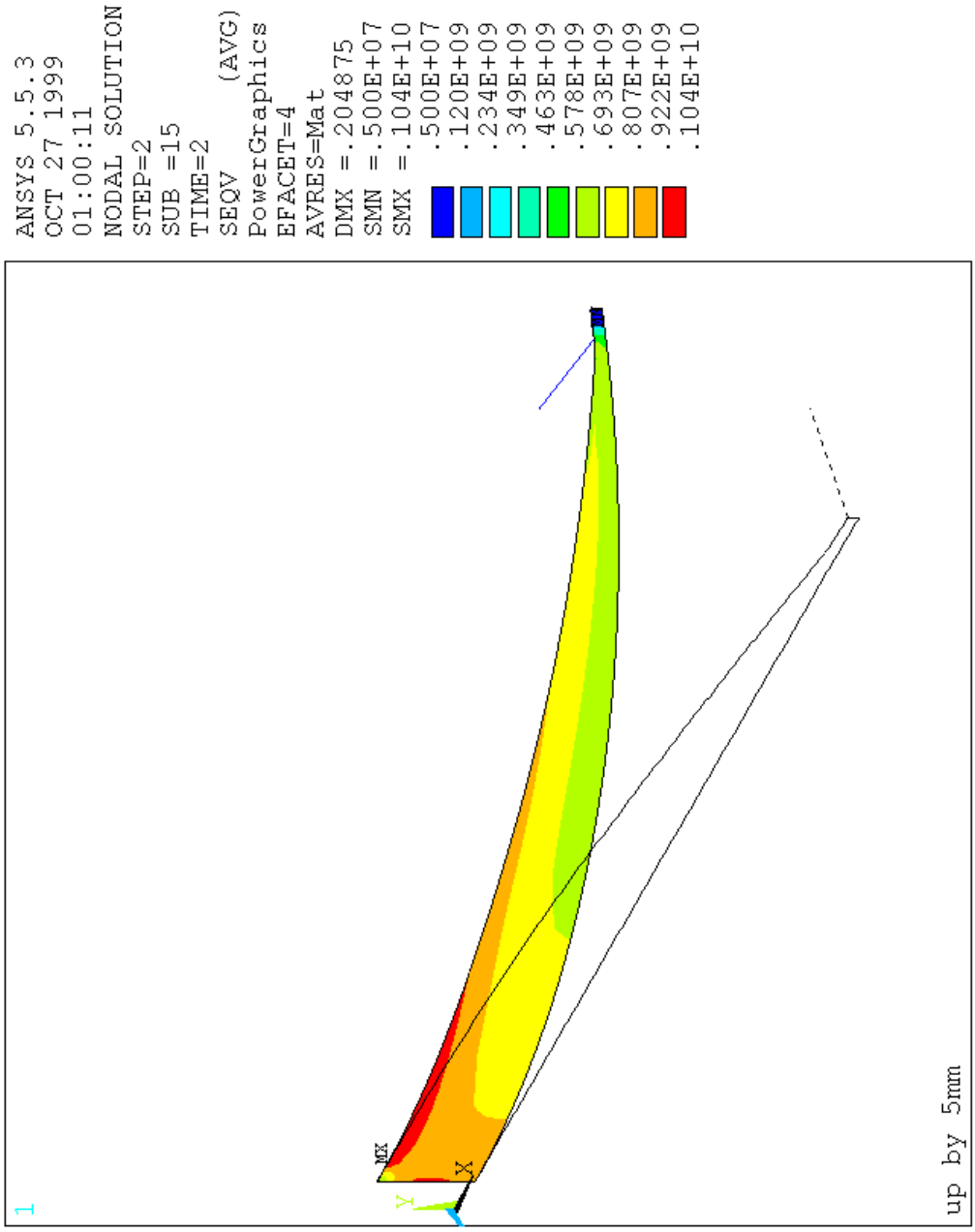

Figure 4.5: ANSYS stress output, up by 5mm

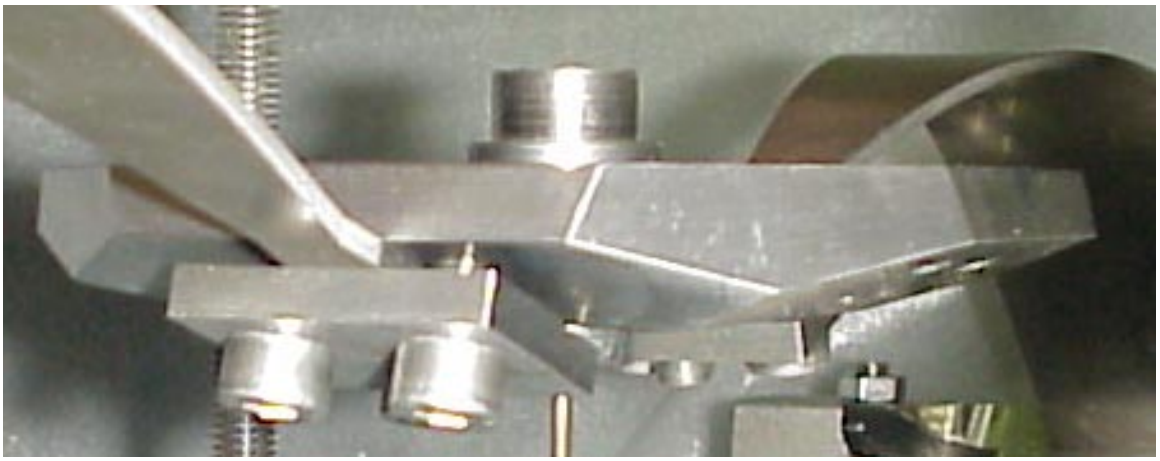

Figure 4.6: Central Block

4.7 Prototype

4.7.1 Description

We started machining a central block that would be able to clamp the four blades and hold the payload. (see fig 4.6) We almost "molded it" on the GAS filter, in the sense that we used its angles and blade-tip distances. It was designed to use the pre-existing GAS blades too, rather than designing new blades at this time of the developpment. Compared to GAS filters, we changed just the minimum number of parts. We changed the central structure and nothing more, therefore we can make easy comparisons, and we are sure where the performance differences come from.

The prototype was made of unistrap rails, and offered possibilities in adjusting the blades distances for example, which is not possible in the usual filter frames (see 4.7).

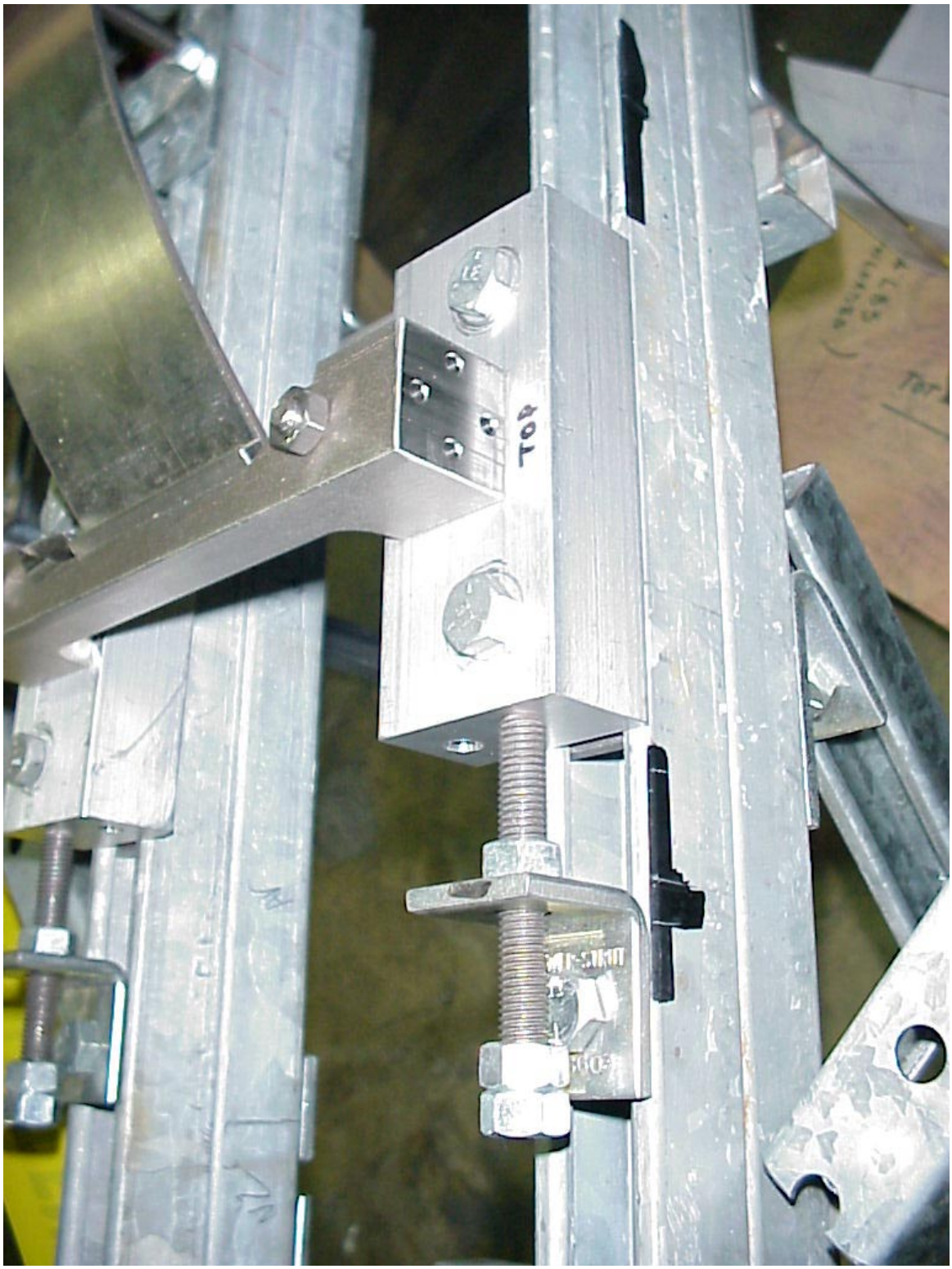

Figure 4.7: Screws for adjustment of the blade compression

4.7.2 Assembly of the prototype

When we first assembled the prototype, the settings and distances were adjusted in order to copy as much as possible the geometry of the GAS filter. We bent the blades on bending tools (figure 4.8 and 4.9), clamped them on the unistrap structure, and then bolted the central block on the blade tips. Next we put a spacer on top of the central block, touching the upper wooden safety plate, so that we could keep the blades bent while we were releasing the bending tools. Once the force was transferred to the safety plate, we hung the payload structure to the central block and began loading it with lead bricks. We kept loading until the safety plate was fully unloaded.

Figure 4.8: Assembly time, bending the blade

Figure 4.9: Assembly time, strap to keep the blade bent

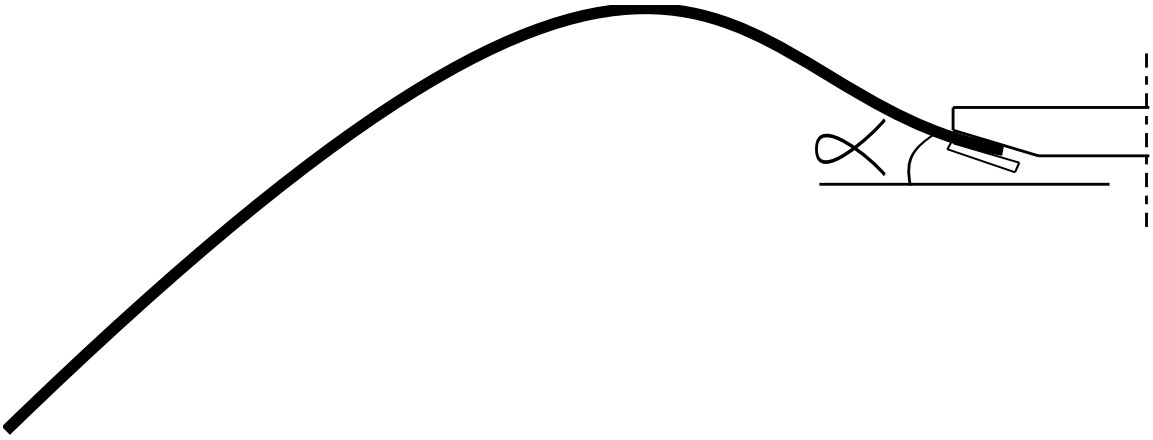

Figure 4.10: Curvature inversion due to too small clamping angle α

4.8 Experiments on the prototype

4.8.1 First results

What we first saw was that the vertical resonant frequency of the filter was higher than for the GAS filter, but not as high as what was expected from the calculations. We obtained 1.3Hz rather than 2.2Hz. But then we realized that we could get lower frequencies by lowering the working point (bringing the nominal position down by loading the filter a bit more). It means that the minimum resonant frequency on the clamped-clamped filter occurs at a lower height setting than what we had for the GAS filter. At this point we stopped respecting the GAS filter's geometry.

It was necessary to bring down the working point by such a distance that on the central block, the blade clamping angles did not fit anymore. The clamping angle was originally designed for a higher working point, and it needed to be increased for a low working point.

Without the central block redesign, we would have gotten a curvature curvature inversion (see 4.10).

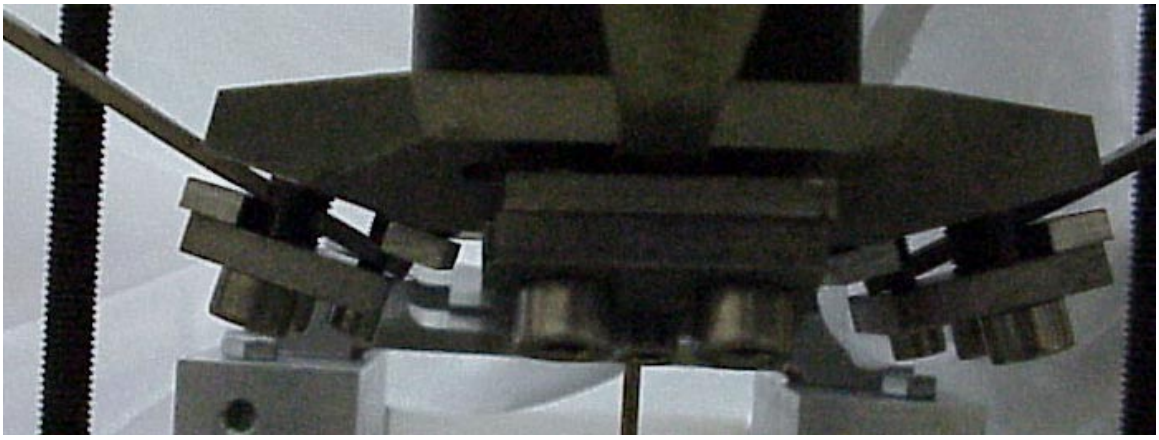

Figure 4.11: Shims to change the clamping angle

4.8.2 Geometry modifications

On this prototype we changed the angle by adding two shims to the blade tips (see 4.11). This solution was not good mechanically, and the shims were only paralelepipeds, not even wedges. But this way we avoided to machine another central block, which would have been too much time and money for such a rough prototype. Furthermore we were not sure by how much we had to change the angle.

We tried two thicknesses of shims, the first try being not enough. We eventually chose quite thick shims, changing the angle from 18^o to about 33^o.

Apart from this geometrical change, we also had to increase the blade curvature. We had to bring the blades roots closer to each other, using the adjustment screws of the unistrap structure (figure 4.7).

4.8.3 Results for the prototype

We measured mainly two properties of the filter. The first one was the relation between vertical resonant frequency (VRF) and height tuning. We excited the filter vertically giving it an impulsion by hand and then measured the oscillating frequency by clocking a certain number of oscillations with a stopwatch. Then we changed the height of the equilibrium position by removing or adding lead bricks, and measured again the frequency. The second property was measured in the same time, we simply wrote down for each position what was the height and its corresponding payload. This gave us the load vs. height curve. We remind the reader that our filter is a nonlinear spring, and we work in a domain where it is very soft. Therefore it holds about 200kg, but we did the height tunings with lead bricks of only 50g.

Once the VRF and load vs. height curves measured, we changed the blade compression with the adjusting screws of the unistrap structure. The first measurements on the prototype with shims gave us minimums of about 1.33 Hz, and we wanted to explore lower frequency configurations.

The relation between horizontal compression and resonant frequency is nonlinear. The frequency sensitivity to the distance becomes higher and higher as we go towards low frequencies and short distances.

Due to this increasing sensitivity, we easily went to a bistable configuration when we were trying to lower the minimum VRF.

Stepping back after getting this bistable setting, we obtained a minimum of 254mHz. At this point we were dealing with eigth of turns on the screws, we had a poor accuracy with this compression setting device.

The experimental data is shown on figures 4.12, 4.13 and 4.14.

We did not try to obtain monostable configurations lower than 254 mhz.

We also noticed a Q factor decrease as we were lowering the frequency. This is only a qualitative observation, we saw the oscillations damp quicker and quicker, but we did not measure it. It might be wiser to measure the Q factor on a better prototype (to be built), because we suspect we have some losses due to the bad tip-clamping system.

Although this prototype allowed us to go to quite low frequencies, for the last configuration (254 mhz) we had reproductivity problems in our measurements, therefore we did not try lower frequencies. Some height drifts were observed. Since we had a low quality factor, we had to give the system great excitation in order to be able to see several periods. These excursions far away from the working point could offset the system, affecting the reproductivity of our measurements. We are not sure of the explanation for that phenomena, it might be hysteresis caused by excursions in the plastic domain. Another theory was that the system was still bistable, we had two stable positions very close to each other, inside the oscilation's domain, and we were randomly stopping on one or the other, causing reproductivity problems.

This problem may be caused by the bad clamping system and may disappear on the next prototype, otherwise it will have to be addressed.

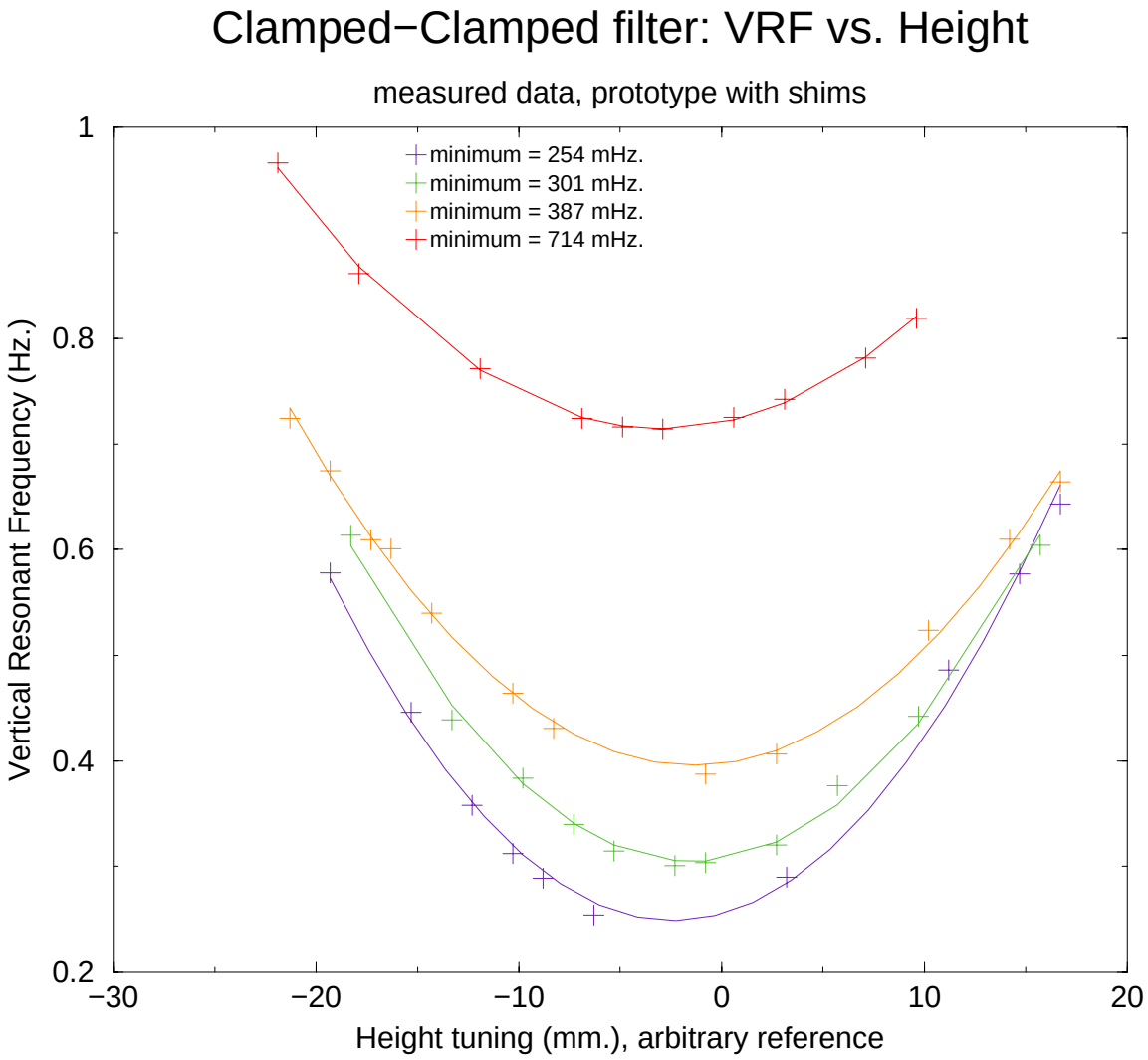

Figure 4.12: Experimental resonant frequencies

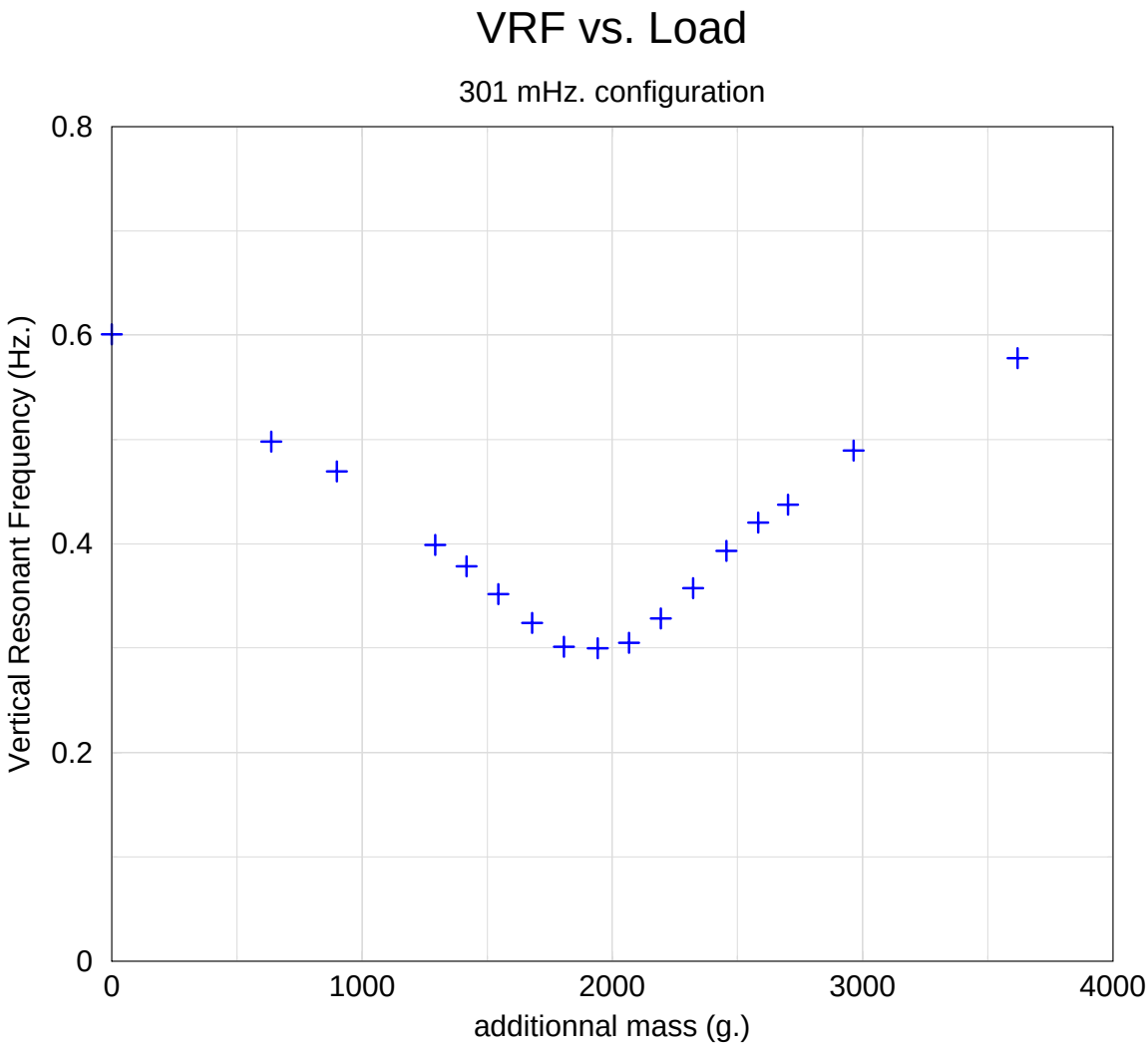

Figure 4.13: Experimental resonant frequencies

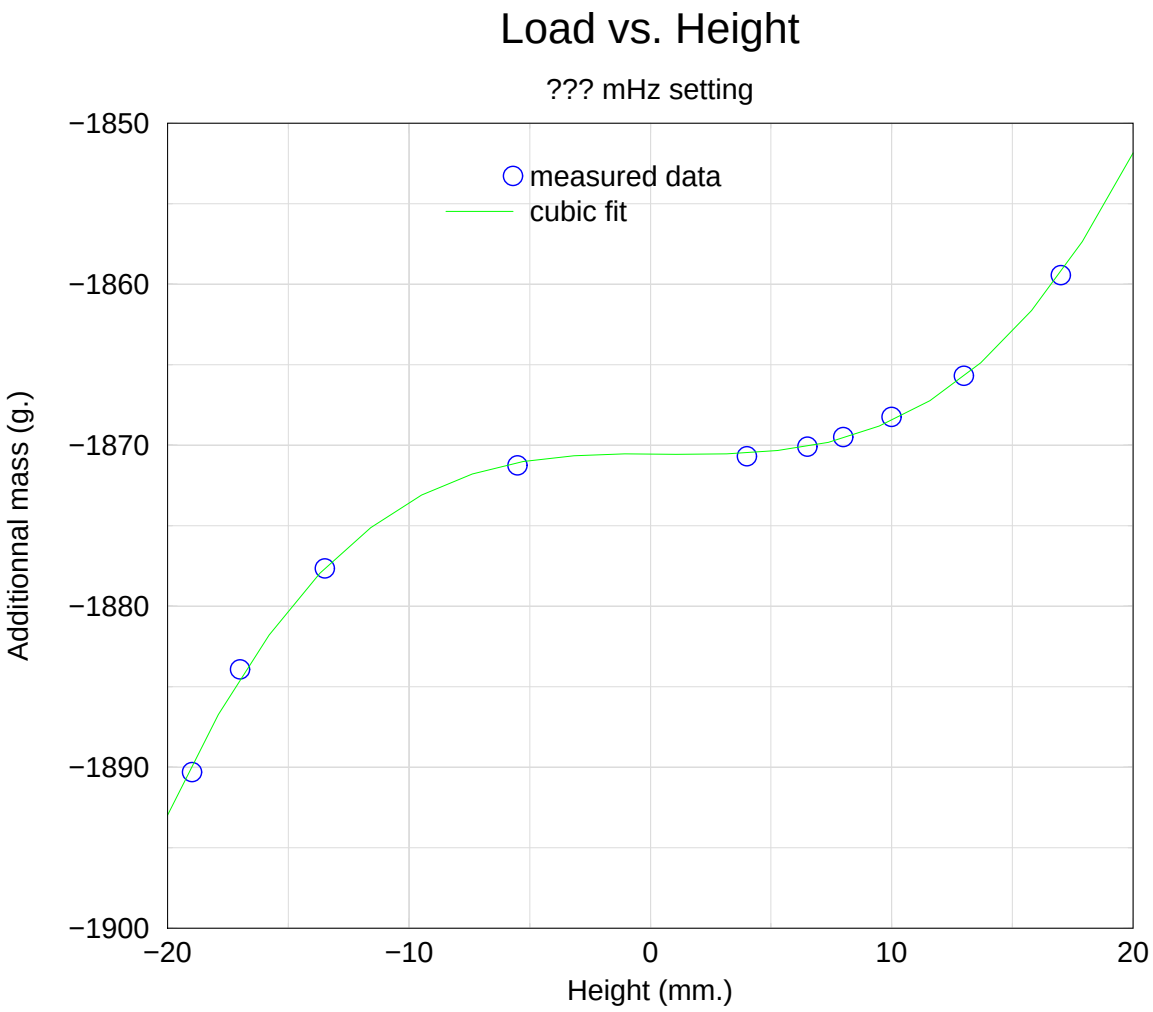

Figure 4.14: Experimental load curve

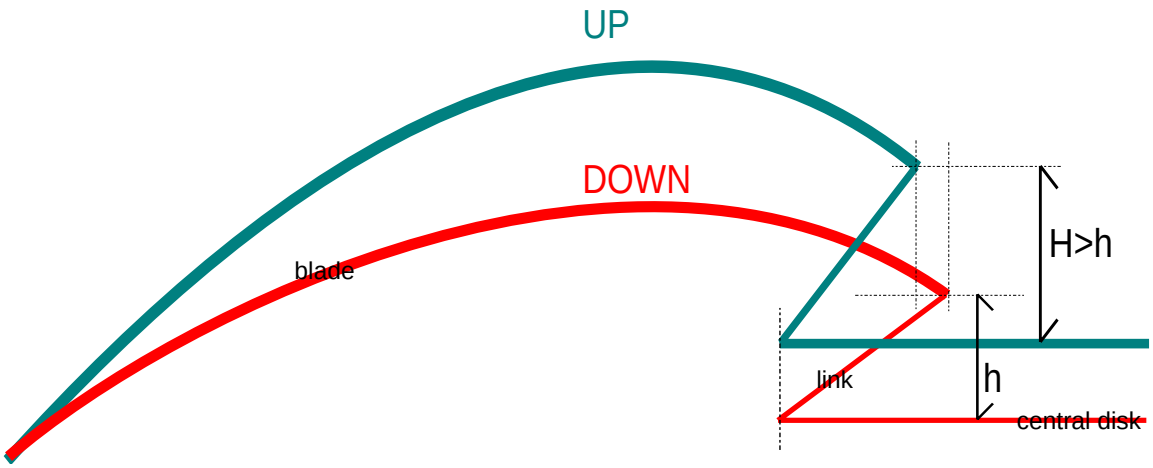

Figure 4.15: Geometric Anti-Springs. When we push the system down, the vertical translation of the blade tip is coupled with an horizontal translation. Since the link cannot vary its length, its angle decreases. The height between the blade tip and the central disk decreases. This is the negative stiffness contribution. The central disk goes down by a lower amount than the blade tip does.

4.9 Comments on the working principle

Obtaining these experimental results from the prototype helped us understand the way the filter works. Before this, we were trying to explain it in the same way we explained the GAS filter. Here it works only with the nonlinearity of the blades, whereas the GAS filter has an additionnal feature to lower the stiffness (figure 4.15).

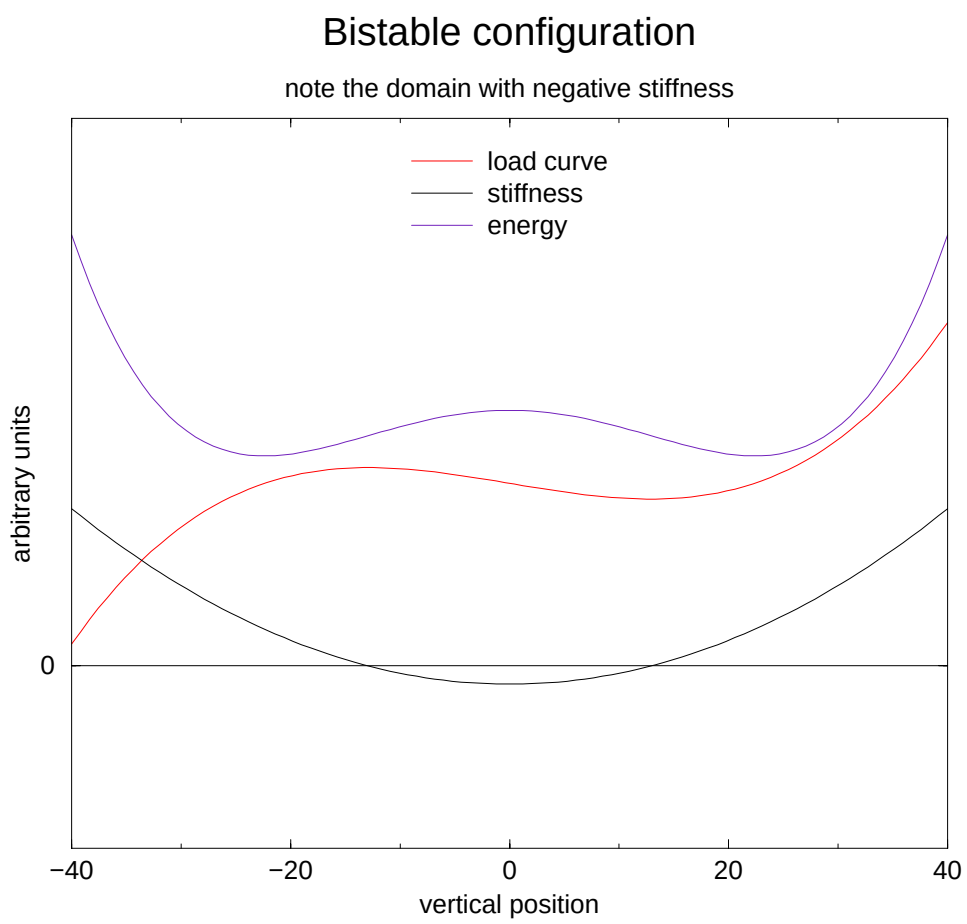

Figure 4.16: T B D

A simple explanation of the wireless filter can be made if we start from a bistable configuration.

We must imagine the filter with the blades highly compressed horizontally, against each other. This way it is quite intuitive that the central block will spontaneously jump up or down rather than staying in a mid-height state. These upper and lower stable positions will give less curvature than any other position in between, they minimize the strain energy contained inside the blades.

Between these two stable positions we get an area with a negative stiffness.

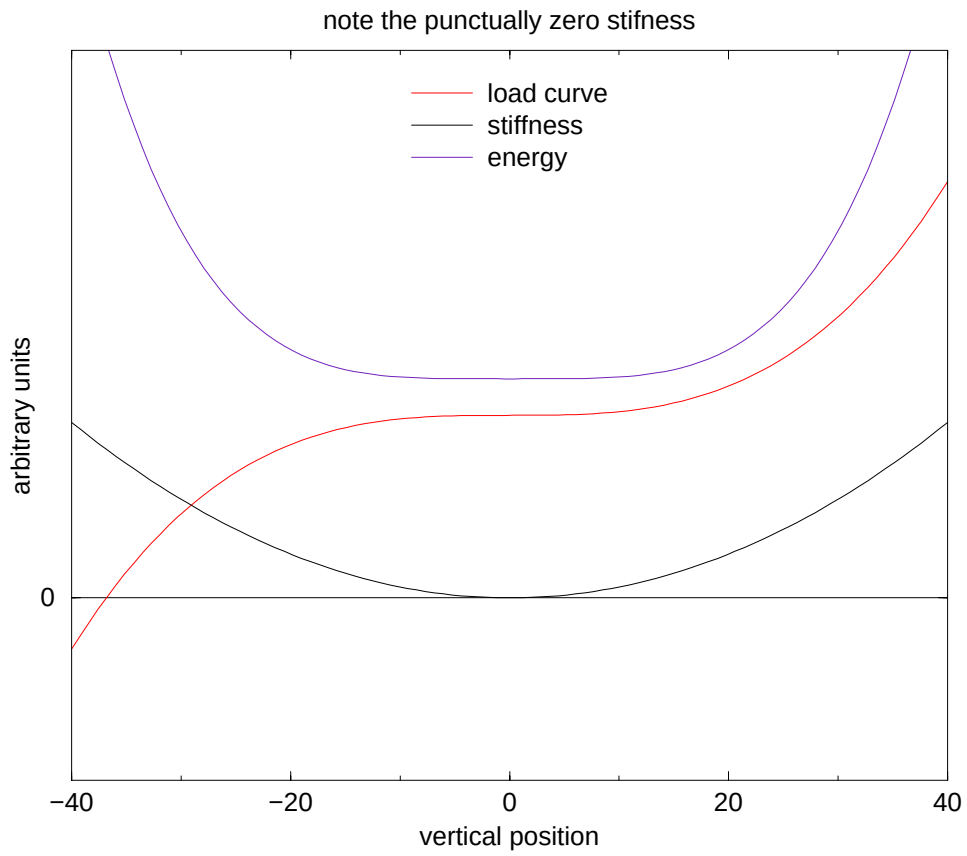

Figure 4.17: T B D

Now if we bring the blades roots farther from each other, the blades become less compressed horizontally, and the bistable behavior becomes less pronounced. The hill in the Energy function will decrease its height. If we keep going this way we will reach a point where we have no hill anymore and we have joined the two wells that were on its sides. This is the limit case between monostability and bistability. We get a load curve that has a flat spot, and locally we get a zero stiffness / zero frequency. In this region, any (even small) friction or creak wins over the elastic forces thus generating chaotic behavior.

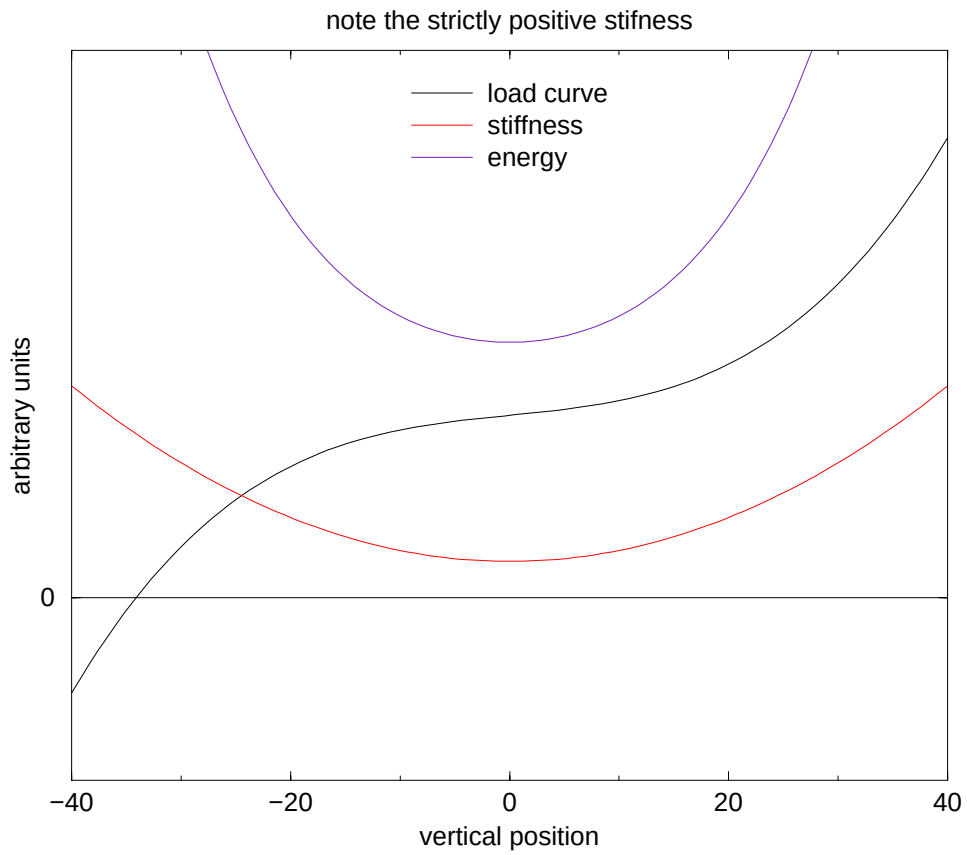

Figure 4.18: T B D

At the begining we had a part with negative stiffness, now we have reduced it into a point with zero stiffness.

If we keep going (releasing the blade compression) then we will get a strictly positive stiffness, with a load curve that is always increasing.

This is the last situation, with locally a low positive stiffness, low VRF, that is of interest for our purposes.

If we decrease again the blade compression then we will increase the minimum stiffness and get a narrower energy curve.

The resonant frequency of the system is what we are interested in, and it varies the same direction as the stiffness. Theoretically we can obtain any desired resonant frequency above zero by giving the right amount of compression to the blades.

On the GAS filters we were tuning the minimum VRF with the diameter of the central disk, here we should increase the size of the central block (or bring the blade roots closer on the unistrap prototype).

The prototype showed us that with a proper geometry, it was possible to obtain low resonant frequencies.

Next we tried to obtain the same from the simulations.

4.10 Simulation of the prototype

4.10.1 Introduction

We measured the geometry of the prototype tuned at 254 mHz. By geometry we mean essentially the coordinates of the root and tip of each blade, the shape of the blade... The idea was to use these data as an input for our simulations, and see if the software would give us the same behavior as the prototype, in terms of resonant frequency, loadcarrying capacity...

Altering a little bit this measured geometry would also allow us to calculate several configurations and plot load curves, resonant frequency curves, curves about the sensitivity to geometric parameters, which we would compare to our experimental data.

All these checks were necessary to correct/calibrate our simulations or confirm that they were reliable. Once they are proven to be reliable, the first thing is that we can have confidence in the simulated stress. This is important because so far no stress (strain) measurement were done, and the computations being our only source of information for the stress, we need to verify them by all possible indirect means. The second thing is we can extrapolate from successful simulations. We can simulate improvements to our first prototype, we can make developments and design a better prototype.

4.10.2 Comments on the prototype's geometry

The main difficulty we faced was the asymetry of the prototype. The blade roots' angles with the horizontal plane were all different from each other. The effective length of the blades were uneven, because of bad clamping wedges (from the recycle bin). We also had two different pairs of available blades, wide and narrow, but at least this was symetric.

Since our system is nonlinear geometrically, the properties of a blade at 45^o is different from what we would find by averaging the properties of a 40^o blade and a 50^o blade. When we take measurements on the filter, what we access is the properties of the four blades together.

The "height vs. load" curve for the whole filter should be the sum of each blade's own curve, and it is also true for the "stiffness vs height" curve. But for the "resonant frequency vs. height" curve, we cannot use the sum of each four blade, because resonant frequency is related to the square root of the stiffness; it is nonlinear and the property of the sum is not generally speaking the sum of the properties.

In our finite element model we have only half a blade. Therefore we ran the calculations several times, each time with the particular geometry of one blade of our prototype, rather than using running our calculations only once, on an "averaged geometry".

4.10.3 Simulation first results

When we first put the measured geometry into the software, the sum of the vertical forces on the four blades was 182.9 kgf. The total payload we measured with a scale/strain gage was 189 kg, therefore the difference was about 3 %.

Then we printed the profile view of the blades and put them aside the protoype to compare the curvature. For the blade # 1 we got a "perfect" match (given our comparison technic) and for the other blades our printings had too much curvature at the ends and not enough in the blade's middle.

Next step was to run the computations for several positions along the vertical axis.

The shape of the curve was unexpected, because near the working point (0mm) the system gets stiffer than anywhere else. We show only the sum of the four curves on picture 4.19. What we expected was a local softening of the load curve instead of this stiffening. This behavior is unexpected but all the four blades show it, it is more or less pronounced but it is always there. Therefore the four simulations are at least coherent with each other.

If we do the sum of the four load curves and superpose it to the measured data, they do not match (4.19); the load was quite well predicted at $h = 0$ but when we move up or down, the shape of the curve is wrong.

To get the resonant frequency we differentiate the load curves, sum them, divide by the sum of the individual payloads. From the square root of the result we can compute the resonant frequency (square root after the sum and not the opposite). Since we had a great error in stiffness we could not get a valid resonant frequency.

From this point of view we have to say that we failed. Putting the measured geometry inside the software, comparing the computed load curve with the measured load curve did not give good results.

To our eyes, the computed and actual profiles seemed to have little difference, but it is possible that it was enough to affect the properties we were looking at. These differences in the curvature may be caused by a bad measurement of the prototype's geometry. For some of the measurements we could use a caliper and get a good accuracy, for some other we had

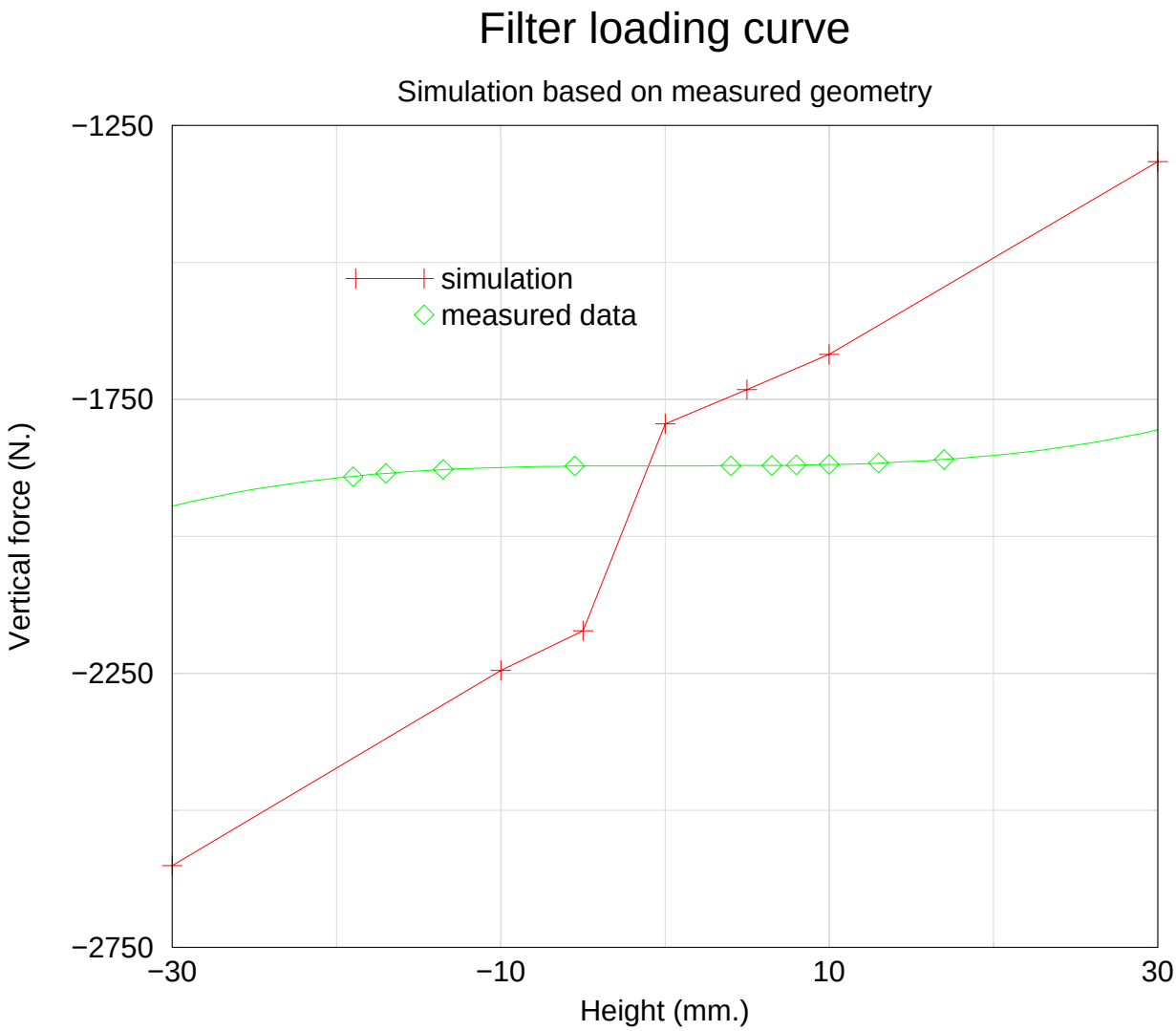

Figure 4.19: Measured and simulated load curves. The measured curve gets softer, very flat in the center. The simulated curve has a sudden step around zero; however note that the slope is smaller between -10 and -5 than between -30 and -10. It also happens between +5 and +10 compared to +10 and +30.

to use a ribbon ruler in inches. The other possibility would be that our measurements were good enough, we had the good coordinates for the tip and the root, but between the two ends the simulation predicts a wrong curvature.

It would be good to check this issue on future prototypes.

4.10.4 Inverse approach

The next approach was to specify the geometry by ourselves, and modify it until we get a load curve close to what we measured. The reason why we did this is that the system seemed highly sensitive to small geometry changes. We mean that if an error of one percent on the geometry leads to an error of 100 % on the stiffness then we will reject the simulation. And we will do so only because the system is too sensitive to an input parameter that we cannot measure accurately enough. Doing the other way, if we need to alter the geometry by only a few percents to get the right resonant frequency, we would consider our simulation valid. Note that this high sensitivity has to be expected as we are substracting large effects (k and $-k$) to a very low value.

4.10.5 Loading procedure

Previously, we had a first loading step defined by pulling on the link ("stepped boundary condition", the software was slowly increasing the force at each substep of the calculation until it reached the specified value). Next was a second load step, in which we removed the link and specified (with displacement boundary conditions) a particular vertical position for the clamped-clamped blade.

Here we want to try arbitrary geometries, we need to move the tip horizontally until we get a certain type of results. Therefore we cannot start anymore the loading process with a load step in which we pull on a link. We would have to change the geometry of the link if we wanted to use it (maybe change the diameter of the central disk where the link is hooked). We want to specify the blade tip's radial position, which has a complicated, non-linear relation with the diameter of the disk. This is why we removed the link and specified the displacements directly on the blade tip.

This change seems minor, but it made the software crash. We could run successfully the very same loading procedure on a model made of simple beam elements, but it would never work on our blade model. Therefore we could not understand the failure from a simplified model.

We could see on the log files that just before the crash certains "dof limits" had been exceeded.

After lots of time-consuming attempts we found a loading procedure that would not cause the software to crash. This procedure can be described as follows:

First step we give only the horizontal displacement. We can "step" the boundary condition during this first step. The vertical and rotationnal boundary conditions on the blade tip remain free. Of course we will see some displacement for these two degree of freedom, what we do vertically will indirectly cause them to move towards a minimal energy geometry.

Second step we specifiy an additonnal parameter, the vertical displacement. What we specify for this parameter will not be very different from what the system had spontaneously reached at the end of step 1. Therefore we do not specify tremendous changes in the geometry compared to the end of step 1. For this second step if we choose stepped boundary condition, the software will step ALL the boundary counditions from ZERO without asking the user.

Until we understood this, the software would keep succeed at step 1 and crash at step 2.

In our particular case the way the software steps the boundary conditions does not work because we have non-zero displacements left from the first step, and we do not want to start again everything from zero. Given this particular feature of the software, we must ramp the boundary conditions during step 2 and 3. For all the iterations that will occur during these steps, all the boundary conditions will be 100 % of their specified values.

Third step is to specify the rotationnal degree of freedom of the blade tip. Again, what we specify will not be very far from was was left from step 2 (the configurations we are interested constrain just a bit the angle). We believe this allows us to avoid the numerical failures we had at the beginning.

We were using only a single load step (still with many iterations), in which we specified all the three boundary conditions at the same time. What caused the numerical failure was certainly that the software ramps all the boundary conditions at the same time from 0 to 100 %. It means the blade tip travels from the straight-unloaded position to final position following a STRAIGHT LINE instead of an unconstrained, "free" curved path. It is likely that the intermediate positions on this straight path would be unrealistic and actually cause the blade to break. By imposing the boundary conditions in three steps, we leave the blade more freedom to follow a low-stress path.

From the computationnal point of view, this was the only difficulty we had to face.

4.10.6 Corrections on blade # 1

We first tried this approach on the blade whose load curve was the easiest to correct, with the lowest stiffness of the four blades. By compressing the blade horizontally by 5mm more than what we had mesured, we actually reduced the stiffness around the working point. It was such a tremendous change that the stiffness became locally negative. Four of these blades would make a bistable system.

Therefore a 5mm correction on the geometry was already too much and switched the stiffness of the system from one extreme to the other. Then with several trys we determined that bringing the stiffness of this blade to the value we had measured on the prototype requires a geometry change of about 2.75mm.

This correction was done on a single blade, the softest one. However, we have four blades, and on our prototype we measured the sum of the four stiffnesses. Therefore when we look for the right geometry change in our simulations, we can find an infinity of combinations that would give such stiffnesses that the sum would match the measured value.

We could correct the geometry of one blade, bring this blade to a negative stiffness to compensate for the others that we leave unchanged, too stiff.

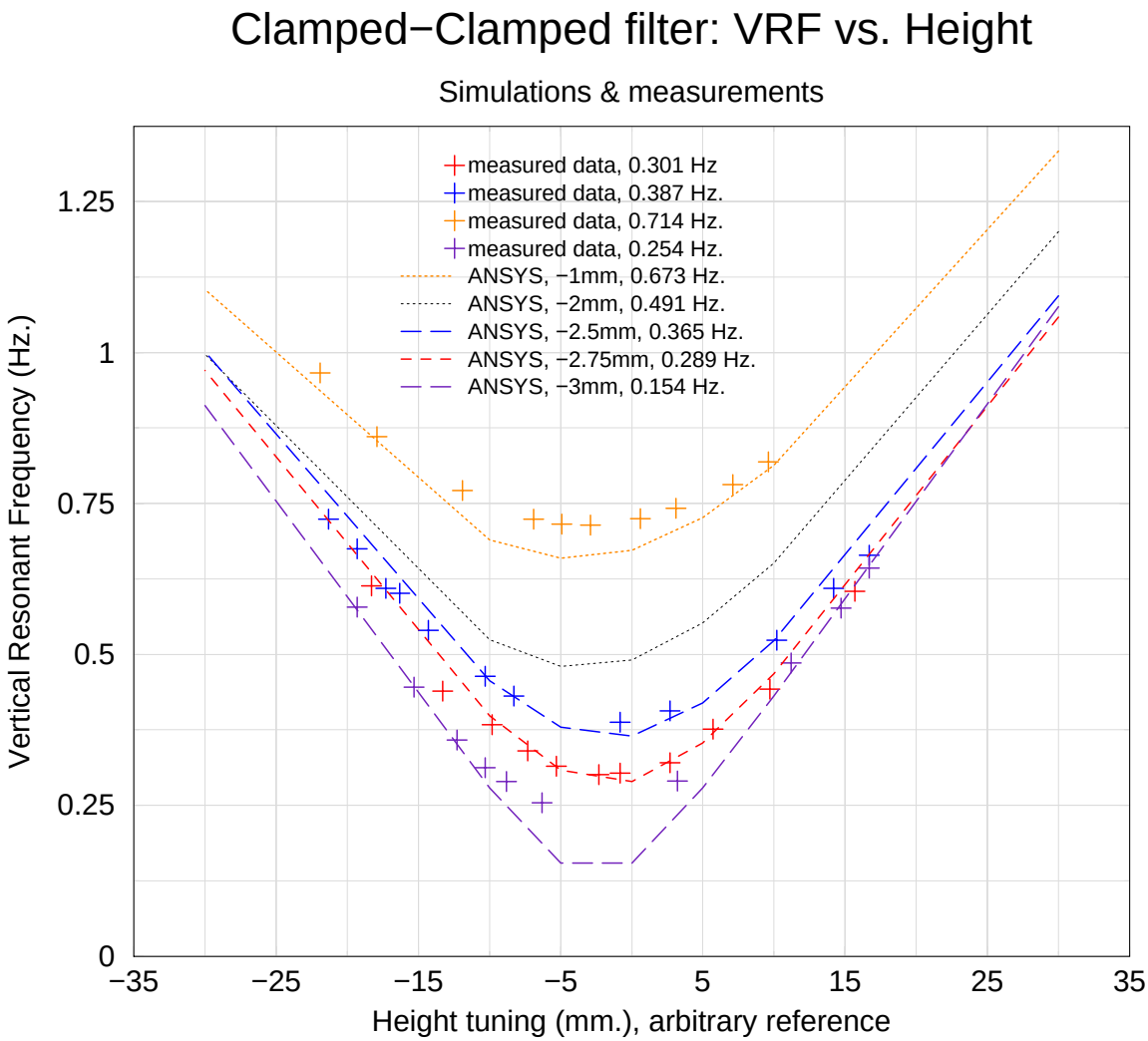
Clamped−Clamped filter: VRF vs. Height
Simulations & measurements
measured data, 0.301 Hz
measured data, 0.387 Hz.
measured data, 0.714 Hz.
measured data, 0.254 Hz.
ANSYS, −1mm, 0.673 Hz.
ANSYS, −2mm, 0.491 Hz.
ANSYS, −2.5mm, 0.365 Hz.
ANSYS, −2.75mm, 0.289 Hz.
ANSYS, −3mm, 0.154 Hz.
Vertical Resonant Frequency (Hz.)
0
0.25
0.5
0.75
1
1.25
−35
−25
−15
−5
5
15
25
35
Height tuning (mm.), arbitrary reference

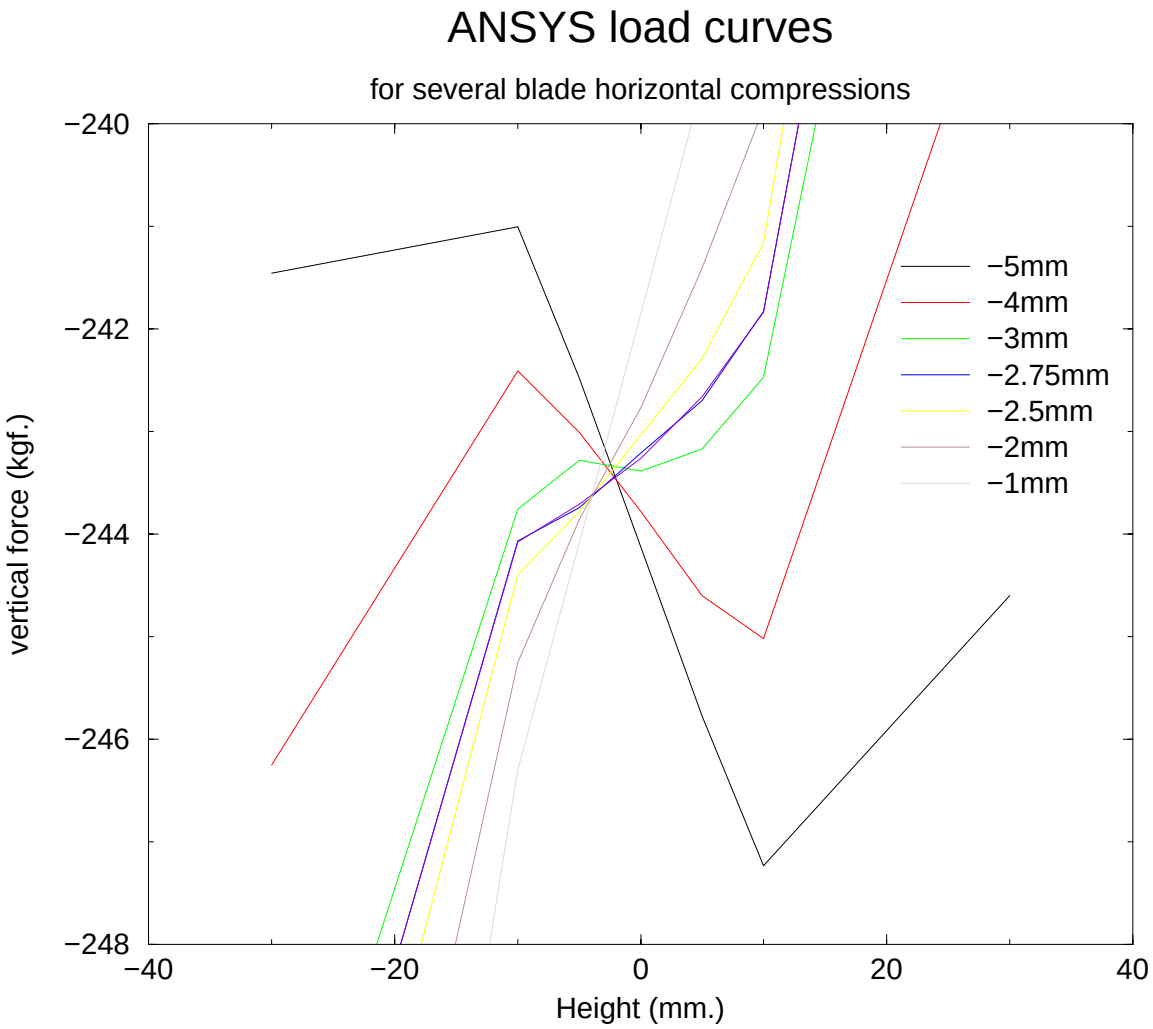
ANSYS load curves
for several blade horizontal compressions
vertical force (kgf.)
Height (mm.)
−240
−242
−244
−246
−248
−40
−20
0
20
40
−5mm
−4mm
−3mm
−2.75mm
−2.5mm
−2mm
−1mm

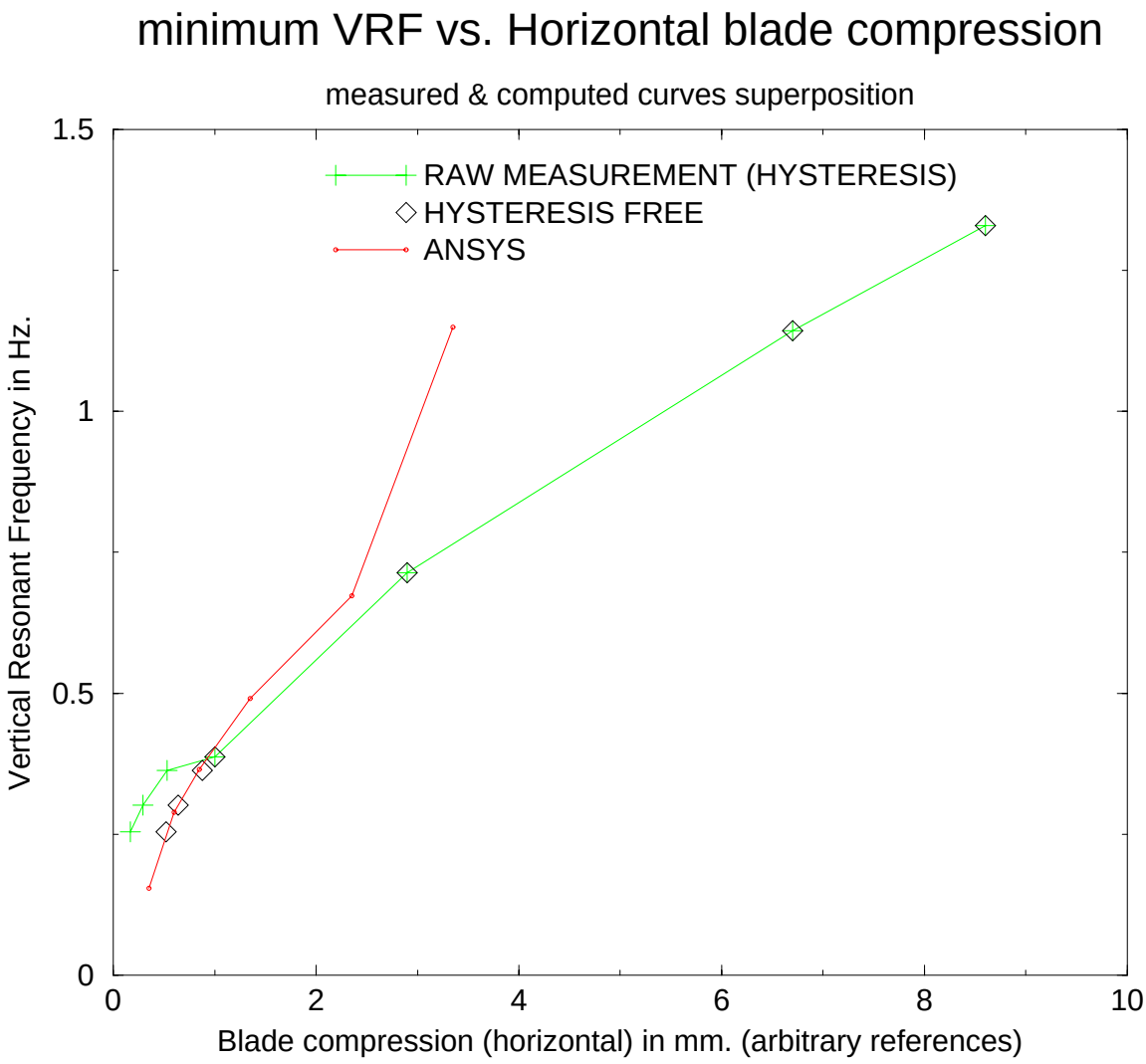
minimum VRF vs. Horizontal blade compression
measured & computed curves superposition
RAW MEASUREMENT (HYSTERESIS)
HYSTERESIS FREE
ANSYS
Vertical Resonant Frequency in Hz.
Blade compression (horizontal) in mm. (arbitrary references)
0
0.5
1
1.5
0
2
4
6
8
10

Or we could try to correct all the four blades by a different amount, to bring them to the same stiffness, a quarter of what we measured on the prototype.

Or we could opt for just any combination...

It does not make much sense to do this, essentially because we cannot access individually the stiffness of each blade on our prototype. Therefore there is no point in trying to calibrate our simulation this way.

But if later on a better prototype is built, with an identical geometry on all its blades, then it will be worth doing this.

Afterwards, we realize that we could have avoided part of these problems. The prototype can still work with two blades. We had two blades with about identical angles. When we were concerned about matching the simulations to the experiments, we could have removed the other blades and kept these two. It might have been a cleaner/simpler system to model.

For now, all we can do is try to see by how much we need to change the worst (stiffest) blade's geometry to bring its stiffness down to reasonable values. This way we will get a rough idea of the range of correction our simulation needs.

4.10.7 Corrections on blade # 3

By compressing blade # 3 by 5mm more than measured we changed its stiffness from 8000 n/m to 700 n/m. The target being about 80n/m we needed a bit more compression. We did not make any further simulation in this direction but from what we saw from blade 1 we can say that blade 3 we would need about 2 more millimeters to reach 80n/m. The total correction would be 5+2=7mm.

This way we get the range of correction our simulation requires, from 2.75mm in the best case to 7mm in the worst case. Of course these values assume that we measured correctly the geometry on the prototype.

4.10.8 Comment on the geometry corrections

Now we can compare the biggest geometry correction (7mm) to the dimensions of the blade. The blades are roughly 400mm long, and when we measured the prototype's geometry we had to deal with similar lengths. The ratio is less than 2 percent.

Even if we compare the 7mm not to the blade length but only to the tip deflexion (roughly 230mm) we get no more than 3 percent.

Therefore we can say that trying to obtain the prototype's performances from our simulation, we reached a geometry that is satisfyingly close to the prototype's.

We first tried the opposite approach and we failed. This is because the properties we are looking at are highly sensitive to the geometry.

4.11 Next prototype

4.11.1 Preambule

The next step in the development of the clamped-clamped filter is to build a second prototype. We will make it symetrical this time, we will manufacture a dedicated filter frame to hold the blades instead of using the unistrap structure. It will not have the bad clampings withs shims that we used here. We could have machined a new central block with the right clamping angle. But on a quick experiment of the resonance frequencies, we found out that the first internal mode of the blades was at 30 Hz. It is quite low, we had 60Hz on the GAS filter. Part of the reason is because our central block is much more massive than the central structure and disk used to hook the links previously.

To push the first internal mode of the blades at higher frequency we want to lighten the central part. Therefore we will manufacture a monolithic blade system, cutting all the blades toghether with the central plate from the same sheet of metal, and then bend it to what used to be the clamping angle, a bit like a flower (figures 4.20 and 4.21).

4.11.2 Simulations

To design such a prototype we needed a few more dimensions. We ran a last time the simulations with a root angle of 45^o, and tried different positions for the tip of the blade until we found the working position giving us a low resonant frequency. Then we could use the blade deflexion/side view to design the filter frame. The simulations also gave us the information on what angle the metal sheet had to be bent. It also gave us a slightly different load curve (see 4.22).

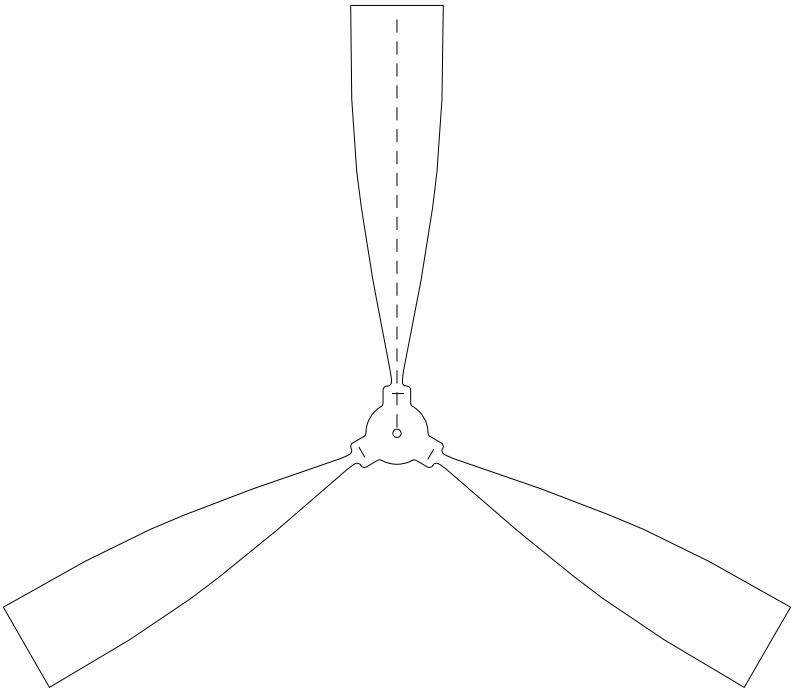

Figure 4.20: Top view of the monolithic "flower"

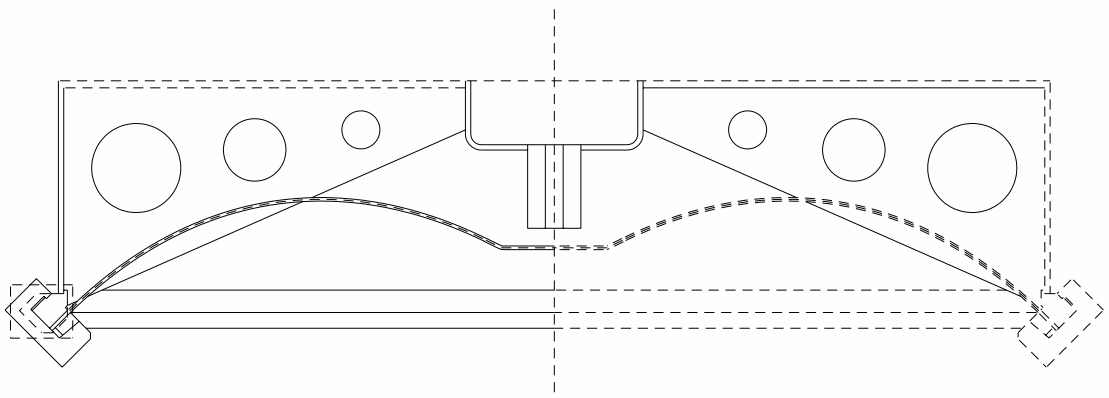

Figure 4.21: Side view of the filter using the "flower"

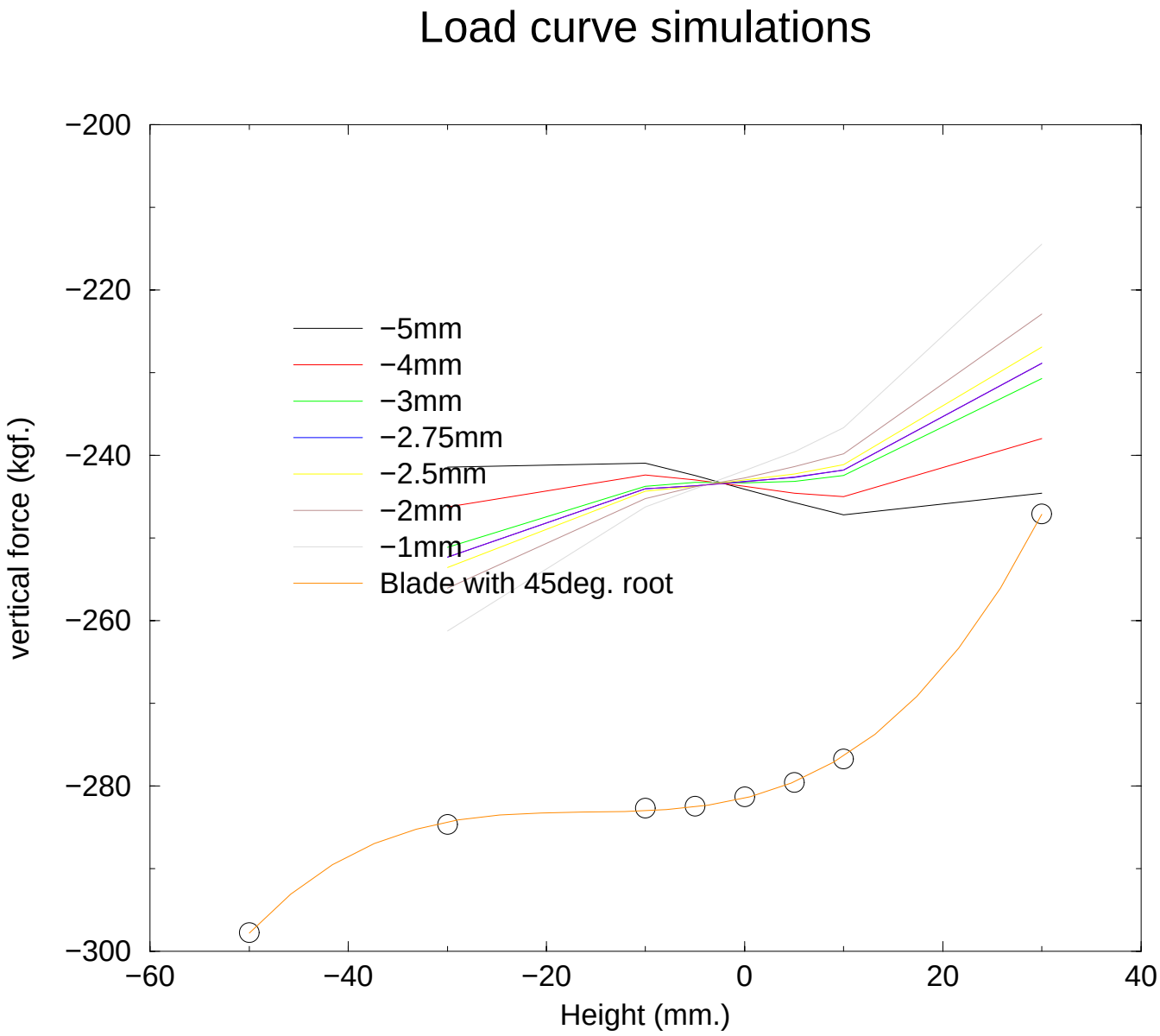

Figure 4.22: 45^o configuration

4.11.3 Limits to the predictions

Possibly when this new prototype will be tested we will find that we need to compress the blades a bit less than what we computed. A "flower filter" was designed featuring clampings that are adjustable radially.

The first prototype of the flower series will be scaled down for the TAMA (300 meter) interferometer. It will have a body diameter of about 60cm instead of 90cm, and the thickness of the blades will be 2mm instead of 3.15mm. The blades may have a different effective length than what we used for our calculations, because their tips have width enlargments (see 4.20). Therefore the above simulations will need to be adapted to this prototype.

4.11.4 Comment on the stress

Without GAS links we need to compress more the blades. They have a shorter radius of curvature. Therefore we find higher levels of stress than what we had for the GAS filters. Early creep measurement experiment indicated that we are still in a safe zone. It will be checked again with the "oven" experiment if maraging steel can actually take this stress and still remain creep-free. Otherwise wider and thinner blades will be used to reduce the peak stress.

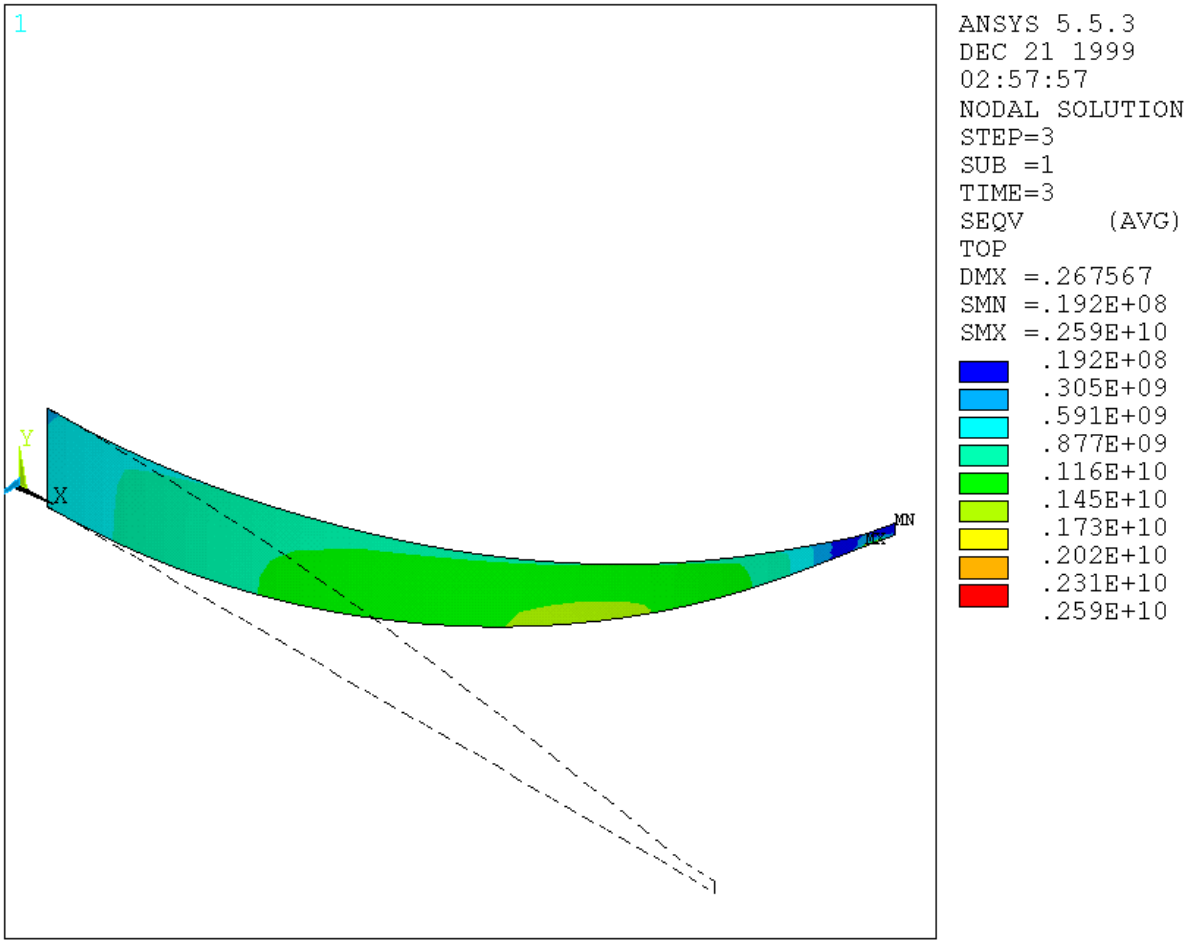

Figure 4.23: down by 20 mm

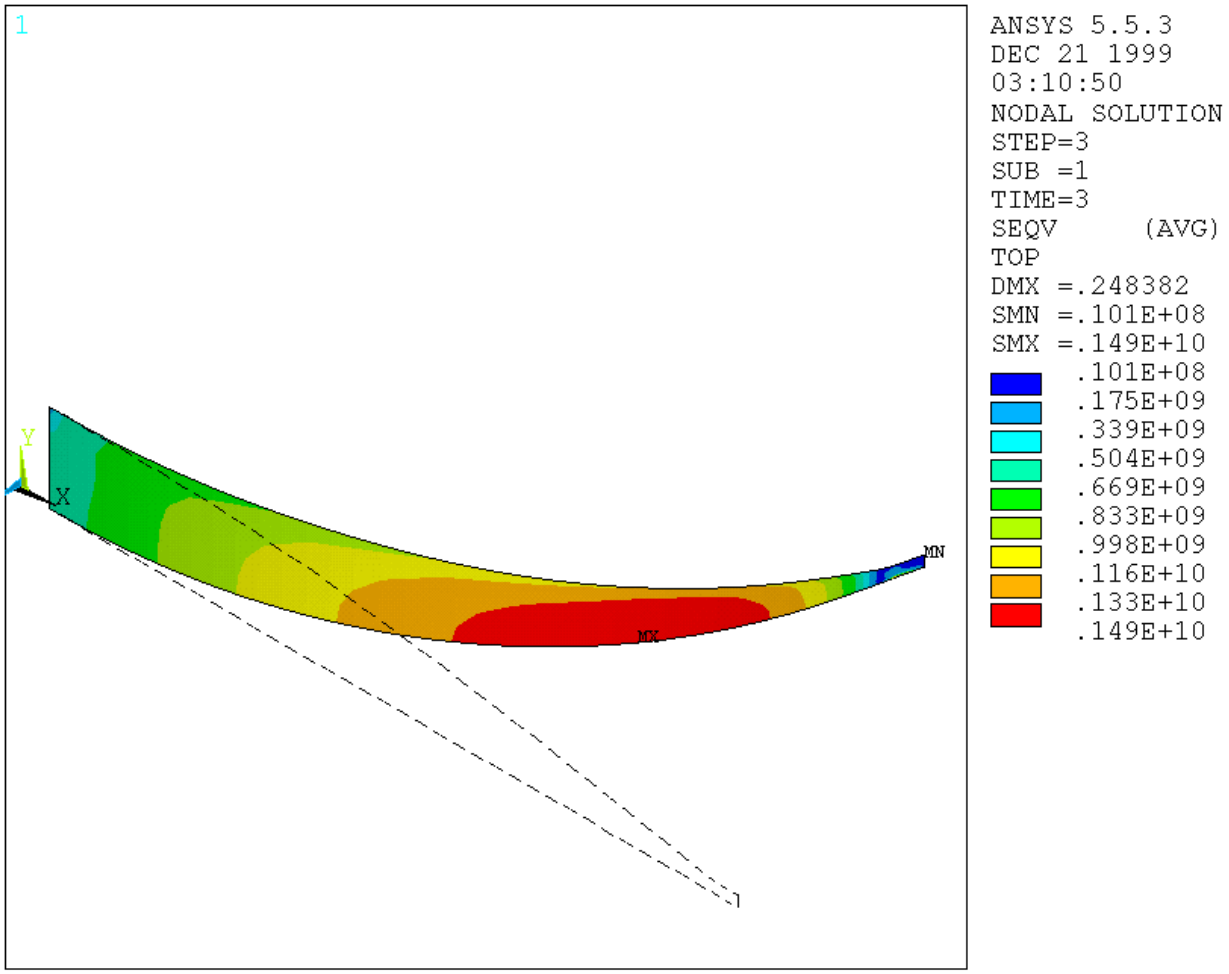

Figure 4.24: nominal position

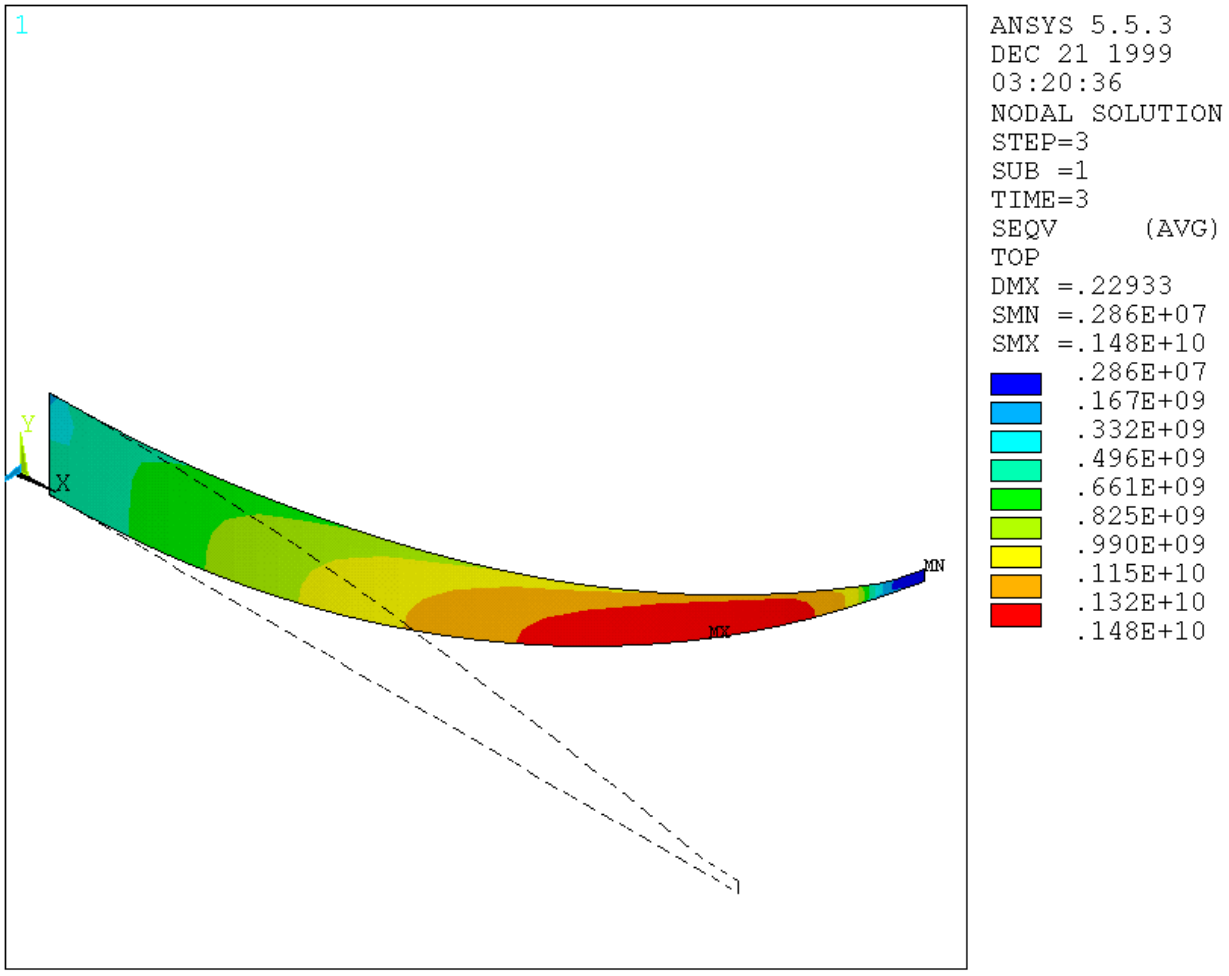

Figure 4.25: up by 20 mm

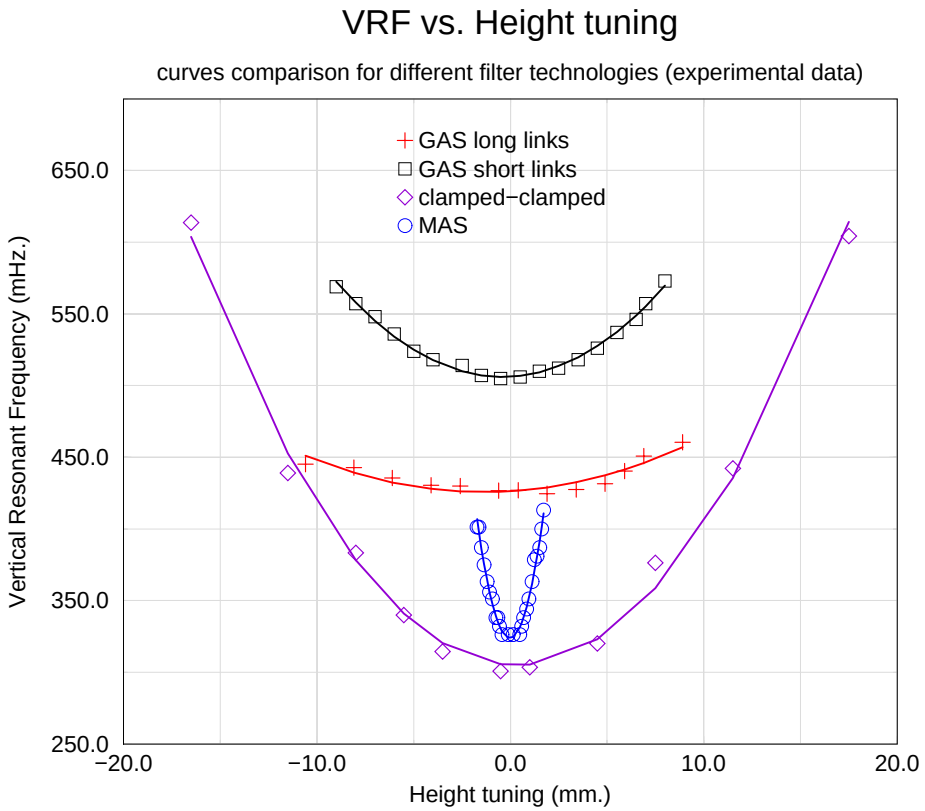

Figure 4.26: comparison Magnetic Anti Springs (VIRGO), Geometric Anti Springs, Clamped-clamped/wireless filters

4.12 Conclusion on the clamped-clamped filter

The clamped-clamped filter does not have the unwanted rotational resonance that the GAS filters had. It is also cheaper, simpler with a reduced number of parts. It can even work with only two blades whereas the GAS needs at least 3. It can be easily reduced in size whereas links were difficult to be made too small.

The clamped-clamped is only at an early stage of development, but is promising. It is difficult to make static simulations of the blades because the system is strongly non-linear and very sensitive to the geometry. The most important was certainly that finite elements calculations convinced us to build a prototype.

Chapter 5

Conclusion

During this internship we showed that Finite Elements simulations could help to design the Seismic Attenuation System. This report describes the study of three particular problems, but many others could be interesting. Among them we could already think of:

- a dynamic analysis of the vertical filter, both in GAS and clamped-clamped configurations
- a dynamic analysis of the whole seismic attenuation system mechanics, including the inverted pendulum and the vertical-filter chain
- a modal analysis of the mechanics of a new accelerometer which is currently being designed, based on a pendulum and an inverted pendulum
- a stress analysis of the classic GAS links
- an optimization of the GAS filter's loading disk in order to minimize its weight

And possibly more!

Chapter 6

Acknowledgements

I would like to thank:

- Dr. Riccardo DeSalvo and Pr. Régis Dufour for being my mentors during this internship.
- Virginio Sannibale and Akiteru Takamori.
- The LMSt laboratory for providing the ANSYS software.

Bibliography

[1] Kip S. Thorne. *Black holes and time warps, Einstein's outrageous legacy.* Norton, 1994.

[2] A. Bertolini, G. Cella, R. DeSalvo, V. Sannibale. *Seismic noise filters, Vertical Resonance Frequency reduction with Geometric Anti-Springs, a feasibility study.* NIM-A article, Jan 10 1998.

[3] G. Losurdo. *Ultra-Low Frequency Inverted Pendulum for the VIRGO Test Mass Suspension.* Tesi di Perfezionamento in Fisica, October 1998.

[4] Pr. R. Dufour. *1998-1999 Finite Element course notes.* INSA de Lyon, Dept. GMD.

[5] M. Lalanne, P. Berthier, J. Der Hagopian. *Mechanical Vibrations for Engineers.* Wiley-Interscience (1984).